Western Graduate&PostdoctoralStudies

Western University
Scholarship@Western

Electronic Thesis and Dissertation Repository

8-25-2021 9:30 AM

Synthesis And Characterization of Re(I) Tricarbonyl Complexes of 1,8-Naphthalimide

Priyanka Jagadeesa Prabhu, *The University of Western Ontario*

Supervisor: Luyt, Leonard G., *The University of Western Ontario*

A thesis submitted in partial fulfillment of the requirements for the Master of Science degree in Chemistry

© Priyanka Jagadeesa Prabhu 2021

Follow this and additional works at: https://ir.lib.uwo.ca/etd

Part of the Organic Chemistry Commons

Recommended Citation

Jagadeesa Prabhu, Priyanka, "Synthesis And Characterization of Re(I) Tricarbonyl Complexes of 1,8-Naphthalimide" (2021). *Electronic Thesis and Dissertation Repository*. 8111.
https://ir.lib.uwo.ca/etd/8111

This Dissertation/Thesis is brought to you for free and open access by Scholarship@Western. It has been accepted for inclusion in Electronic Thesis and Dissertation Repository by an authorized administrator of Scholarship@Western. For more information, please contact wlswadmin@uwo.ca.

Abstract

1,8-Naphthalimide fluorophores with amino-substituents absorb and emit in the visible region. The photophysical properties of this class of fluorophores can be modulated by altering the degree of Intramolecular Charge Transfer (ICT) in the excited state. Thus, several metal complexes with the 1,8-naphthalimide motif have been developed as cell imaging agents. In this project, four 1,8-naphthalimide ligands were synthesized by incorporating rigid linkers. Among these, three ligands also allowed the extension of π-conjugation to the naphthalimide moiety. In addition, a ligand was also synthesized without the use of a linker. Re(I) tricarbonyl complexes of these ligands were also synthesized and their photophysical properties were studied. Extension of π-conjugation was seen to shift the emission of the fluorophores to shorter wavelengths that are not ideal for cell imaging. However, ligands that lack the extended π-conjugation fluoresce at ca. 420 nm, implying their use as fluorescence imaging agents and possible development as SPECT tracers.

Keywords

1,8-naphthalimide derivatives, extended π-conjugation, rigid linkers, fluorescence, optical imaging agents, dual SPECT/fluorescence imaging agents.

Summary for Lay Audience

Optical imaging is an imaging technique that is non-invasive and uses light to image the tissue and organs. Due to the scattering of light by the tissues and cell components, specific drug-like molecules, called imaging probes, are used to enhance the contrast of the tissue. Molecules that exhibit fluorescence are often used as probes for optical imaging. 1,8-Naphthalimde is one such molecule that shows fluorescence behaviour when irradiated by visible light. The wavelength of light emitted by 1,8-naphthalimide can be modified by adding certain molecules, called linkers. Simple hydrocarbon chains have been previously utilized as linkers to make 1,8-naphthalimide based imaging agents. In this study, we use 4 different rigid molecules such as a benzene ring, as linkers and analyze the changes in the wavelength of emitted light. Another derivative was also synthesized without the use of a linker. Complexes of rhenium metal are also known to be good cell imaging agents. In addition, they also allow the possibility of developing imaging probes for a different imaging technique, that utilizes gamma rays from radioactive metals to image the organs. Hence, complexes were synthesized by using 1,8-naphthalimide derivatives as ligands to from rhenium metal complexes. Measurement of the fluorescence properties of these ligands and rhenium complexes revealed that the use of rigid linkers resulted in emission of light which has a wavelength below 400 nm. Since the microscope that is used to image cells utilizes light in the range of 400 to 800 nm, the newly synthesized ligands and their rhenium complexes may not be useful as cell imaging agents. However, successful formation of rhenium complexes implies the possibility of using ^{99m}Tc as the radioactive metal to develop nuclear imaging probes.

Co-Authorship Statement

Most of the work in this project was done by the author except the following:

L$_1$ and **L**$_2$ were designed and initially synthesized by Maryam Majeed, NSERC-summer intern in Dr. Len Luyt's Lab. These were then optimized for yield by the author.

HRMS measurements were carried out by Haidy Metwally, the facility manager at the Western Chemistry Mass Spectroscopy facility.

Absolute quantum yields of all ligands and rhenium complexes were obtained by Francis Buguis, Ph.D. candidate in Dr. Joe Gilroy's Lab.

Acknowledgements

Firstly, I would like to thank my supervisor Dr. Len Luyt, for the opportunity to work in his lab. I appreciate his patience and timely advice through all the ups and downs of graduate student life and research. He has taken great care to keep everyone connected and timely informed during the pandemic and lockdown in the last year.

I would like to Dhvani Oza and Julia Mason for being good friends and colleagues. They have been my first point of contact for anything and everything for the past two years. A thank you to Dr. Mark Milne, Dr. Carlie Charron and Dr. Marina Childs for the training and mentorship in the lab.

I am grateful to Dr. Robert Hudson for the permission and to Mria Chowdury for the training, in carrying out the fluorimetry studies in their lab.

Most of all I am extremely thankful to my parents for their support and encouragement, all my life. Thank you for listening to all my happy and worried ramblings from halfway across the world.

Table of Contents

Abstract……i

Summary for Lay Audience…….....ii

Co-Authorship Statement……...iii

Acknowledgements…….....iv

Table of Contents…….....v

List of Tables…….vii

List of Figures……...viii

List of Schemes……...ix

List of Appendices……...x

List of Abbreviations……..xi

Chapter 1: Introduction…….……..……..…1

1.1 Molecular Imaging……..…….…….….1

1.2 Imaging Probes……..……..……..2

1.3 Dual Modality Imaging Probes…….…..…..……..3

1.4 Single-Photon Emission Computed Tomography (SPECT)…….……...……..6

1.5 Technetium-99m…….……...……7

1.6 Rhenium…….……...…….8

1.7 Optical Imaging ……..……...…….10

1.8 Derivatives of 1,8-Naphthalimide……11

1.9 Scope Of The Thesis……12

1.10 References……..13

Chapter 2: Synthesis and Characterization of Re(I) tricarbonyl Complexes of 1,8-Naphthalimide Derivatives……16

2.1 Introduction……..16

2.2. Results and Discussion……...21

2.2.1 Design of 1,8-Naphthalimide Derivatives……21

2.2.2 Optimization and Synthesis of Ligands……22

2.2.3 Synthesis of Re(I) tricarbonyl Complexes……...….29

2.2.4 Structural Characterization……...30

2.2.5 Photophysical Properties……...32

2.3 Conclusions……..34

2.4 Experimental……34

2.5 References……44

Chapter 3: Conclusions and Future Work……..48

3.1 References……50

Appendices.……..……..52

Curriculum Vitae…….105

List of Tables

Table 1.1: Comparison of some *in vivo* imaging modalities……..……4

Table 1.2 : List of commonly used radioisotopes in SPECT imaging……...…7

Table 2.1 : Conditions attempted for the synthesis of **L**$_5$……..29

Table 2.2 : Photophysical properties of synthesized ligands and their Re(I) tricarbonyl complexes……..33

List of Figures

Figure 1.1: Steps in a molecular imaging study……...2

Figure 1.2: Schematic representation of an imaging probe…….3

Figure 1.3: Example of SPECT-fluorescence dual-imaging probe for potential imaging of prostate cancer…….6

Figure 1.4: Decay scheme of ^{99}Mo to ^{99}Ru……..8

Figure 1.5: Example of a Re(I) tricarbonyl complexes as cellular imaging agents with a) polypyridyl, b) dipicolylamine and c) bis-quinoline ligands……...9

Figure 1.6: Examples of fluorescent organic dyes used in cell imaging……...11

Figure 1.7: Naphthalimide derivative as donor-π-acceptor systems……..12

Figure 2.1: a) Re(I) tricarbonyl complexes of 1.8-naphthalimde derivatives for cell imaging. b) Structure of dual-modality T140 analogue for CXCR4 expression……...19

Figure 2.2: 1,8-Naphthalimde derivative with variable linker lengths for potential SPECT/fluorescence imaging……20

Figure 2.3: Positively, neutral and negatively charged Re(I) complexes of 1,8-naphthalimde derivatives……...20

Figure 2.4: Structures of 1,8-naphthalimide derivative to study the effect of rigid linkers……22

Figure 2.5: Effect of linker on methylene protons of the dipicolylamine arms ……..….31

Figure 2.6: Diastereotopic splitting of the methylene protons on the chelator, in rhenium complexes……..32

List of Schemes

Scheme 2.1: Synthesis of **L_1** using **1**…...……...…….……..22

Scheme 2.2: Attempts in synthesis of **L_2** using **1**.…….…...…….....23

Scheme 2.3: Pathways for the synthesis of **L_3** using 4-fluorophenylboronic acid and 4-nitrophenylboronic acid…….24

Scheme 2.4: Synthesis of **L_4** using **1**…...……....……..25

Scheme 2.5: Scheme for synthesis of **L_5** using **1**…….....25

Schene2.6: Attempts at synthesizing **L_6** using **1**.....……...…….……..……...…..26

Scheme 2.7: Synthesis of **L_2** using **12**……...…….…...……26

Scheme 2.8: Synthesis of precursors for **L_3**-**L_5** and **L_6** using 12 ..……..…....…….…27

Scheme 2.9: Synthesis of **L_3** and **L_4**..……...……..28

Scheme 2.10: Attempted synthesis of **L_5**…….. 28

Scheme 2.11: Synthesis of **L_6** ……...……29

Scheme 2.12: Scheme for synthesis of Re(I) tricarbonyl complex of 1.8-naphthalimde derivative……29

List of Appendices

Appendix A : ^{1}H and ^{13}C NMR Spectroscopy Data of Synthesized Compounds……52

Appendix B : High Resolution Mass Spectroscopy (HRMS) Data of Synthesized Compounds……90

Appendix C : UV/Vis Absorbance and Fluorescence Spectra of Ligands and Rhenium Complexes……100

List of Abbreviations

Boc	tert-butyloxycarbonyl
CT	Computed Tomography
CXCR4	C-X-C-Chemokine Receptor 4
DCM	dichloromethane
DMF	*N*,*N*-Dimethylformamide
DMSO	dimethyl sulfoxide
DOTA	1,4,7,10-tetraazacyclododecane-1,4,7,10-tetraacetic acid
DPA	2,2'-picolyl)amine
EDG	electron donating group
ESI	electrospray isonization
Et_3N	triethylamine
EtOAc	ethylacetate
EtOH	ethanol
eV	electron volt
HOMO	highest occupied molecular orbital
HPLC	high-performance liquid chromatography
HRMS	high resolution mass spectroscopy
ICT	intramolecular charge transfer

LUMO	lowest unoccupied molecular orbital
mAb	monoclonal antibodies
MeOH	methanol
MLCT	metal-to-ligand charge transfer
MRI	magnetic resonance imaging
NMR	nuclear magnetic resonance
OI	optical imaging
OTf	trifluoromethanesulfonate
PET	positron emission tomography
PSMA	prostate-specific membrane antigen
RT	room temperature
SPECT	single-photon emission tomography
TBAF	tetra-n-butylammonium fluoride
TFA	trifluoroacetic acid
THF	tetrahydrofuran
UV/Vis	ultraviolet/visible

Chapter 1 : Introduction

1.1 Molecular Imaging

Molecular imaging aids in the visualization and evaluation of internal biochemical processes that take place in living beings. Over the years, the application of molecular imaging has gone beyond merely differentiating between healthy and diseased tissues. Today, it is used for early detection, to gain insight into disease progression and to monitor response to therapy in conditions such as cancer. Steps involved in a typical molecular imaging study are shown in **Figure 1.1**. The first step requires the selection of a biochemical process that can be visualized directly or indirectly using a molecular target. These targets are often receptors, enzymes, or cellular events that are altered in a diseased tissue as opposed to healthy tissue. An imaging modality is then chosen to study the target. Examples of imaging modalities include Magnetic Resonance Imaging (MRI), Optical Imaging (OI), Single-Photon Emission Computed Tomography (SPECT) and Positron Emission Tomography (PET). Imaging probes allow interaction with the molecular target and enhance the contrast of images. Choosing an imaging probe depends on the type of imaging modality, which in turn decides the further steps involved in the study including the design, synthesis, *in vitro* and *in vivo* evaluation of the probe, as well as the final image acquisition and processing.

An ideal imaging modality would allow for imaging of the whole body with short acquisition time, high specificity to the targets and high resolution of the images. All currently available imaging modalities have their advantages and disadvantages. For instance, the more readily available MRI that is seen as a very safe imaging method has limited sensitivity due to its dependence on the difference between the high and low energy states of the atoms. OI which offers high sensitivity along with spatial resolution lacks the required depth of tissue penetration, for clinical use. On the other hand, while radiation-based imaging modalities offer high sensitivity and tissue penetration depth,

they run the risk of exposing the patient to ionizing radiation. Above all, availability, cost and possible side effects influence the choice of imaging modality.

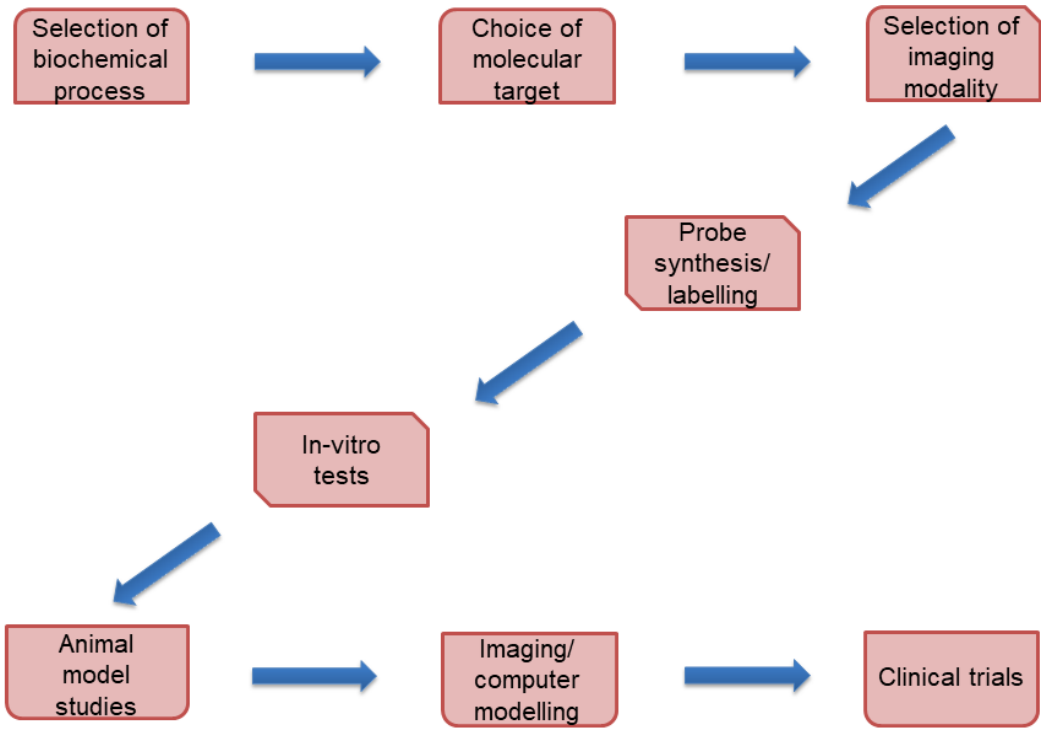

***Figure 1.1**: Steps in a molecular imaging study*

1.2 Imaging Probes

As represented in **Figure 1.2**, a typical imaging probe comprises two major components: an imaging entity and a targeting entity, which are often linked to each other using a linker moiety. The role of the imaging entity is to produce a signal or enhance the contrast of the image. Structure and design of the imaging entity are dictated by the imaging modality in which the probe is intended to be used. For example, bioluminescent or fluorescent molecules are used to visualize the specific molecular targets in OI while nuclear imaging techniques such as SPECT and PET rely on emissions from the radioactive decay of the atoms. The targeting entity allows binding of the probe to the molecular target with high affinity and specificity. Hence, targeting entities are typically peptides, antibodies, nucleic acids, or small molecules that are designed to interact with

the molecular targets. Since binding of the probe to its target is predominantly affected by its size, charge, lipophilicity and binding affinity, these factors along with the imaging entity influence the choice of targeting entity.

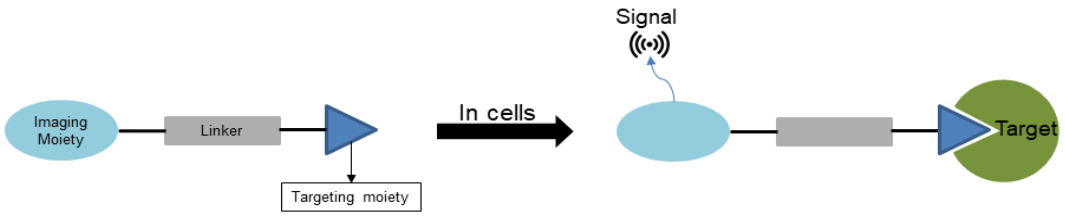

Figure 1.2: *Schematic representation of an imaging probe*

Monoclonal antibodies (mAb), due to their large size can accommodate larger imaging components like metal chelators and large fluorophores. While mAbs can bind to unique targets, their long retention times in the blood leads to a low signal to background ratio, resulting in poor quality images. In contrast, small molecules offer better pharmacokinetics, but their small size limits the type of imaging entity that can be incorporated without affecting their binding affinity and specificity. Peptides that generally weigh less than their mAb counterparts, allow for better pharmacokinetics, like small molecules, while also tolerating larger imaging entities. Moreover, the ease of synthesis gives peptides better leverage to be modified for improved properties.

A synthetic linker molecule is often used to couple the imaging and targeting entities which help in minimizing the interaction between the two moieties as well as modify the pharmacokinetics of the imaging probe.[1] Linkers have been documented to affect the biodistribution of the probe.[2–4] Fine-tuning of factors such as length, flexibility and hydrophilicity can be achieved using linkers.

1.3 Dual-modality Imaging Probes

Dual-modality imaging probes permit the use of two imaging techniques, which is a convenient way of obtaining additional information for the diagnosis, treatment and monitoring of disease. The amount of information gathered using an imaging modality

depends on factors such as the mechanisms of signal production, specific sensitivity, spatial and temporal resolution. Imaging methods such as Computed Tomography (CT) and MRI provide the structural detail whereas modalities such as SPECT and PET provide morphological and functional information. Comparison between the commonly used imaging modalities is shown in **Table 1.1**.

Table 1.1: *Comparison of some in vivo imaging modalities*[5]

	CT	**MRI**	**PET/SPECT**	**Optical**
Source	X-ray	Magnetic field, radiofrequency	γ-rays	Light
Spatial resolution	50–200 μm	25–100 μm	2–10 mm	1–5 mm
Penetration depth	unlimited	unlimited	unlimited	1–10 cm
Information	Anatomical, Physiological	Anatomical, Physiological, Functional	Anatomical, Physiological, Functional	Physiological, Molecular
Advantages	High resolution, unlimited penetration depth	High resolution, no radiation, unlimited penetration depth	Unlimited penetration depth	No radiation, sensitive to probe dose
Disadvantages	Radiation, poor soft tissue delineation, low sensitivity	Poor sensitivity to probes, expensive	Radiation, expensive, low resolution	Low penetration depth, low resolution

Since each modality has certain advantages and disadvantages, when more than one modality is used, it can widen the extent of information that can be obtained, combine the advantages, and eliminate some of the disadvantages. In a clinical scenario, this ensures better accuracy in the detection of diseased areas which translates to better treatment methods. Combining the information from different modalities can be achieved by

merging the images taken at different times using digital image manipulation software. However, this approach has a major restriction due to the positioning of the patient on different devices. Images thus merged, are less accurate due to inconsistent alignment.[6] In addition, this approach often requires the use of different probes that might diffuse differently *in vivo*, leading to increased toxicity.

Inconsistency in alignment of the images can be resolved by simultaneous image acquisition. This approach was first enforced in 1990 by using a hybrid device capable of performing SPECT and CT scans at the same time.[7] Commercial introduction of SPECT/CT and PET/CT systems later in the decade has led to increased clinical use of dual-modal imaging and spurred advances of other dual/multi-modality platforms. Use of such systems requires multi-modality imaging probes that can produce a signal in each modality. In recent years, continued progress is being made in dual-modality tracers that often involve modalities that provide complementary or additional clinically useful information. Nuclear–optical probes are one such example. In addition to the high detection sensitivity of both modalities, their complementary nature also helps to cross-validate the information. While images from nuclear imaging provide a whole-body image with localization of tumours, fluorescence imaging can aid in detection as well as image-guided surgery.[8,9]

The imaging agent shown in **Figure 1.3** is the first reported dual-modality SPECT/near-infrared fluorescence imaging agent for imaging prostate cancer. It utilizes a near-infrared dye, IRDye800CW, for *in vivo* fluorescent imaging while the radioactive ^{111}In chelated to DOTA acts as the SPECT imaging component. Lysine-urea-glutamate serves as the targeting moiety which binds to Prostate-Specific Membrane Antigen (PSMA) which is overexpressed in prostate cancer cells.[10] In the past decade, a few other SPECT-fluorescence probes have also been successfully synthesized which have potential applications in sequential pre-operative imaging via SPECT and intra-operative imaging via near-infrared fluorescence imaging.[11–15]

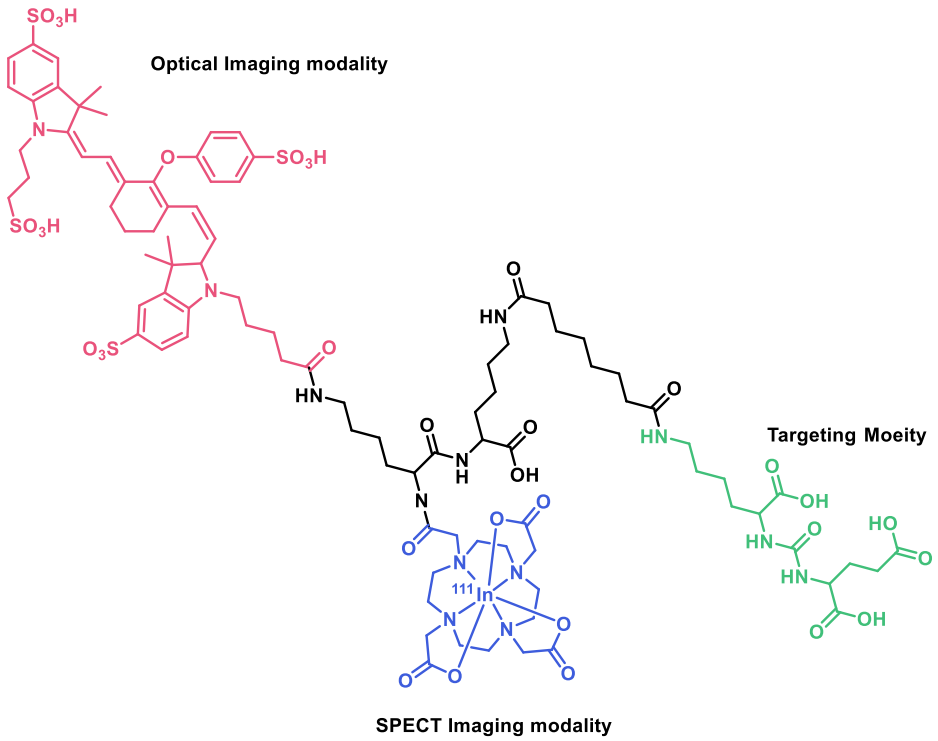

Figure 1.3: *Example of SPECT-fluorescence dual-modality probe for potential imaging of prostate cancer*

1.4 Single-Photon Emission Computed Tomography (SPECT)

Single-photon emission computed tomography (SPECT) is a nuclear imaging technique that is used to study the localization of radiotracers in the body. SPECT radiotracers use radioactive isotopes such as ^{67}Ga, ^{99m}Tc, ^{111}In and ^{123}I that emit single gamma rays with typical energies in the range 100-300 keV, which are optimal for tissue penetration without harming the tissues. Decay energies and half-lives of commonly used SPECT radioisotopes are listed in **Table 1.2**. Photons emitted by the decay of radioisotopes are detected by a gamma camera fitted with a collimator, to derive the directional information. The detector is rotated around the patient to collect images from different angles which are then used to build the 3-D images. The collimator consists of narrow, long holes that are made of lead or tungsten. In theory, optimal resolution can be obtained by using infinitely narrow holes. But in practice, since the holes cannot be infinitely

narrow, this limits the spatial resolution. Moreover, collimators only detect photons that travel at right angles to the detector leading to most photons being undetected and thus, limiting the sensitivity of SPECT images.[16]

Table 1.2: *List of Commonly used radioisotopes in SPECT imaging*

Radionuclide	Half-life (hours)	Principal photon emission energy (keV) (Intensity)
^{67}Ga	78.28	93 (39%), 185 (21%), 300 (16)
^{99m}Tc	6.01	140 (90%)
^{111}In	67.39	171 (90%)
^{123}I	13.22	159 (89%)

Longer half-lives of SPECT radioisotopes ranging from 6 hours to 3 days, allow sufficient time for the radiosynthesis, purification, administration as well as longer imaging time while the lower energy of gamma emission ensures low radiation dose to patients and technicians. Availability of onsite generators or cyclotrons and less expensive gamma cameras also make SPECT imaging less costly and more widely available for clinical use.

1.5 Technetium-99m

^{99m}Tc was first isolated in 1938 from the radioactive decay of ^{99}Mo (**Figure 1.4**). It has a radioactive half-life of 6.01 hours and emits gamma rays of 140 keV. Today it is commonly used as a radionuclide in SPECT imaging applications, due to its favourable nuclear properties and its easier availability from ^{99}Mo/^{99m}Tc generators as sodium pertechnate where it has an oxidation state of +7. It is then reduced to lower oxidation states of +1, +3 and +5 that are commonly seen in medical applications. A widely successful method of reducing ^{99m}Tc is by carbonylation to form *fac*-

$[^{99m}Tc(CO)_3(H_2O)_3]^+$. The labile H_2O is exploited to allow the chelation of bifunctional chelators that are tethered to biological targets.[17] *fac*-$[^{99m}Tc(CO)_3(H_2O)_3]^+$ can be conveniently synthesized in a single-step procedure using IsoLink formulations. These formulations contain a solution of sodium boranocarbonate, sodium tartarate, sodium borate and sodium carbonate, where the boranocarbonate acts as the carbonyl source.[18] This has ensured more accessibility and higher yields of ^{99m}Tc complexes. Absence of α and β radiation from ^{99m}Tc also allows for easier handling of radiotracers.

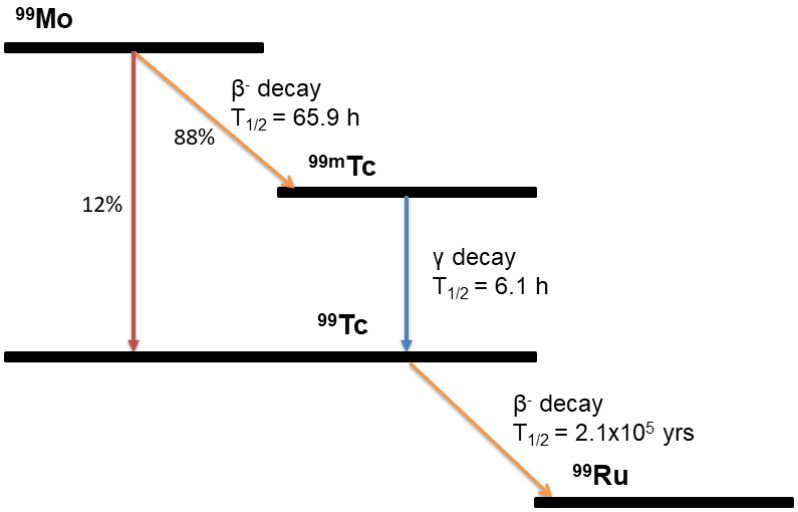

Figure 1.4: *Decay scheme of ^{99}Mo to ^{99}Ru*

1.6 Rhenium

Due to its radioactive nature, ^{99m}Tc causes practical limitations in studying the structural properties of its complexes. Alternatively, its non-radioactive heavier congener, rhenium, is used to characterize the complexes before radiolabelling with ^{99m}Tc. Naturally occurring rhenium exists as a mixture of the stable isotope ^{185}Re (37.4%) and the unstable isotope ^{187}Re (62.6%) with a very long half-life. Radioactive isotopes such as ^{186}Re and ^{188}Re have also been used as radiotherapeutics. Belonging to group 7 transition metals, technetium and rhenium have similar atomic radii due to lanthanide contraction leading to similar chemical reactivity, coordination geometries as well as similar biodistribution

profiles.[19] Moreover, rhenium complexes themselves have been gaining attention as photodynamic therapy agents, organic light-emitting diodes, sensors and in bioimaging applications.[20–23] Re(I) tricarbonyl complexes of nitrogen-containing ligands with low lying π* orbitals such as diimine ligands and dipicolylamine exhibit luminescent properties due to Metal to Ligand Charge Transfer (MLCT) excited states.[24] Their high photostability leads to reduced photobleaching while large Stoke's shift and long luminescence lifetimes allow the signal to be detected above the autofluorescence of the cells, making Re(I) tricarbonyl complexes ideal agents for cellular imaging. Examples of Re(I) tricarbonyl complexes with polypyridyl[25] and bis-quinoline[26] and dipicolylamine[27] ligands as cellular imaging agents are shown in

Figure *1.5*.

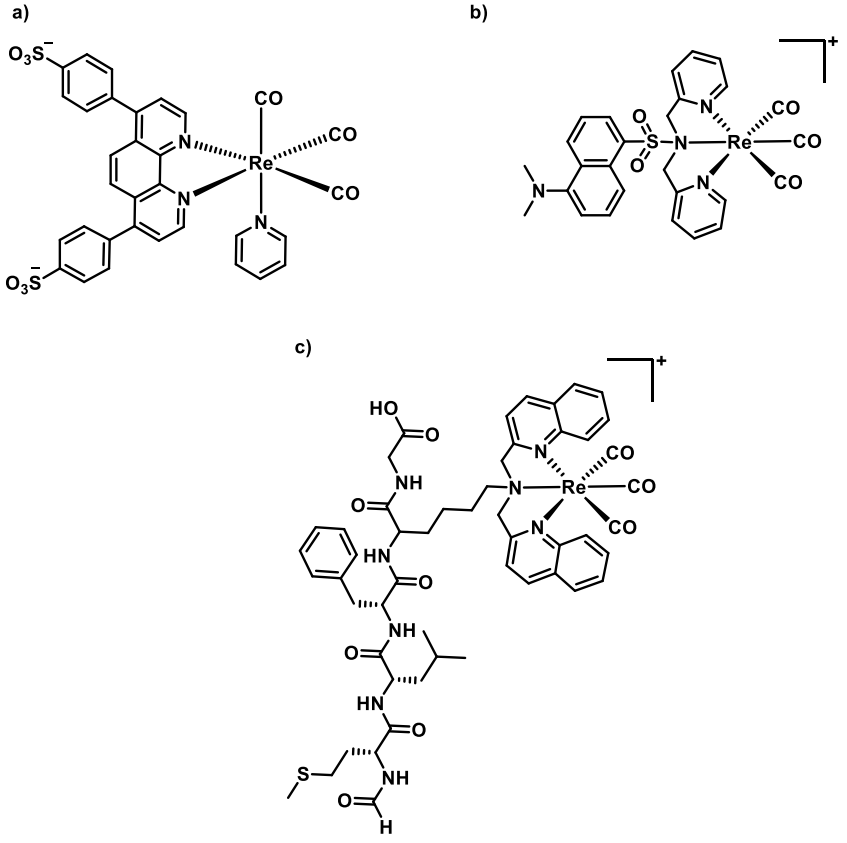

Figure 1.5: *Example of Re(I) tricarbonyl complexes as cellular imaging agents with* ***a)****polypyridyl,* ***b)*** *dipicolylamine and* ***c)*** *bis-quinoline ligands*

1.7 Optical Imaging

Optical imaging provides a non-invasive method of imaging the body using visible, ultraviolet or infrared light to form detailed images of the organs and tissues. It is an emerging domain in cell visualization and cancer diagnosis, relying on the evolution of modern optical systems, genomics, and proteomics. Optical imaging modalities show high sensitivity to probes and are low cost. However, their signal gets attenuated in deep tissues due to the low energy of photons. Thus, depth of penetration poses a major disadvantage of optical imaging.

Fluorescence is described as the emission of electromagnetic radiation when a molecule is irradiated by electromagnetic radiation of higher energy. Since the energy of emission is typically less than the energy absorbed, fluorescence emissions are red-shifted compared to excitations, giving rise to Stoke's shift. Thus fluorescent molecules with emissions in the visible light spectrum with large Stoke's shift are the most useful in molecular imaging. Optical fluorescence imaging is especially sought after for image-guided surgery[28] as well as *ex vivo* imaging. However, conventional fluorescence imaging probes that emit light in the visible spectra are not optimal for image-guided surgery due to the non-specific background signal associated with the visible spectrum of light.[29] Thus, imaging probes that utilize the red, far-red and near-infrared light have gained traction in the imaging of tissues and organs, especially in image-guided surgery.

Biological fluorophores and synthetic organic dyes and are the most used fluorescent materials for imaging. Biological fluorophores (e.g. green fluorescent protein) are introduced into cells or organs *via* the expression of plasmids. In addition to being a laborious process, it may lead to alteration of biological functions and cytotoxicity.[30] Synthetic organic dyes, in comparison, are smaller and can be easily linked to biomarkers

to monitor specific molecular processes. **Figure 1.6** shows examples of fluorescent organic dyes commonly used for cell imaging.

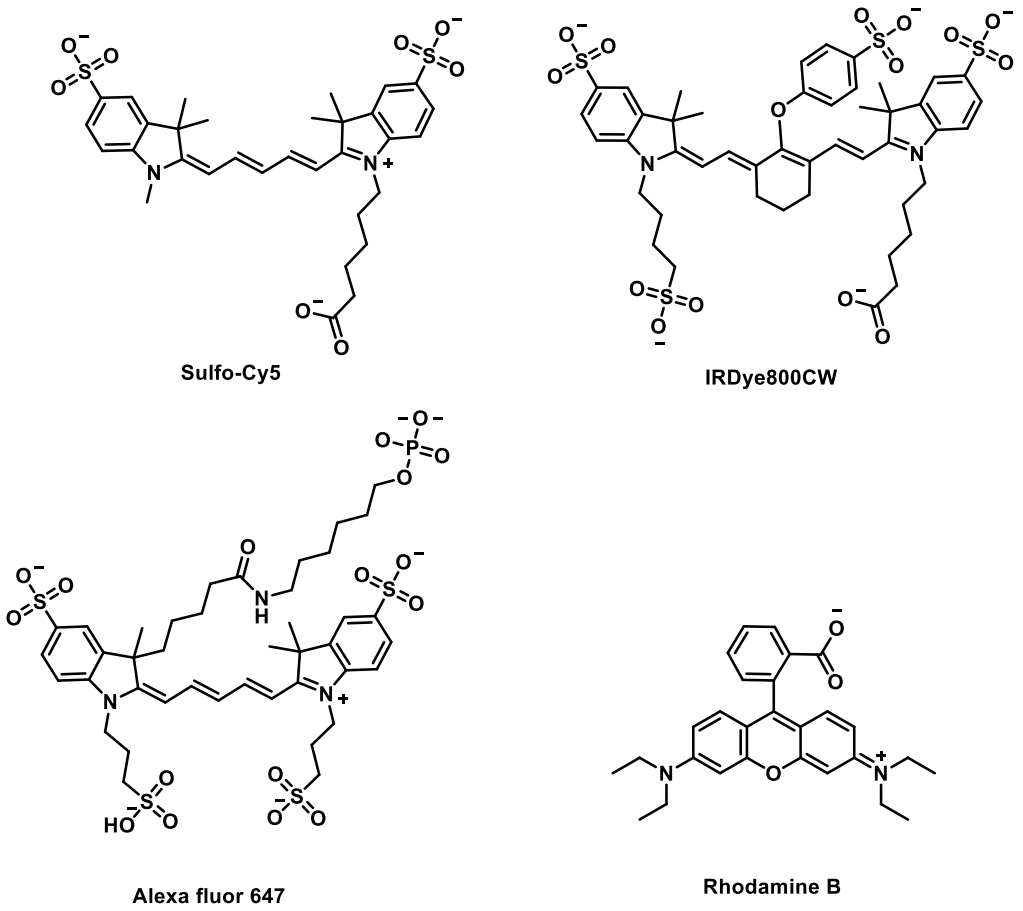

Figure 1.6: *Examples of fluorescent organic dyes used in cell imaging*

1.8 Derivatives of 1,8-Naphthalimide

1,8-Napthalimide is a fluorophore that emits in the visible region of the electromagnetic spectra. Owing to its high light and thermal stability, it has been used in the development of fluorescent chemo-sensors, molecular imaging, analytical chemistry as well as in material chemistry.[31–34] Possibility of electron transfer within donor-acceptor systems has been commonly exploited in the design of novel fluorescent materials. On excitation,

electrons can jump from a donor to an acceptor while the inclusion of small spacers/bridges can lead to faster transfer rates.[35] **Figure 1.7** represents a generic derivative of 1,8-naphthalimide that constitutes a donor-π-acceptor system with an electron-donating group on the naphthalene ring acting as the donor, naphthalene ring as the π bridge and the imide part acting as the acceptor.[36] Thus chemical modifications on the naphthalene ring or the imide-N have been explored for the design of various fluorescent tags.[37,38] Especially, amine group substitutions at 4 and 5 positions have been extensively studied for their effect on the fluorescence wavelength.[39,40] In addition, quantum yields of 1,8-naphthalimide based fluorescent tags exhibit solvatochromism because polarity of solvents affect the efficiency of intersystem crossing between the excited states.[41]

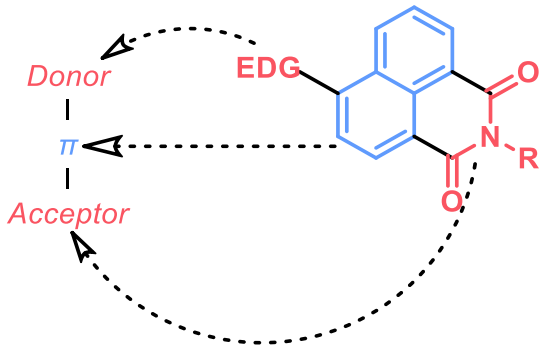

Figure 1.7: *Naphthalimide derivatives as donor-π-acceptor systems*

1.9 Scope of the Thesis

The purpose of this thesis is to design and evaluate potential dual imaging probes for use in SPECT and optical fluorescence imaging. 1,8-Naphthalimide based rhenium complexes have been reported to be useful as fluorescence imaging agents in cells. Since the emissive properties of these complexes remain unaffected by substituents on the imide-nitrogen, it serves as an ideal site for attachment of a targeting moiety.[42] Using a CXCR4 targeting peptide, T140, these complexes have been used as targeted fluorescence imaging agents while their ^{99m}Tc analogues show potential as SPECT

tracers.[43] Thus, this report aims to explore the effect of substituents on 1,8-naphthalimide based imaging agents.

The primary objective, discussed in Chapter 2, is the synthesis and spectroscopic characterization of 1,8-naphthalimide based ligands with different substituents at position 4, which has been shown to have the most effect on its electronic properties.[44] Their corresponding rhenium complexes were also synthesized and characterized. The photophysical properties of these ligands and rhenium complexes are analyzed on basis of their structural properties. Results from this study would aid in the development of potential dual-imaging probes for use in fluorescence and SPECT imaging modalities.

1.10 References

(1) Massoud, T. F.; Gambhir, S. S. *Genes Dev.* **2003**, *17* (5), 545.

(2) Liu, S.; Edwards, D. S. *Bioconjug. Chem.* **2001**, *12* (1), 7.

(3) Haubner, R.; Wester, H. J.; Weber, W. A.; Mang, C.; Ziegler, S. I.; Goodman, S. L.; Senekowitsch-Schmidtke, R.; Kessler, H.; Schwaiger, M. *Cancer Res.* **2001**, *61* (5), 1781.

(4) Chen, X. *Mini Rev. Med. Chem.* **2006**, *6* (2), 227.

(5) Wallyn, J.; Anton, N.; Akram, S.; Vandamme, T. F. *Pharm. Res.* **2019**, *36* (6), 78.

(6) Hutton, B. F.; Braun, M. *Semin. Nucl. Med.* **2003**, *33* (3), 180.

(7) Hasegawa, B. H.; Gingold, E. L.; Reilly, S. M.; Liew, S.-C.; Cann, C. E. In *Proc.SPIE*; 1990; Vol. 1231.

(8) Lee, S.; Chen, X. *Mol. Imaging* **2009**, *8* (2), 7290.2009.00013.

(9) Tipirneni, K. E.; Rosenthal, E. L.; Moore, L. S.; Haskins, A. D.; Udayakumar, N.; Jani, A. H.; Carroll, W. R.; Morlandt, A. B.; Bogyo, M.; Rao, J.; Warram, J. M. *Mol. Imaging Biol.* **2017**, *19* (5), 645.

(10) Banerjee, S. R.; Pullambhatla, M.; Byun, Y.; Nimmagadda, S.; Foss, C. A.; Green, G.; Fox, J. J.; Lupold, S. E.; Mease, R. C.; Pomper, M. G. *Angew. Chemie Int. Ed.* **2011**, *50* (39), 9167.

(11) Rijpkema, M.; Oyen, W. J.; Bos, D.; Franssen, G. M.; Goldenberg, D. M.; Boerman, O. C. *J. Nucl. Med.* **2014**, *55* (9), 1519 LP.

(12) Liu, C.; Zhang, X.; Song, Y.; Wang, Y.; Zhang, F.; Zhang, Y.; Zhang, Y.; Lan, X. *Atherosclerosis* **2016**, *254*, 263.

(13) Feng, G.-K.; Liu, R.-B.; Zhang, M.-Q.; Ye, X.-X.; Zhong, Q.; Xia, Y.-F.; Li, M.-Z.; Wang, J.; Song, E.-W.; Zhang, X.; Wu, Z.-Z.; Zeng, M.-S. *J. Control. Release* **2014**, *192*, 236.

(14) Welling, M. M.; Bunschoten, A.; Kuil, J.; Nelissen, R. G. H. H.; Beekman, F. J.; Buckle, T.; van Leeuwen, F. W. B. *Bioconjug. Chem.* **2015**, *26* (5), 839.

(15) Hekman, M. C. H.; Rijpkema, M.; Bos, D. L.; Oosterwijk, E.; Goldenberg, D. M.; Mulders, P. F. A.; Boerman, O. C. *J. Nucl. Med.* **2017**, *58* (5), 706.

(16) Hutton, B. F. Grupen, C., Buvat, I., Eds.; Springer Berlin Heidelberg: Berlin, Heidelberg, 2012; pp 917–933.

(17) Bilton, H. A.; Ahmad, Z.; Janzen, N.; Czorny, S.; Valliant, J. F. *J. Vis. Exp.* **2017**, No. 120, 55188.

(18) Alberto, R.; Ortner, K.; Wheatley, N.; Schibli, R.; Schubiger, A. P. *J. Am. Chem. Soc.* **2001**, *123* (13), 3135.

(19) Papagiannopoulou, D. *J. Label. Compd. Radiopharm.* **2017**, *60* (11), 502.

(20) Liew, H. S.; Mai, C.-W.; Zulkefeli, M.; Madheswaran, T.; Kiew, L. V; Delsuc, N.; Low, M. L. *Molecules* . 2020,.

(21) Zhao, G.-W.; Zhao, J.-H.; Hu, Y.-X.; Zhang, D.-Y.; Li, X. *Synth. Met.* **2016**, *212*, 131.

(22) Liu, Z.; He, W.; Guo, Z. *Chem. Soc. Rev.* **2013**, *42* (4), 1568.

(23) Raszeja, L. J.; Siegmund, D.; Cordes, A. L.; Güldenhaupt, J.; Gerwert, K.; Hahn, S.; Metzler-Nolte, N. *Chem. Commun.* **2017**, *53* (5), 905.

(24) Balasingham, R. G.; Coogan, M. P.; Thorp-Greenwood, F. L. *Dalt. Trans.* **2011**, *40* (44), 11663.

(25) Fernández-Moreira, V.; Thorp-Greenwood, F. L.; Amoroso, A. J.; Cable, J.; Court, J. B.; Gray, V.; Hayes, A. J.; Jenkins, R. L.; Kariuki, B. M.; Lloyd, D.; Millet, C. O.; Williams, C. F.; Coogan, M. P. *Org. Biomol. Chem.* **2010**, *8* (17), 3888.

(26) Stephenson, K. A.; Banerjee, S. R.; Besanger, T.; Sogbein, O. O.; Levadala, M. K.; McFarlane, N.; Lemon, J. A.; Boreham, D. R.; Maresca, K. P.; Brennan, J. D.; Babich, J. W.; Zubieta, J.; Valliant, J. F. *J. Am. Chem. Soc.* **2004**, *126* (28), 8598.

(27) Darshani, T.; Thushara, N.; Weerasuriya, P.; Fronczek, F. R.; Perera, I. C.; Perera, T. *Polyhedron* **2020**, *185*, 114592.

(28) Bu, L.; Shen, B.; Cheng, Z. *Adv. Drug Deliv. Rev.* **2014**, *76*, 21.

(29) Richards-Kortum, R.; Sevick-Muraca, E. *Annu. Rev. Phys. Chem.* **1996**, *47* (1), 555.

(30) Liu, H. S.; Jan, M. S.; Chou, C. K.; Chen, P. H.; Ke, N. J. *Biochem. Biophys. Res. Commun.* **1999**, *260* (3), 712.

(31) Dai, F.; Jin, F.; Long, Y.; Jin, X.-L.; Zhou, B. *Free Radic. Res.* **2018**, *52* (11–12), 1288.

(32) Ge, S.; Li, B.; Meng, X.; Yan, H.; Yang, M.; Dong, B.; Lu, Y. *Dye. Pigment.* **2018**, *148*, 147.

(33) Bao, X.; Wu, X.; Berry, S. N.; Howe, E. N. W.; Chang, Y.-T.; Gale, P. A. *Chem. Commun.* **2018**, *54* (11), 1363.

(34) Liu, J.; Tu, G.; Zhou, Q.; Cheng, Y.; Geng, Y.; Wang, L.; Ma, D.; Jing, X.; Wang, F. *J. Mater. Chem.* **2006**, *16* (15), 1431.

(35) Daly, B.; Ling, J.; de Silva, A. P. *Chem. Soc. Rev.* **2015**, *44* (13), 4203.

(36) Szakács, Z.; Rousseva, S.; Bojtár, M.; Hessz, D.; Bitter, I.; Kállay, M.; Hilbers, M.; Zhang, H.; Kubinyi, M. *Phys. Chem. Chem. Phys.* **2018**, *20* (15), 10155.

(37) Bojinov, V.; Konstantinova, T. *Dye. Pigment.* **2002**, *54* (3), 239.

(38) Tian, Y.; Su, F.; Weber, W.; Nandakumar, V.; Shumway, B. R.; Jin, Y.; Zhou, X.; Holl, M. R.; Johnson, R. H.; Meldrum, D. R. *Biomaterials* **2010**, *31* (29), 7411.

(39) Poteau, X.; Brown, A. I.; Brown, R. G.; Holmes, C.; Matthew, D. *Dye. Pigment.* **2000**, *47* (1), 91.

(40) Banerjee, S.; Veale, E. B.; Phelan, C. M.; Murphy, S. A.; Tocci, G. M.; Gillespie, L. J.; Frimannsson, D. O.; Kelly, J. M.; Gunnlaugsson, T. *Chem. Soc. Rev.* **2013**, *42* (4), 1601.

(41) Wintgens, V.; Valat, P.; Kossanyi, J.; Biczok, L.; Demeter, A.; Bérces, T. *J. Chem. Soc. Faraday Trans.* **1994**, *90* (3), 411.

(42) Langdon-Jones, E. E.; Symonds, N. O.; Yates, S. E.; Hayes, A. J.; Lloyd, D.; Williams, R.; Coles, S. J.; Horton, P. N.; Pope, S. J. A. *Inorg. Chem.* **2014**, *53* (7), 3788.

(43) Turnbull, W. L.; Yu, L.; Murrell, E.; Milne, M.; Charron, C. L.; Luyt, L. G. *Org. Biomol. Chem.* **2019**, *17* (3), 598.

(44) Ali, H. D. P.; Kruger, P. E.; Gunnlaugsson, T. *New J. Chem.* **2008**, *32* (7), 1153.

Chapter 2 : Synthesis and Characterization of Re(I) Tricarbonyl Complexes of 1,8-Naphthalimide Derivatives

2.1 Introduction

All bioimaging modalities have their specific advantages and disadvantages. No single modality can provide comprehensive information about a disease. This drives the need for multimodality imaging where more than one modality is used to image the diseased organ/tissue. Recent advances in technology have resulted in bringing together imaging modalities like Positron Emission Tomography (PET) and Computed Tomography (CT) onto a single platform. On a platform like PET/CT, the patient receives both PET and CT scans simultaneously. Images from both scans are then fused using computer software which often provides additional information than what would be available from a single imaging modality. Depending on the type of imaging modalities used, combining information from different imaging modalities often provides additional or complementary information, which is helpful in cross-validation. From a clinical perspective, this would allow more precise diagnosis leading to better disease monitoring and treatment plans.

Each imaging modality makes use of a unique imaging probe that helps enhances the signal or contrast of the image. Due to the different ways each probe interacts within the body, introduction of different probes can lead to increased toxicity or sub-par image results. Thus, development of multimodal imaging platforms also warrants the need for multimodal imaging probes which are capable of signal production in more than one imaging technique. Based on the structure of imaging probes, designing of multimodality probe would require incorporation of a different imaging entity for each modality.[1,2] For example, a dual-modality probe that can be used in nuclear imaging and optical

fluorescence imaging would require a radioactive entity capable of emitting gamma rays and a fluorophore that provides detectable fluorescence emission.

Single Photon-Emission Computed Tomography (SPECT) is a type of nuclear imaging technique that is used to study the distribution of radiolabelled tracers within the body. Although clinically used SPECT scanners have lower spatial resolution, they provide similar sensitivity while being less expensive and more widely available than other nuclear imaging techniques like PET. SPECT utilizes radioactive metals such as ^{67}Ga, ^{99m}Tc, ^{111}In, and ^{123}I, which emit single gamma rays. Among these radionuclides, ^{99m}Tc is more commonly used, due to its favourable nuclear properties and its easier availability from ^{99}Mo/^{99m}Tc generators.[3] However, due to the lack of stable isotopes, its third-row congener, rhenium is often used as a surrogate to study the fundamental inorganic chemistry of technetium complexes. Moreover, rhenium complexes themselves have been gaining attention as photodynamic therapy agents, organic light-emitting diodes, sensors and in bioimaging applications.[4–7] Re(I) tricarbonyl complexes of nitrogen-containing ligands with low lying π^* orbitals such as diimine ligands and dipicolylamine exhibit luminescent properties due to Metal to Ligand Charge Transfer (MLCT) excited states.[8] Their low toxicity and cell uptake capabilities have resulted in the complexes being studied as biological and cell imaging probes.[9]

As opposed to nuclear imaging techniques, optical fluorescence imaging utilizes non-ionizing radiation in the visible or near-infrared wavelengths and suitable fluorophores, to form images of the tissues/organs. It is a non-invasive imaging method capable of producing images with higher spatial resolution. In addition to being useful in microscopic studies of cells and tissues, it is also sought after for image-guided surgery[10] as well as *ex vivo* imaging.

Combining SPECT and optical fluorescence imaging, due to their high detection sensitivity, facilitate cross-validation of information. A clinical translation of dual-SPECT/optical fluorescence imaging technology would allow whole-body imaging

through SPECT to guide surgical resection of tumours or in optical biopsy using endoscopes.[11] Pre- and intra-operative utility of SPECT/fluorescence imaging probes has been demonstrated for mapping lymph nodes in nude mice.[12,13] However, with currently available devices, simultaneous imaging using both modalities is not feasible. Hence, dual-modality SPECT/fluorescence imaging probes can be used sequentially to provide high sensitivity images for localization of tracers using SPECT followed by fluorescence imaging for cross-validation of disease localization or in image-guided surgery.[14]

1,8-Napthalimide is a fluorophore that emits in the visible region of electromagnetic spectra. Owing to its high light and thermal stability, it has been used in the development of fluorescent chemosensors, molecular imaging, analytical chemistry as well as in material chemistry.[15–18] Derivatives of 1,8-naphthalimide constitute a donor-π-acceptor system which can lead to an Intramolecular Charge Transfer (ICT) process.[19] Thus, chemical modifications on the naphthalene ring or the imide-nitrogen have been explored for their effect on ICT excited states, which permits them to be customized as the fluorescent tags for various imaging applications.[20,21] Especially, amine group substitutions at 4 and 5 positions have been extensively studied for their effect on the fluorescence wavelength.[22,23]

Langdon-Jones et al. reported Re(I) tricarbonyl complexes of fluorescent 1,8 naphthalimide ligands (**Figure 2.1a**) to be useful in conventional fluorescence microscopy applications.[24] The authors observed that the fluorescence emission of these ligands and complexes was largely insensitive to the different substitutions at the imide-nitrogen. This aspect was utilized by Turnbull et al. to synthesize a 1,8-naphthalimide derivative appended with a CXCR4 targeting peptide - T140, at the imide-nitrogen.[25] Rhenium(I) tricarbonyl complex of this ligand (**Figure 2.1b**) was used in confocal microscopy imaging, which showed potential in differentiating between healthy, benign, and malignant prostate cancer cells. Further, radiolabelling with ^{99m}Tc and subsequent

bio-distribution studies in murine xenografts established their potential use as SPECT/fluorescence imaging tracer.

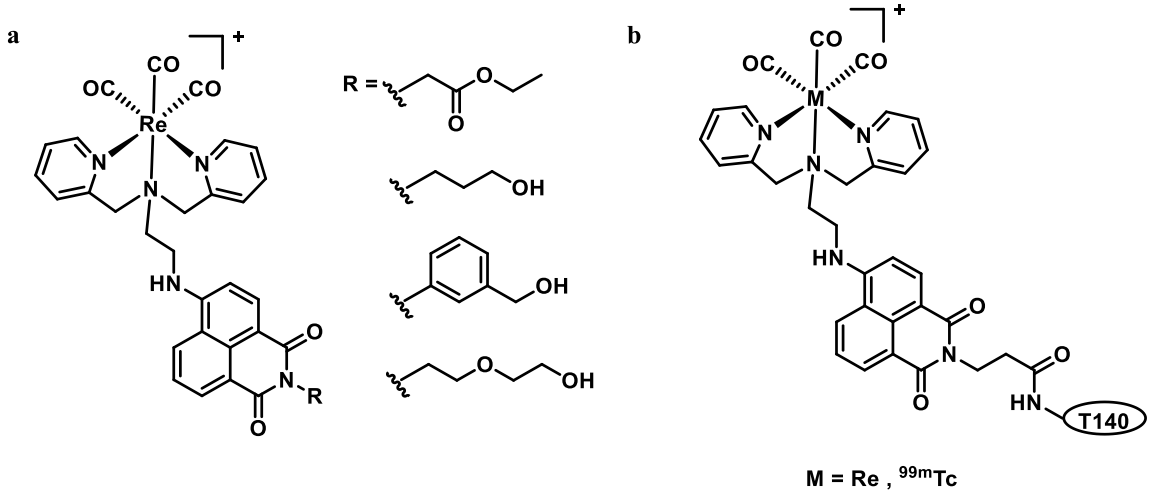

***Figure 2.1: a**)Re(I) tricarbonyl complexes of 1,8-naphthalimide derivatives for cell imaging.* ***b**) Structure of dual-modality T140 analogue for CXCR4 expression*

Here, we define 'linker' as the substitution at the 4th position of 1,8-naphthalimide, which connects to the chelator. In their work, Day et al. employed linkers of various lengths to explore the effect of lipophilicity and their use as imaging agents[26] (**Figure 2.2**). Lipophilicity plays important role in cell permeability, localization of imaging probes in cells as well as its excretion pathway. Their results indicated that photophysical properties were insensitive to the length of the linker. However, *in vivo* assessment of the radiolabelled tracer indicated that increasing lipophilicity leads to increased cellular uptake and rapid clearance of the tracer from the body.

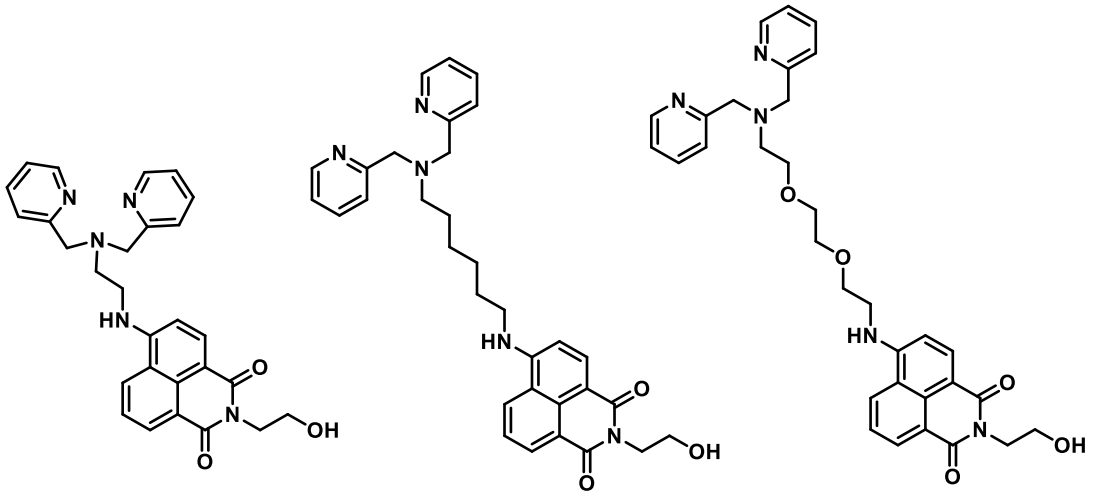

Figure 2.2: *1,8-Naphthalimide derivatives with variable linker lengths for potential SPECT/fluorescence imaging*

Re(I) tricarbonyl complexes with 2,2'-dipicolylamine (DPA) has an overall positive charge. Additionally, neutral and negatively charged complexes were also synthesized by introducing N-(2-pyridylmethyl)glycinate and iminoacetate respectively, as chelators[27] (**Figure 2.3**). The photophysical properties were largely unaffected by the charge on the complexes. However, the positively charged complex was observed to have better cell permeability than the neutral and negatively charged complexes.

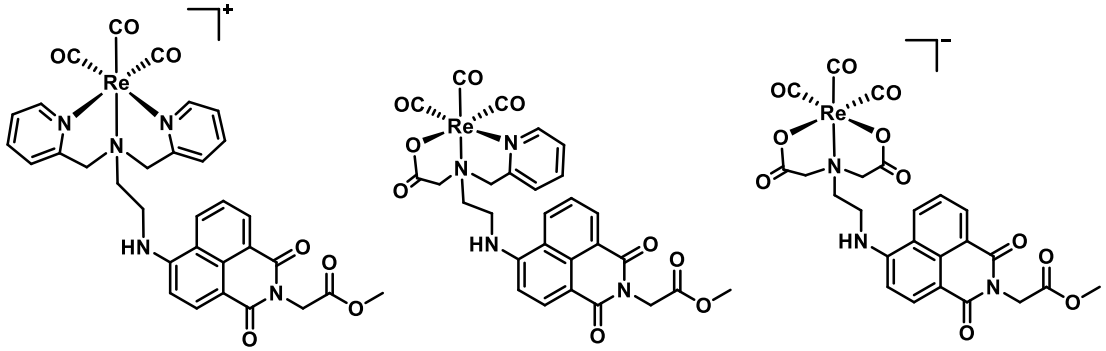

Figure 2.3: *Positively, neutral and negatively charged Re(I) complexes of 1,8-naphthalimide derivatives*

In this work, we introduce planar rigid linkers to increase the conjugation of the naphthalimide moiety. Increased conjugation leads to strong π-π interactions which will

alter the fluorescence emission wavelength of the 1,8-naphthalimide derivatives.[28] Derivatives lacking extended π-conjugation are also synthesized by incorporating a cyclic amine as well as without the use of a linker moiety. DPA chelator is used to aid the formation of Re(I) carbonyl complexes, due to its positive effects on cell permeability. Photophysical properties of ligands and their corresponding rhenium complexes will be analyzed to corroborate their effect on fluorescence wavelength. Results from this report will aid in better design of fluorophores for SPECT/fluorescence imaging probes, whose clinical translation will lead to improved diagnosis and treatment of various diseases including cancer.

2.2 Results and Discussion

2.2.1 Design of 1,8-Naphthalimide Derivatives

Incorporation of rigid linkers decreases the energy lost due to rotational and vibrational motions, leading to large Stoke's shift.[29] Extension of π-conjugation decreases the HOMO-LUMO gap resulting in absorption and emission of longer wavelengths.[30,31] Thus, extended π-conjugation in naphthalimide derivatives is expected to cause a bathochromic shift in fluorescence emission. However, electron-donating capacity of the substituents is also known to take precedence over the resonance effects.[32] Therefore, four derivatives (**L_1-L_4**) were designed by incorporating cyclic groups as linkers between 1,8-naphthalimide and the DPA chelator. These groups were chosen to have varying effects of electron-donation and extended π-conjugation. A derivative with an ethylene linker (**L_5**) was also proposed to discern the effect of conjugation and flexibility of the linkers on their photophysical properties. Additionally, to compare the effects of electron donation without resonance effects, a ligand was designed to directly link DPA chelator to the 4th position of 1,8-naphthalimide without the use of a linker (**L_6**). Structures of these derivatives are shown in **Figure 2.4**.

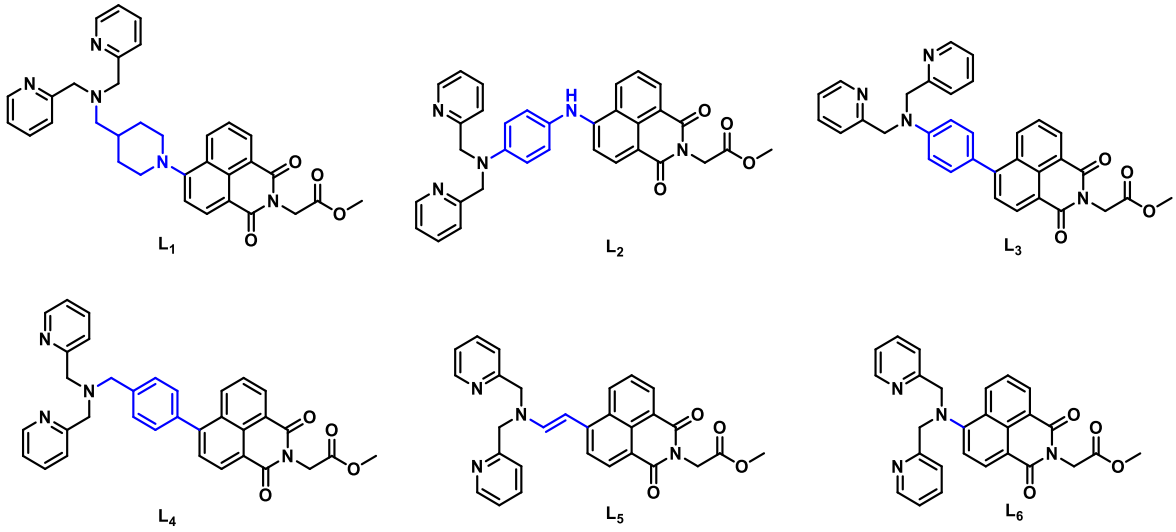

Figure 2.4: *Structures of 1,8-naphthalimide derivatives to study the effect of rigid linkers*

2.2.2 Optimization and synthesis of ligands

The naphthalimide precursor **1,** previously reported by *Turnbull et.al*., was synthesized using the same procedure.[27] Compound **2** was synthesized in 91% by the reaction of **1** with *N*-boc-4-(aminomethyl)piperidine. Removal of Boc protecting group was achieved by treatment with TFA to yield **3**, which underwent reductive amination with 2-pyridinecarboxaldehyde to form **L_1** in 68% yield. Scheme for synthesis of **L_1** is shown in **Scheme 2.1**.

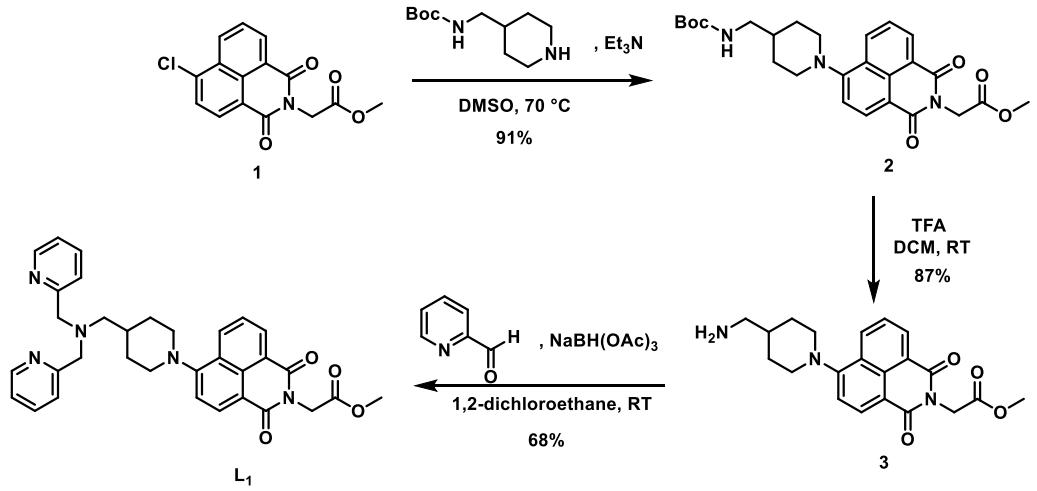

Scheme 2.1: Synthesis of **L_1** using **1**

Synthesis of **L2** was attempted in a similar fashion using *N*-boc-*p*-phenylenediamine (**Scheme 2.2a**). Due to insufficient yield of **4**, even with elevated temperature and extended reaction time, an alternative synthetic route shown in **Scheme 2.2b** was utilized. Low nucleophilicity of the aniline derivative compared to alkylamines, led to the failure of its reaction with 2-(chloromethyl)pyridine hydrochloride to form **5**. Reductive amination using 2-pyridinecarboxaldehyde favoured the production of **5** followed by Boc-deprotection produced **6,** which then reacted with **1** to give **L2**. Several attempts to purify **L2** using silica column chromatography were unsuccessful due to the co-elution of unreacted **1**. Although precipitation using hexane-ethanol mixture was useful in removing a small amount of **1**, pure **L2** was not obtained. Use of a more reactive precursor was implied to reduce the amount of unreacted material, as discussed later in this section.

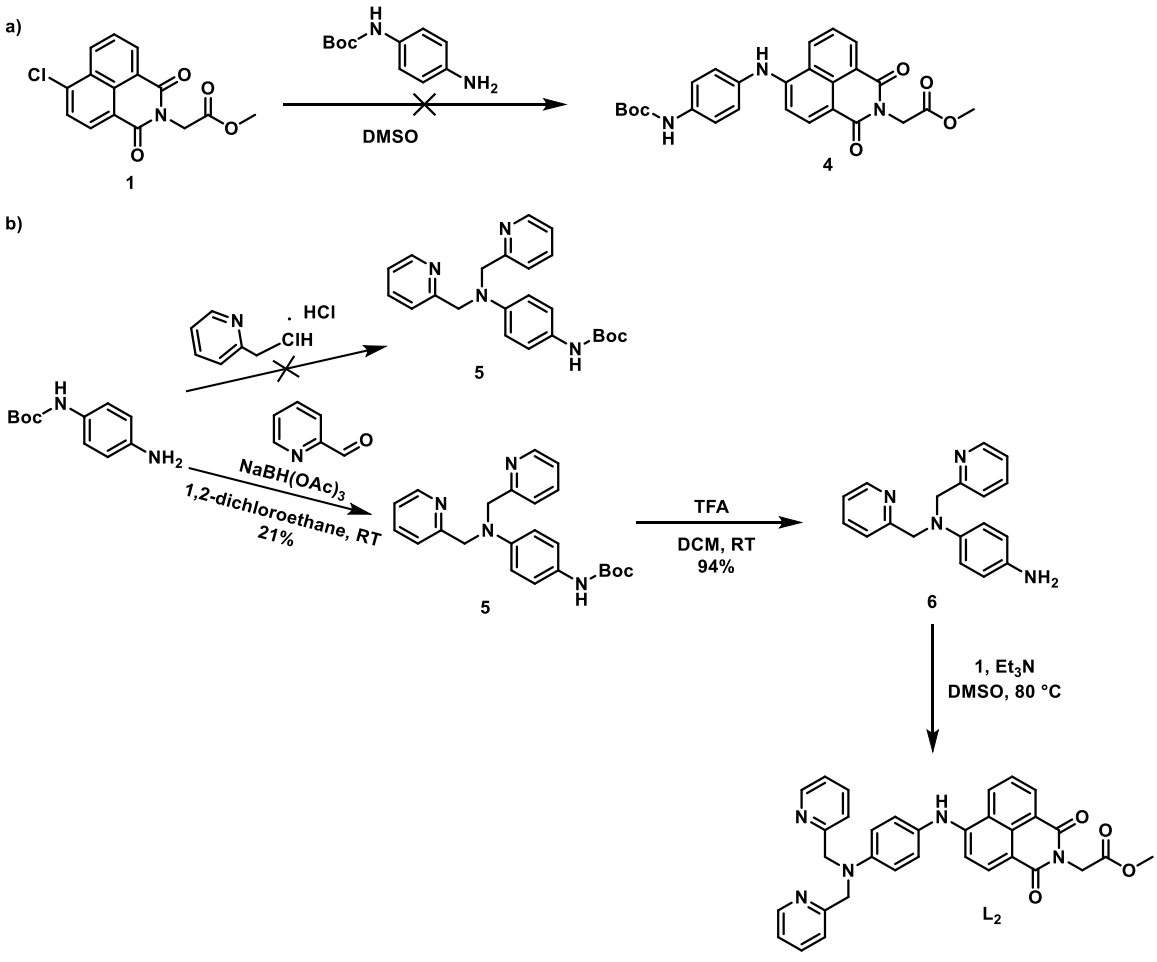

Scheme 2.2: *Attempts in synthesis of* ***L2*** *using* ***1***

Scheme 2.3. outlines the attempts made to synthesize **L3**. **7** was formed by the coupling of **1** with 4-fluorophenylboronic acid under Suzuki coupling conditions. Linking of DPA with **7** was proposed for the synthesis of **L3**. However, subsequent failure of several attempts to achieve this, prompted the use of a different synthetic route using 4-nitrophenylboronic acid to form **8.** However, pure **7** or **8** were not isolated due to co-elution of **1** during silica column chromatography. Longer reaction time to decrease the amount of unreacted **1** was also found to be unhelpful in isolating pure products. Although further reactions with the impure product were attempted, increased amount of side products led to difficult separations and very low yields.

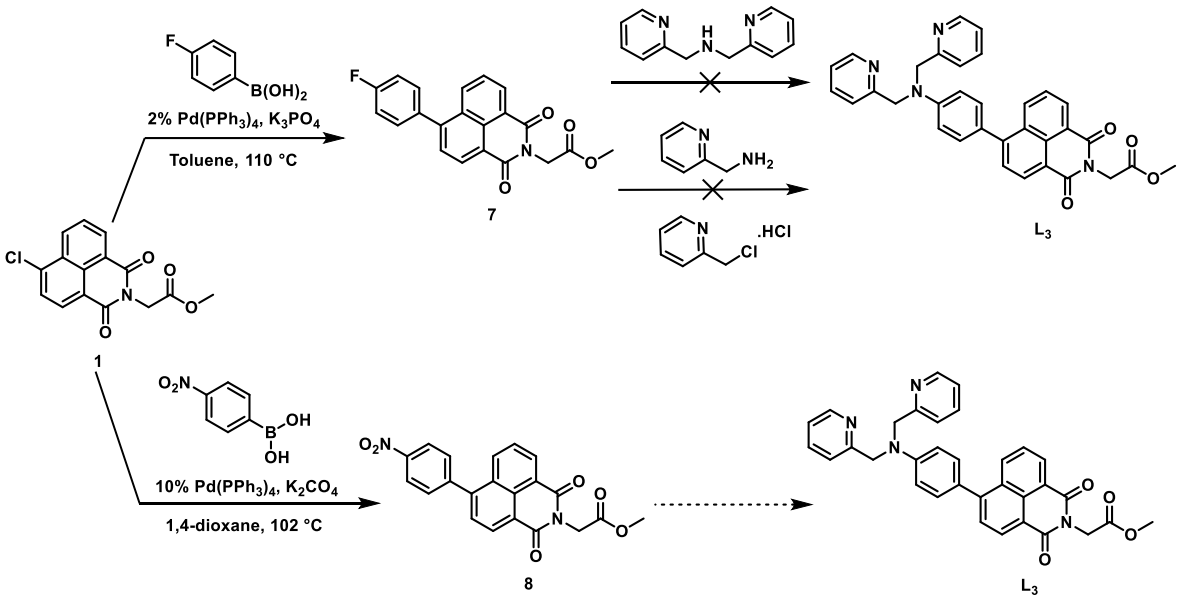

Scheme 2.3: *Pathways for synthesis of* ***L3*** *using 4-fluorophenylboronic acid and 4-nitrophenylboronic acid*

A similar synthetic route was used for the synthesis of **L4** using 4-bromomethyl phenylboronic acid (**Scheme 2.4**). **9** was successfully synthesized however, a sufficiently pure product that could be used to synthesize **L4**, could not be isolated.

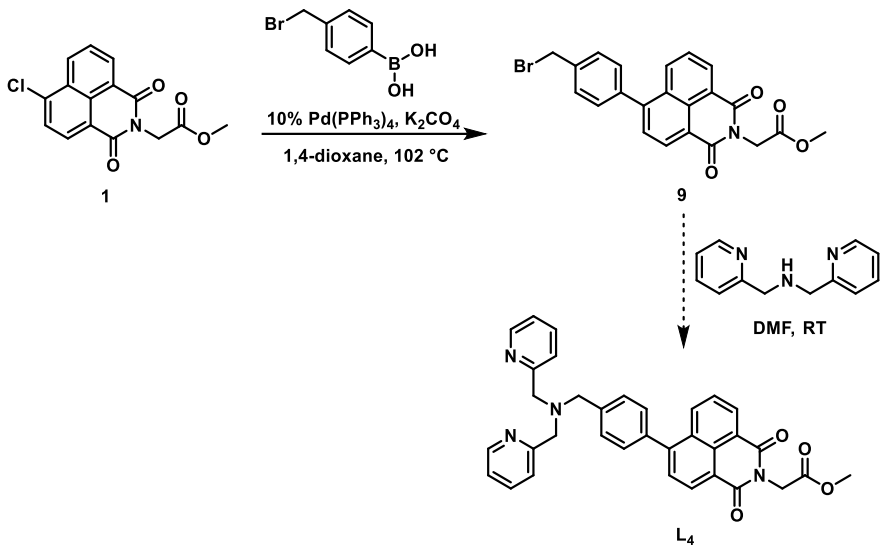

Scheme 2.4: *Synthesis of* ***L4*** *using* ***1***

Sonogashira coupling using trimethylsilyl acetylene was utilized for the synthesis of **10** followed by removal of trimethylsilyl group using tetrabutylammonium fluoride (TBAF) to give **11** (**Scheme 2.5**)**.** The method previously reported by McAdam et al. was used for the synthesis.[31] Even though adequate purity of **11** was not achieved, attempts were made in synthesizing $\mathbf{L_5}$. Due to several side products, the reaction mixture was analyzed by mass spectroscopy, for the presence of the desired product. However, the mass associated with $\mathbf{L_5}$ was not observed.

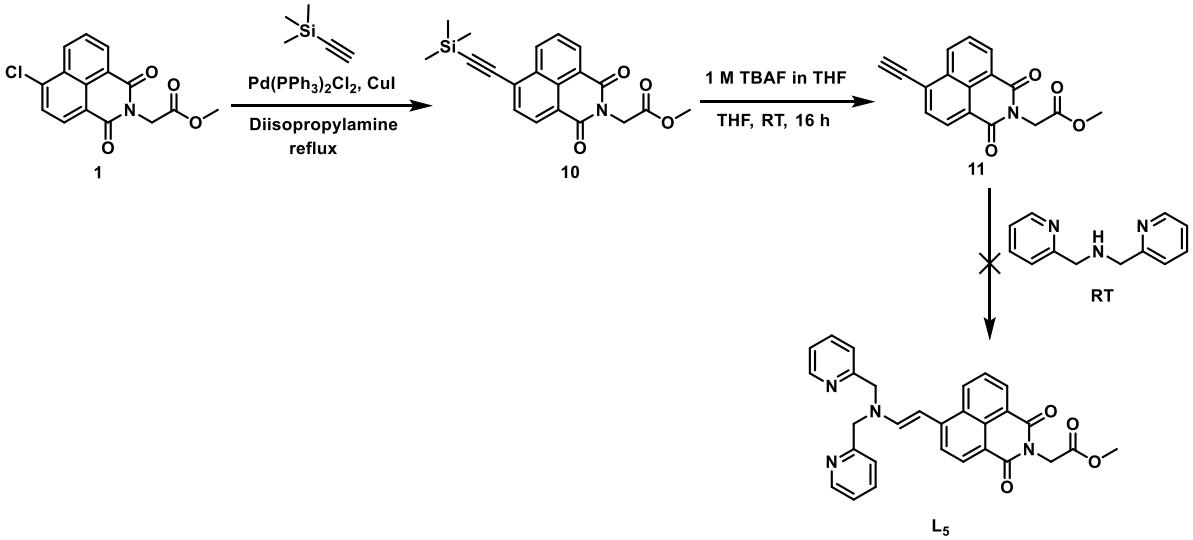

Scheme 2.5: *Scheme for synthesis of* ***L5*** *using* ***1***

Synthesis of **L_6** was initially adapted from the report by Zhang et al. by using a solution of **1** in diethyleneglycol diethylether.[33] Another attempt was made without the use of a solvent at elevated temperature, as shown in **Scheme 2.6**. Both attempts failed to yield the desired ligand in sufficient amounts.

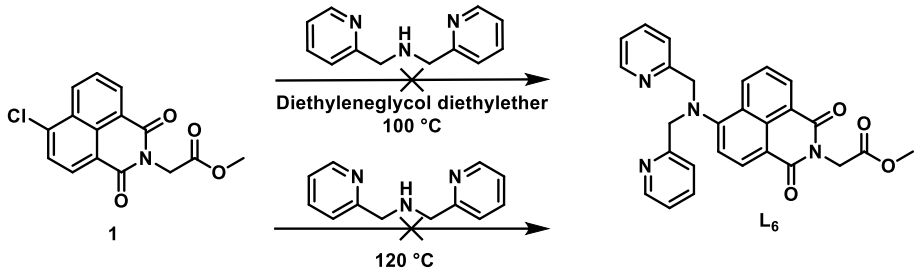

Scheme 2.6: *Attempts in synthesizing* ***L_6*** *using* ***1***

Although **L_1** was successfully synthesized, failure or lower yields of subsequent ligands hinted at the lesser reactivity of precursor **1**. Hence, precursor **12** was synthesized using 4-bromo-1,8-naphthalic anhydride, using the same method as **1** in 75% yield. **L_2** was then synthesized by reaction of compound **6** with **12** (**Scheme 2.7**). The product was isolated in 51% yield.

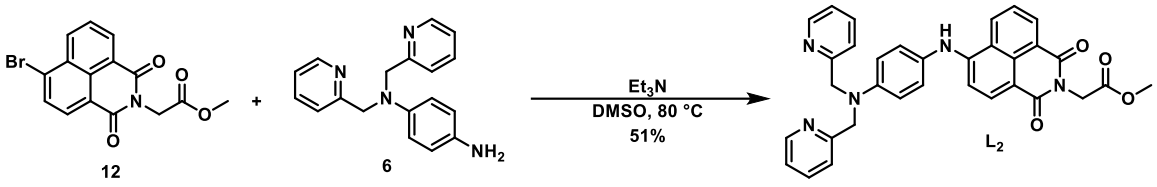

Scheme 2.7: *Synthesis of* ***L_2*** *using* ***12***

Precursors for ligands **L_3-L_5** as well as ligand **L_6** were then synthesized by using **12** as shown in **Scheme 2.8**. Increased reactivity of the bromo-precursor relative to the chloro-precursor, resulted in reduced amount of unreacted **12** as well as facile purification of the products.

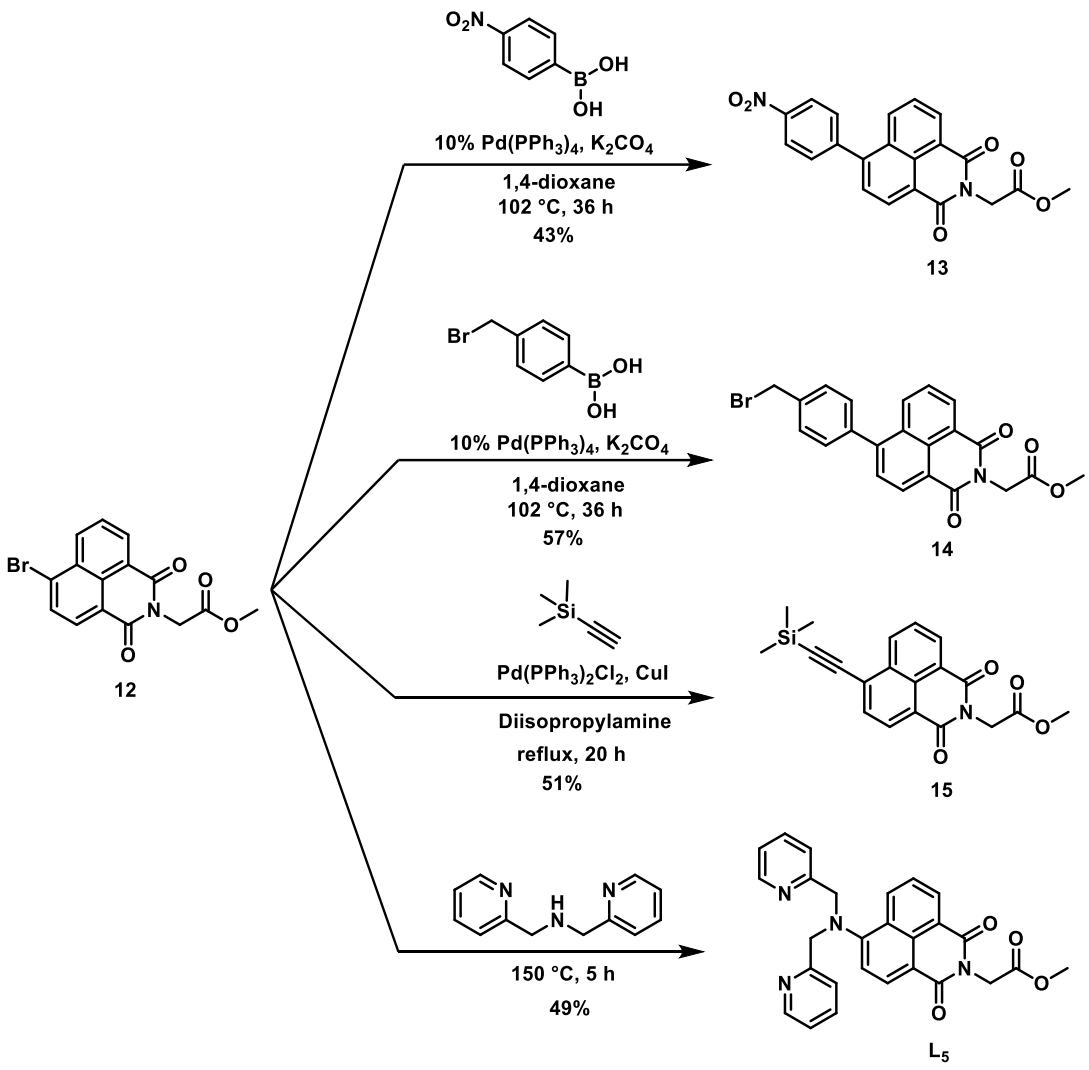

Scheme 2.8: *Synthesis of precursors for* ***L3-L5*** *and* ***L6*** *using* ***12***

To synthesize **L3**, **13** was reduced using Tin(II) chloride dihydrate and HCl followed by reaction with 2-pyridinecarboxaldehyde, yielding 65% product. **L4** was synthesized from **14** by the reaction with 2,2'-dipicolylamine, in 65% yield. Successful synthetic routes to **L3** and **L4** are shown in **Scheme 2.9**.

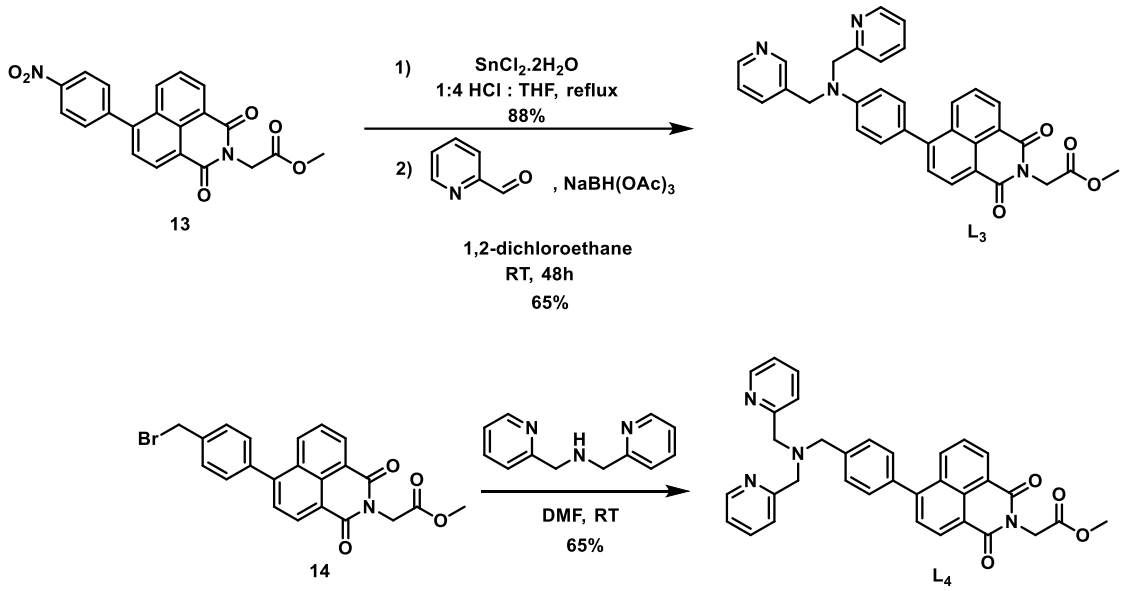

Scheme 2.9: *Synthesis of* ***L₃*** *and* ***L₄***

Attempts were made at the synthesis of $\mathbf{L_5}$ with purified **15** (**Scheme 2.10**). However, none of the reactions yielded the desired product. Although hydroamination reaction proceeds with the help of metal-based catalysts, such reactions were not attempted since the DPA chelator in the product, is known to form complexes with other metals including palladium and platinum.[34–36]

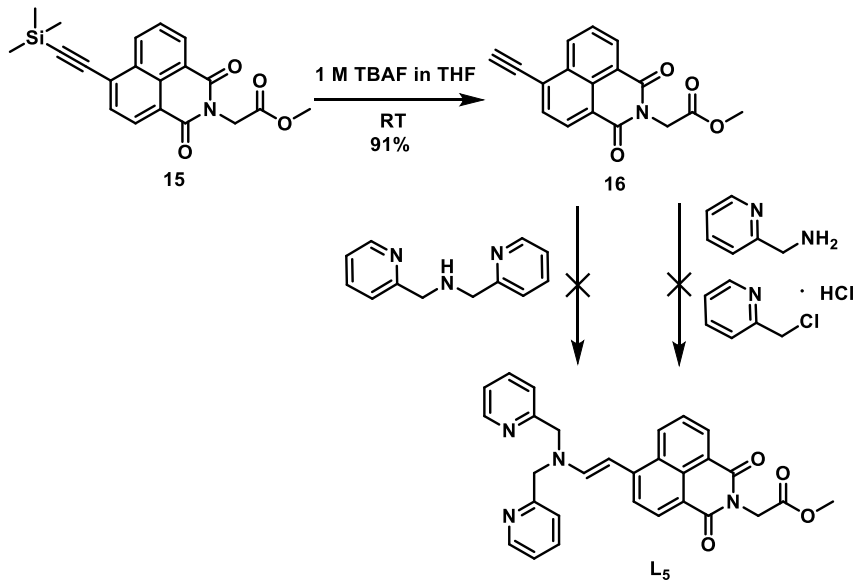

Scheme 2.10: *Attempted synthesis of* ***L₅***

Based on the procedure reported by McAdam et al., synthesis of **L5** was modified by allowing longer reaction time, using higher temperatures, different solvents and addition of base. The different conditions that were attempted is summarised in **Table 2.1**.

Table 2.1: *Conditions attempted for the synthesis of* ***L5***

Solvent	Temperature	Time
Acetonitrile	RT	Up to 72 h
DMSO	RT	Up to 72 h
DMF	RT	Up to 72 h
DMSO	50 °C	48 h
DMSO	100 °C	48 h
NMP, K^{t}BuO	RT	48 h

Finally, **L6** was synthesized using **12** and DPA in 49% yield (**Scheme 2.11**). Temperature of the reaction was elevated to 150 °C, following the procedure reported by Fulop et al. for the synthesis of a similar ligand.[37]

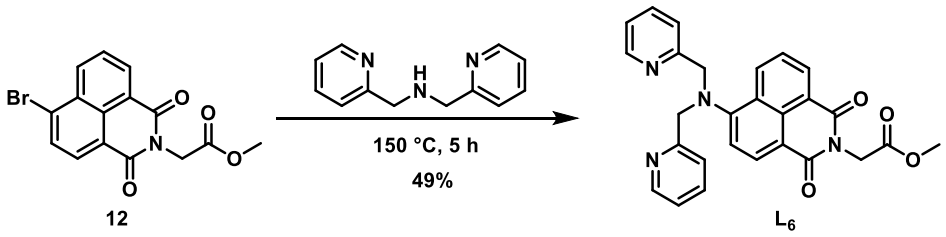

Scheme 2.11: *Synthesis of* ***L6***

2.2.3 Synthesis of Re(I) tricarbonyl complexes

$[Re(CO_3)_5]OTf$ and the aqua complex $[Re(CO)_3(H_2O)_3]OTf$ were synthesized by previously reported procedures.[38,39] Ligands **L1**-**L4** and **L6** were poorly soluble in water, as is observed in other naphthalimide based ligands.[40,41] Hence, the ligands were dissolved in 2:1 methanol-water mixture. Re(I) tricarbonyl complex, **ReL1** was synthesized by heating **L1** with $[Re(CO)_3(H_2O)_3]OTf$ in microwave conditions as per **Scheme 2.12**. Removal of methanol resulted in precipitation of the pure product in 84%

yield. **ReL$_2$, ReL$_3$, ReL$_4$** and **ReL$_6$** were synthesized from their corresponding ligands using the same procedure.

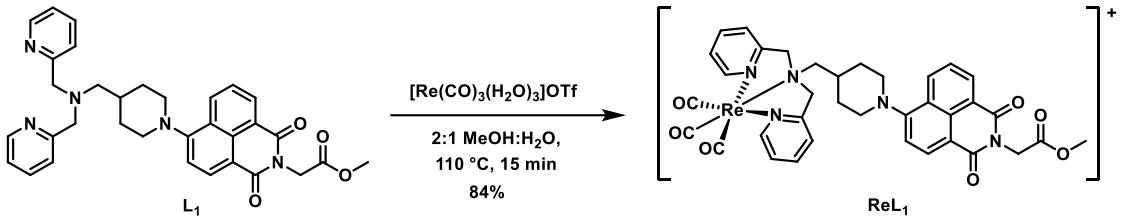

Scheme 2.12: *Scheme for the synthesis of Re(I) tricarbonyl complex of 1,8-naphthalimide derivative*

2.2.4 Structural Characterization

All precursors, ligands and Re(I) tricarbonyl complexes were characterized by NMR spectroscopy. Comparing the ^{1}H NMR spectra of **L$_1$**–**L$_4$** and **L$_6$** demonstrate the effect of the linker on the chemical shifts of the methylene protons of the chelator arms. These protons are seen at 4.95 ppm, 4.96 ppm and 4.75 ppm in **L$_2$**, **L$_3$** and **L$_6$** respectively. In **L$_1$** and **L$_4$**, they are more shielded as seen at 3.86 ppm and 3.9 ppm respectively, due to the inductive effect of methylene protons of the linker. In **Figure 2.5**, peaks corresponding to these protons are marked with asterisk.

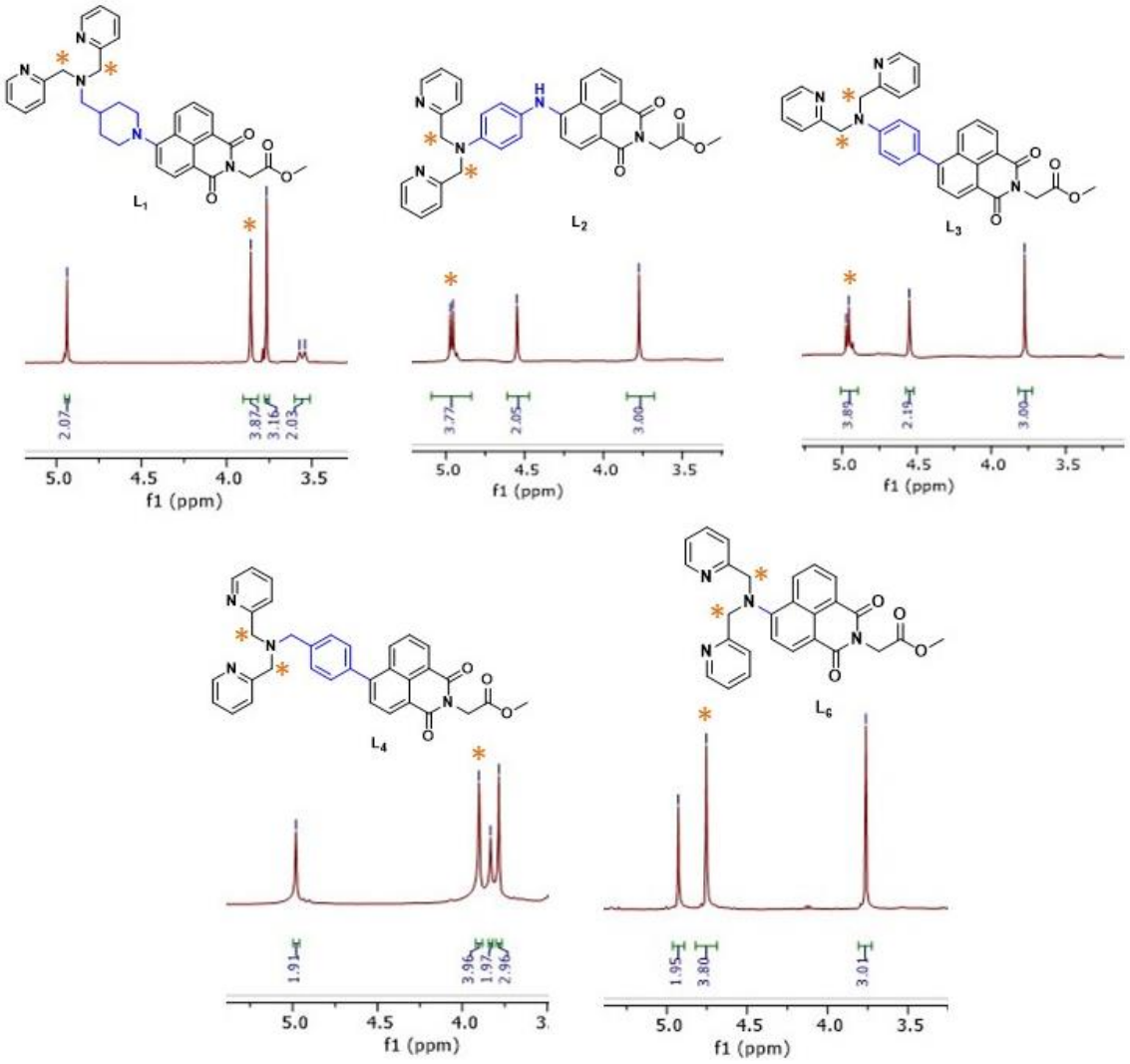

Figure 2.5: *Effect of linker on methylene protons of the dipicolylamine arms*

In ^{1}H NMR spectra of rhenium complexes, the methylene protons from the chelator arms were de-shielded compared to the corresponding ligands. The characteristic diastereotopic splitting of these methylene protons was also observed. In **Figure 2.6**, this peak splitting pattern is shown by comparing **L$_6$** and **ReL$_6$**, as an example. The calculated coupling constant was 16-17 Hz, indicative of geminal coupling. Peaks at ca. 197 ppm and ca. 196.5 ppm in ^{13}C NMR spectra of the rhenium complexes, prove the presence of equatorial and axial carbonyl ligands. These observations confirm the formation of rhenium complexes.

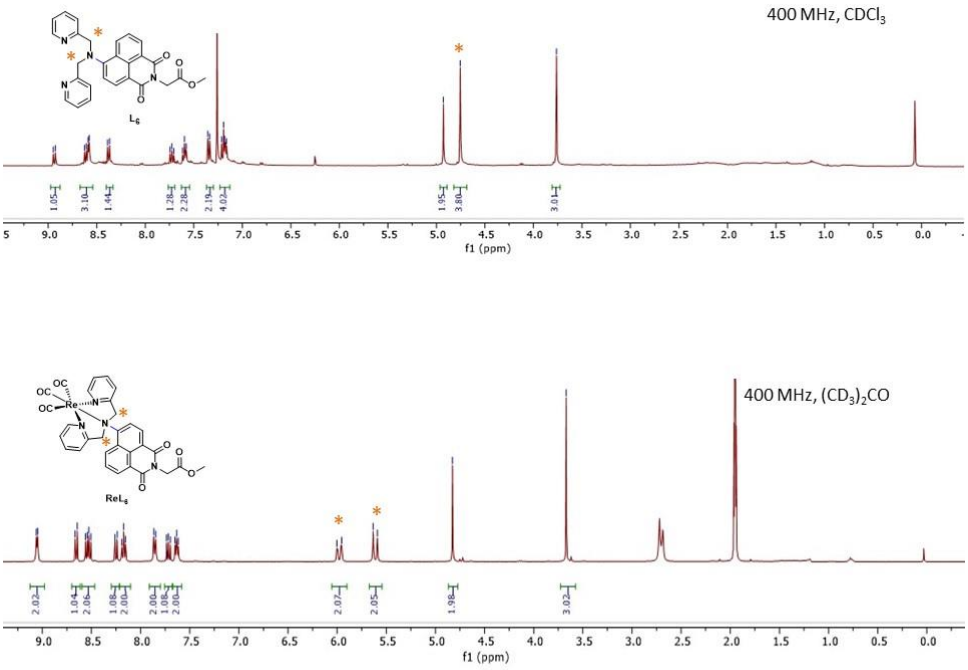

Figure 2.6: *Diastereotopic splitting of the methylene protons on the chelator, in rhenium complexes*

2.2.5 Photophysical properties

The photophysical properties of ligands and their rhenium complexes are given in **Table 2.2**. UV/Vis absorption and fluorescence properties were recorded in MeCN solutions. In the absorption spectra of all ligands and rhenium complexes, a broad lower energy peak was observed that can be assigned to the characteristic Intramolecular Charge Transfer (ICT) transition of substituted 1,8-naphthalimides. In **L_1** and **L_6,** maxima of this peak was observed at 420 nm and 422 nm respectively. It is worth noting that the absorption maxima of ligands **L_2-L_4** are lower**,** indicating an increase in energy required for ICT transition. The electron-donating ability of an aromatic amine is less than secondary alkyl amine while phenyl and benzyl groups are only weakly electron-donating. The reduced electron-donating ability can be attributed to the higher energy ICT transitions in **L_2-L_4**. On formation of the corresponding positively charged Re(I) complexes, only minor shifts were seen in the absorption spectra probably due to perturbation of ICT transition by the

positive charge.[26] The molar extinction coefficients of **ReL$_1$**, **ReL$_2$** and **ReL$_6$** showed a decrease compared to **L$_1$**, **L$_2$** and **L$_6$** while **ReL$_3$** and **ReL$_4$** showed a significant increase compared to **L$_3$** and **L$_4$**. The fluorescence spectra of the ligands and their corresponding Re(I) complexes showed a trend similar to that of the absorption spectra. Rhenium coordination resulted in the hypsochromic shift of 18 nm in the emission maxima of **L$_1$**, while all other ligands showed smaller shifts of 6-9 nm.

Table 2.2: *Photophysical properties of synthesized ligands and their Re(I) tricarbonyl complexes*

Compound	**λ_{Abs} (nm)[a]**	**ε (L.mol^{-1}cm^{-1})**	**λ_{Ex} (nm)[a]**	**λ_{Em} (nm)[a]**	**Stoke's Shift (cm^{-1})**	**Φ_f[b]**
L_1	420	1400	417	539	5428	0.024 (0.027[c])
ReL_1	415	1300	410	521	5196	0.159
L_2	346	1000	361	492	7376	0.146
ReL_2	342	970	360	485	7159	0.010
L_3	352	1300	361	489	7251	0.132
ReL_3	348	2100	357	483	7307	0.130
L_4	352	500	355	436	5233	0.074
ReL_4	350	1800	353	425	4799	0.071
L_6	422	530	418	522	4766	0.239 (0.272[d])
ReL_6	420	430	414	515	4737	0.150

[a]20 μM in CH_3CN. [b]Absolute quantum yield at λ_{Ex} = 390 nm. [c]λ_{Ex} = 417 nm. [d]λ_{Ex} = 418 nm.

Absolute quantum yields were recorded at an excitation wavelength of 390 nm. In donor-acceptor pairs with two π-systems, Twisted Intramolecular Charge Transfer (TICT) mechanism has been linked to fluorescence quenching as well as dual fluorescence in certain cases.[42] TICT mechanism allows non-radiative relaxation of the excited states due to the rotation between π-systems.[43] This can be correlated to the lower quantum yields of ligands **L_1-L_4**. Moreover, restrictions due to instrumentation that limited the excitation wavelength between 390 – 800 nm, resulted in samples being excited at less-than-ideal wavelengths. This led to lower quantum yields as can be observed in the case of **L_1** and **L_6** which were the only systems excited at their excitation maxima.

2.3 Conclusions

In summary, the synthesis and photophysical properties of four 1,8-naphthalimide based ligands and their corresponding Re(I) tricarbonyl complexes are reported. The effect of rigid linkers on their optical properties were analysed. In comparison to ligands with alkyl linkers,[26,27] introduction of rigid linkers leads to a blue shift in their fluorescence emission. The extent of blue shift can be correlated to the electron-donating capacity of the substitutions. The planar nature of the linkers can lead to TICT states which results in lower emission intensities. Naphthalimide based Re(I) tricarbonyl complexes have been previously studied for potential confocal microscopy applications. Due to 400-800 nm being the ideal excitation wavelength for confocal microscopes, rhenium complexes **ReL_1-ReL_3** may not be suitable for such applications. Successful formation of rhenium complexes implies the possibility of radiolabelling with ^{99m}Tc to produce SPECT traces. However, lower-than-ideal emission wavelengths limit the potential use as dual-modality probes for optical fluorescence imaging.

2.4 Experimental

All reagents were purchased from commercial sources and used without further purification. NMR spectra were recorded on a Bruker AvIII HD 400 spectrometer. All

chemical shifts are reported in ppm and referenced to the residual solvent peaks. High resolution mass spectra were recorded on a Bruker micrOTOF II for ESI in either positive or negative mode. Analytical reversed-phase HPLC-MS was performed on a system consisting of an Agilent Zorbax SB-C18 column (5 μm, 4.6 x 150 mm), Waters 600 controller and binary solvent pump and a Waters Quattro Micro API mass spectrometer (System I). The linear gradient solvent system comprised of solvent A (CH_3CN + 0.1 % TFA) and solvent B (H_2O + 0.1 % TFA) at a flow rate of 1.5 mL/min over 10 minutes with a 5 minute wash cycle at 95% solvent A. The UV/Vis absorbance was detected using a Waters 2998 photodiode array detector. Mass spectra were collected using an ESI source in positive ion mode. UV-Vis spectra were recorded on an Agilent Cary 60 UV-Vis spectrophotometer. Fluorescence spectra were recorded on a Photon Technologies International, Inc. Quanta Master – 7/2005. Solution state emission quantum yields were measured in aerated acetonitrile using a Hamamatsu C11347-11 Quantaurus Absolute PL Quantum Yield Spectrometer.

Methyl 2-(6-chloro-1,3-dioxo-1H-benzo[de]isoquinolin-2(3H)-yl)acetate (1)

Compound **1** was synthesized using the previously reported procedure.[27] 4-Chloro-1,8-napthalic anhydride (2.00 g, 8.6 mmol), triethylamine (1.17 mL, 8.4 mmol) and glycine methyl ester hydrochloride (1.53 g, 12.2 mmol) were added to ethanol (50 mL) and heated to reflux for 16 hours. The orange solution was cooled to room temperature, resulting in the formation of the product as an off-white precipitate that was collected by filtration, washed with cold ethanol and then dried under vacuum (2.2 g, 84%). ^{1}H NMR (400 MHz, $CDCl_3$) δ 8.69 (dd, *J* = 7.3, 1.0 Hz, 1H), 8.65 (dd, *J* = 8.5, 1.0 Hz, 1H), 8.53 (d, *J* = 7.9z Hz, 1H), 7.90 – 7.84 (m, 2H), 4.95 (s, 2H), 3.79 (s, 3H). ^{13}C NMR (100 MHz, $CDCl_3$) δ 168.4, 163.4, 163.1, 139.6, 132.5, 131.6, 131.2, 129.5, 129.3, 127.9, 127.5, 122.7, 121.1, 52.6, 41.3. HRMS (ESI): *m/z* calculated for $C_{15}H_{10}ClNO_4$ $[M]^+$ 303.0298; found 303.0309.

Methyl 2-(6-(4-(((tert-butoxycarbonyl)amino)methyl)piperidin-1-yl)-1,3-dioxo-1H-benzo[de]isoquinolin-2(3H)-yl)acetate (2)

To a solution of compound **1** (100 mg, 0.33 mmol) in 1 mL DMSO, *N*-boc-4-(aminomethyl)piperidine (106 mg, 0.49 mmol) and triethylamine (91 μL, 0.66 mmol) were added and heated to 70 °C for 18 hours. The bright yellow solution was cooled to room temperature and diluted with DCM (30 mL). The organic layer was washed with water and brine, dried over Na_2SO_4, filtered and evaporated under reduced pressure to give the product as a yellow solid. Yield: 144 mg, 91% ^{1}H NMR (400 MHz, $CDCl_3$) δ 8.58 (dd, *J* = 7.3, 1.0 Hz, 1H), 8.50 (d, *J* = 8.1 Hz, 1H), 8.39 (dd, *J* = 8.5, 1.0 Hz, 1H), 7.67 (m, 1H), 7.18 (d, *J* = 8.2 Hz, 1H), 4.94 (s, 2H), 3.76 (s, 3H), 3.62 (d, *J* = 12.3 Hz, 2H), 3.17 (t, *J* = 6.3 Hz, 2H), 2.91 (m, 2H), 1.93 (d, *J* = 11.4 Hz, 2H), 1.67-1.57 (m, 3H), 1.46 (s, 9H). ^{13}C NMR (100 MHz, $CDCl_3$) δ 168.9, 164.4, 163.8, 157.3, 156.3, 133.2, 131.6, 131.1, 130.3, 126.5, 125.7, 122.8, 115.1, 52.6, 46.2, 41.3, 41.1, 36.9, 30.3, 28.6. HRMS (ESI): *m/z* calculated for $C_{26}H_{31}N_3O_6$ $[M+H]^+$: 482.2291, found 482.2273.

Methyl 2-(6-(4-(aminomethyl)piperidin-1-yl)-1,3-dioxo-1H-benzo[de]isoquinolin-2(3H)-yl)acetate (3)

Compound **2** (135 mg, 0.28 mmol) was dissolved in DCM (2.5 mL), followed by the addition of trifluoroacetic acid (2.5 mL), and stirred for 12 hours. The solvent was removed under reduced pressure. The resulting brownish-yellow oil was dissolved in water, the pH adjusted to 9 with 1 M NaOH, and extracted with DCM. The organic layer was washed with water and brine, dried over Na_2SO_4, filtered and evaporated under reduced pressure to give the product as a yellow solid. Yield: 93 mg, 87%. ^{1}H NMR (400 MHz, $CDCl_3$) δ 8.58 (dd, *J* = 7.3, 1.0 Hz, 1H), 8.50 (d, *J* = 8.1 Hz, 1H), 8.39 (dd, *J* = 8.5, 1.0 Hz, 1H), 7.68 (m, 1H), 7.19 (d, *J* = 8.2 Hz, 1H), 4.94 (s, 2H), 3.77 (s, 3H), 3.64 (d, *J* = 12.4 Hz, 2H), 2.93 (t, *J* = 11.1 Hz, 2H), 2.77 (s, 2H), 1.97 (d, *J* = 8.7 Hz, 2H), 1.61 (b, 3H). ^{13}C NMR (100 MHz, $CDCl_3$) δ 168.9, 164.4, 163.8, 157.4, 133.2, 131.6, 131.1,

130.3, 126.5, 125.6, 122.8, 115.7, 115.0, 52.6, 48.0, 41.3, 41.2, 39.3, 30.4. HRMS (ESI): *m/z* calculated for $C_{21}H_{23}N_3O_4$ $[M+H]^+$: 382.1767, found 382.1786.

Methyl 2-(6-(4-((bis(pyridin-2-ylmethyl)amino)methyl)piperidin-1-yl)-1,3-dioxo-1H-benzo[de]isoquinolin-2(3H)-yl)acetate (L_1)

To a solution of **3** (76 mg, 0.2 mmol) in 1,2-dichloroethane (5 mL) 2-pyridinecarboxaldehyde (48 μL, 0.5 mmol) was added, and the solution stirred for 2 hours under a nitrogen atmosphere. The solution was cooled to 0 °C on an ice-water bath, and sodium triacetoxyborohydride (127 mg, 0.6 mmol) was added. The solution was allowed to warm to RT, and then stirred for 48 hours. Water was added, and the product was extracted with chloroform. The organic layer was washed with water and brine, dried over Na_2SO_4, filtered and concentrated to a minimum volume. The product was precipitated by the addition of hexanes and collected by filtration as a bright yellow solid. Yield: 76 mg, 68%. ^{1}H NMR ($CDCl_3$, 400 MHz) δ 8.56 (m, 3H), 8.49 (d, *J* = 8.1 Hz, 1H), 8.33 (dd, *J* = 8.5, 1 Hz, 1H), 7.67 (m, 3H), 7.58 (s, 1H), 7.56 (s, 1H), 7.18 (m, 2H) 7.15 (d, *J* = 8.1 Hz, 1H), 4.94 (s, 2H), 3.86 (s, 4H), 3.76 (s, 3H), 3.55 (d, *J* = 12.3 Hz, 2H), 2.87 (t, *J* = 11.1 Hz, 2H), 2.56 (d, *J* = 7.2 Hz, 2H), 2.03 (d, *J* = 11.6 Hz, 1H), 1.45 (m, 3H). ^{13}C NMR (100 MHz, $CDCl_3$) δ 168.6, 164.1, 163.5, 159.6, 157.2, 148.9, 136.2, 132.9, 131.3, 130.8,130.0, 126.1, 125.2, 122.8, 122.5, 121.9, 115.3, 114.6, 61.0, 60.3, 52.2, 40.9, 34.0, 30.8, 29.5. HRMS (ESI): *m/z* calculated for $C_{33}H_{33}N_5O_4$ $[M+H]^+$: 564.2611, found 564.2607

***Tert*-butyl (4-(bis(pyridin-2-ylmethyl)amino)phenyl)carbamate (5)**

To a solution of *N*-boc-p-phenylenediamine (105 mg, 0.5 mmol) in 1,2-dichloroethane (10 mL) 2-pyridinecarboxaldehyde (119 μL, 1.25 mmol) was added, and the solution stirred for 2 hours under a nitrogen atmosphere. The solution was cooled to 0 °C on an ice-water bath, and sodium triacetoxyborohydride (318 mg, 1.5 mmol) was added. The solution was allowed to warm to RT, and then stirred for 48 hours. Water was added, and

the product was extracted with chloroform. The organic layer was washed with water and brine, dried over Na_2SO_4, filtered and concentrated under reduced pressure. Purification using column chromatography (silica gel, 60-80% EtOAc in hexanes + 1% Et_3N) gave the desired product as a brownish orange solid. Yield: 41 mg, 21 %. ^{1}H NMR ($CDCl_3$, 400 MHz) δ 8.59 (d, *J* = 5.6 Hz, 2H), 7.61 (m, 2H), 7.25 (d, *J* = 7.9 Hz, 2H), 7.15 (dd, *J* = 14.7, 8.9 Hz, 4H), 6.64 (d, *J* = 9.1 Hz, 2H), 4.80 (s, 2H), 3.76 (s, 3H), 1.48 (s, 9H). ^{13}C NMR (100 MHz, $CDCl_3$) δ 158.9, 149.7, 144.7, 136.9, 128.6, 122.0, 121.4, 121.0, 113.1, 57.7, 28.5. HRMS (ESI): *m/z* calculated for $C_{23}H_{26}N_4O_2$ $[M+H]^+$: 391.2134, found 391.2122

N^1,N^1-bis(pyridin-2-ylmethyl)benzene-1,4-diamine (6)

Compound **5** (40 mg) was dissolved in DCM (2 mL), followed by the addition of trifluoroacetic acid (2 mL), and stirred for 24 hours. The solvent was removed under reduced pressure. The resulting brownish oil was dissolved in water, the pH adjusted to 9 with 1 M NaOH, and extracted with DCM. The organic layer was washed with water and brine, dried over Na_2SO_4, filtered, and evaporated under reduced pressure to give the product as an orange solid. Yield: 28 mg, 94%. ^{1}H NMR ($CDCl_3$, 400 MHz) 8.59 (d, *J* = 5.6 Hz, 2H), 7.60 (m, 2H), 7.23 (d, *J* = 7.5 Hz, 2H), 7.13 (dd, *J* = 14.2, 8.4 Hz, 4H), 6.64 (d, *J* = 9.1 Hz, 2H), 4.80 (s, 2H), 3.76 (s, 3H). 2.79 (b, 2H). ^{13}C NMR (100 MHz, $CDCl_3$) δ 159.0, 149.8, 136.9, 122.1, 121.0, 113.2, 57.8. HRMS (ESI): *m/z* calculated for $C_{18}H_{18}N_4$ $[M+H]^+$: 291.1610, found 291.1616.

Methyl 2-(6-bromo-1,3-dioxo-1H-benzo[de]isoquinolin-2(3H)-yl)acetate (12)

Synthesized same as compound **1** but with 4-bromo-naphthalic anhydride (2g, 7.22 mmol), triethylamine (1.5 mL g, 10.83 mmol) and glycine methyl ester hydrochloride (1.36 g, 10.83 mmol). Yield = 1.88 g (75%). ^{1}H NMR (400 MHz, $CDCl_3$) δ 8.66 (dd, *J* = 7.3, 1.1 Hz, 1H), 8.59 (dd, *J* = 8.5, 1.1 Hz, 1H), 8.42 (d, *J* = 7.9 Hz, 1H), 8.05 (d, *J* = 7.9 Hz, 1H) 7.86 (dd, *J* = 8.5, 7.3 Hz, 1H), 4.94 (s, 2H), 3.78 (s, 3H). ^{13}C NMR (100 MHz,

$CDCl_3$) δ 168.5, 163.4, 133.9, 132.6, 131.7, 131.0, 130.9, 129.3, 128.3, 122.7, 121.9, 52.7, 41.4. HRMS (ESI): *m/z* calculated for $C_{15}H_{10}BrNO_4$ $[M]^+$ 347.9872; found 347.9889

Methyl 2-(6-((4-(bis(pyridin-2-ylmethyl)amino)phenyl)amino)-1,3-dioxo-1H-benzo[de]isoquinolin-2(3H)-yl)acetate (L_2)

Compound **12** (35 mg, 0.1 mmol) and compound **6** (44 mg, 0.15 mmol) were dissolved in 2 mL DMSO. Triethylamine (28 μL, 0.2 mmol) was added and the solution was heated to 80 °C for 48 hours. The brown solution was cooled to room temperature and diluted with DCM (30 mL). The organic layer was washed with water and brine, dried over Na_2SO_4, filtered and evaporated under reduced pressure. Purification using column chromatography (silica gel, 50-80 % EtOAc in hexanes + 1% Et_3N) gave the desired product as an orange solid Yield: 28 mg, 51%. ^{1}H NMR ($CDCl_3$, 400 MHz) δ 8.61 (dd, *J* = 7.2, 4.4 Hz, 5H), 8.42 (d, *J* = 8.5 Hz, 1H), 7.68 (t, *J* = 8.1 Hz, 4H), 7.36 (m, 4H), 6.83 (d, *J* = 8.4 Hz, 3H), 4.95 (d, *J* = 7.2 Hz, 4H), 4.55 (s, 2H), 3.77 (s, 3H). ^{13}C NMR (101 MHz, $CDCl_3$) δ168.8, 168.3, 164.0, 157.9, 149.4, 148.4, 148.1, 136.9, 133.7, 131.3, 130.3, 129.3, 127.6, 126.6, 122.5, 121.8, 113.1, 61.7, 52.6, 49.1, 45.3, 41.5. HRMS (ESI): *m/z* calculated for $C_{33}H_{27}N_5O_4$ $[M+H]^+$ 558.2141; found 558.2189

Methyl 2-(6-(4-nitrophenyl)-1,3-dioxo-1H-benzo[de]isoquinolin-2(3H)-yl)acetate (13)

Compound **12** (174 mg, 0.5 mmol) and 4-nitrophenylboronic acid (125 mg, 0.75 mmol) were dissolved in 1,4-dioxane (10 mL) and then degassed. To the resultant solution $Pd(PPh_3)_4$ (58 mg, 10 mol%) and K_2CO_3 (207 mg, 1.5 mmol) were added and the reaction mixture was heated to reflux and stirred for 36 h. The reaction was then diluted with EtOAc (50 mL), washed with water and brine then dried over Na_2SO_4, filtered, and concentrated under reduced pressure. Purification using column chromatography (silica gel, 0-15% EtOAc in hexanes) gave the desired product as a yellow solid. Yield: 84 mg, 43%. ^{1}H NMR (400 MHz, $CDCl_3$,) δ 8.67 (dd, *J* = 15.9, 8.7 Hz, 2H), 8.53 (d, *J* = 7.9 Hz,

1H), 8.37 (d, *J* = 8.8 Hz, 2H), 7.87 dd, *J* = 15.5, 7.6 Hz, 2H), 7.79 (d, *J* = 8.8 Hz, 2H), 4.95 (s, 2H), 3.79 (s, 3H). ^{13}C NMR (100 MHz, $CDCl_3$) δ 145.4, 144.6, 133.2, 132.2, 132.1, 131.2, 131.0, 128.7, 128.6, 128.1, 127.6, 124.1, 52.7, 41.5, 29.9. HRMS (ESI): *m/z* calculated for $C_{21}H_{14}N_2O_6$ $[M+H]^+$ 391.0931; found 391.0946

Methyl 2-(6-(4-(bis(pyridin-2-ylmethyl)amino)phenyl)-1,3-dioxo-1H-benzo[de]isoquinolin-2(3H)-yl)acetate (L_3)

To a solution of **13** (80 mg, 0.2 mmol) in THF (4 mL), anhydrous Tin(II) chloride (144 mg , 1 mmol) were added followed by addition of 1 mL HCl. The solution was heated to reflux for 3 hours. The solution was cooled to room temperature and concentrated to minimum volume. 50 mL of EtOAc was added and the solution was filtered through silica gel, which was washed with additional 50 mL of EtOAc. The organic layer were combined and evaporated to give an orange oil. Yield: 63 mg, 88%. ^{1}H NMR (400 MHz, $CDCl_3$,) δ 8.62 (dd, *J* = 7.3 3.3 Hz, 2H), 8.39 (d, *J* = 8.5 Hz, 2H) 7.68 (dd, *J* = 7.42, 3.6 Hz, 1H), 7.30 (d, *J* = 8.4 Hz, 2H), 6.83 (d, *J* = 8.4 Hz, 2H), 4.96 (s, 2H), 3.79 (s, 3H), 3.52 (b, 2H). ^{13}C NMR (100 MHz, $CDCl_3$) δ 168.8, 168.3, 164.3, 148.0, 147.1, 133.6, 131.3, 130.4, 129.2, 127.7, 126.6, 122.5, 120.5, 115.1, 61.7, 52.6, 45.8, 41.6, 29.8, 14.3, 8.8. HRMS (ESI): *m/z* calculated for $C_{21}H_{16}N_2O_4$ $[M+H]^+$ 361.1188; found 361.1181

To a solution of the above compound (50 mg, 0.14 mmol) in 1,2-dichloroethane (4 mL) 2-pyridinecarboxaldehyde was added (33 μL, 0.35 mmol), and the solution was stirred for 2 hours under a nitrogen atmosphere. The solution was cooled to 0 °C on an ice-water bath, and sodium triacetoxyborohydride (89 mg, 0.42 mmol) was added. The solution was allowed to warm to RT, and then stirred for 48 hours. Water was added, and the product was extracted with chloroform. The organic layer was washed with water and brine, dried over Na_2SO_4, filtered and concentrated to a minimum volume. Purification using column chromatography (silica gel, 50-80% EtOAc in hexanes + 1% Et_3N) gave the desired product as a orangish-yellow solid Yield: 56 mg, 74%. ^{1}H NMR (400 MHz, $CDCl_3$,) δ 8.61 (dd, *J* = 7.3, 4.5 Hz, 5H) 8.42 (dt, *J* = 8.5, 1.4 Hz, 2H), 7.68 (ddd, *J* = 10.1,

6.8, 1.6 Hz, 3H), 7.36 (m, 4H), 6.83 (d, *J* = 8.2 Hz, 3H), 4.96 (d, *J* = 7.2 Hz, 4H), 4.55 (s, 2H), 3.77 (s, 3H). ^{13}C NMR (100 MHz, $CDCl_3$) δ 157.8, 149.3, 136.8, 133.6, 131.4, 131.2, 127.5, 126.4, 122.4, 121.7, 113.0,61.5, 52.5, 49.0, 41.4. HRMS (ESI): *m/z* calculated for $C_{33}H_{26}N_4O_4$ $[M+H]^+$ 543.2033; found 543.2049.

Methyl 2-(6-(4-(bromomethyl)phenyl)-1,3-dioxo-1H-benzo[de]isoquinolin-2(3H)-yl)acetate (14)

Compound **12** (174 mg, 0.5 mmol) and 4-(bromomethyl)phenylboronic acid (161 mg, 0.75 mmol) were dissolved in 1,4-dioxane (10 mL) and then degassed. To the resultant solution $Pd(PPh_3)_4$ (58 mg, 10 mol%) and K_2CO_3 (207 mg, 1.5 mmol) were added and the reaction mixture was heated to reflux and stirred for 36 h. The reaction was then diluted with EtOAc (50 mL), washed with water and brine then dried over Na_2SO_4, filtered, and concentrated under reduced pressure. Purification using column chromatography (silica gel, 0-10% EtOAc in hexanes) gave the desired product as a bright yellow solid Yield: 124 mg, 57%. ^{1}H NMR (400 MHz, $CDCl_3$) δ 8.66 (dd, *J* = 7.4, 2.6 Hz, 2H), 8.28 (d, *J* = 8.4 Hz, 1H), 7.71 (m, 2H), 7.59 (d, *J* = 8.2 Hz, 2H), 7.50 (d, *J* = 8 Hz, 2H), 4.99 (s, 2H), 4.61 (s, 2H), 3.79 (s, 3H). ^{13}C NMR (100 MHz, $CDCl_3$;) δ 169.0, 164.3, 134.9, 132.1, 127.4 122.6, 121.6 52.9, 41.6. HRMS (ESI): *m/z* calculated for $C_{22}H_{16}BrNO_4$ $[M]^+$ 437.0263; found 437.0253.

Methyl 2-(6-(4-((bis(pyridin-2-ylmethyl)amino)methyl)phenyl)-1,3-dioxo-1H-benzo[de]isoquinolin-2(3H)-yl)acetate (L_4)

To a solution of compound **14** (50 mg, 0.11mmol) in DMF (3mL), 2,2'-dipicolylamine (30 μL, 0.165 mmol) was added. The solution was stirred at room temperature under a nitrogen atmosphere for 48 hours. Water was added to the solution, and the product was extracted with DCM, dried over Na_2SO_4, filtered, and concentrated under reduced pressure. Purification using column chromatography (silica gel, 50-80% EtOAc in hexanes + 1% Et_3N) gave the desired product as a bright yellow solid. Yield: 40 mg, 65%.

^{1}H NMR (400 MHz, $CDCl_3$,) δ 8.64 (dd, *J* = 7.3, 3.5 Hz, 2H), 8.56 (5.2, 1.8 Hz, 2H), 8.29 (d, *J* = 8.5 Hz, 1H), 7.69 (dd, *J* = 7.4, 1.9 Hz, 3H), 7.64 (d, *J* = 7.8 Hz, 3H), 7.60 (d, *J* = 7.9 Hz, 2H), 7.45 (d, *J* = 7.9 Hz, 2H), 7.18 (ddd, *J* = 6.8, 4.8, 1.4 Hz, 2H), 4.98 (s, 2H), 3.9 (s, 4H), 3.83 (s, 2H), 3.78 (s, 3H). ^{13}C NMR (100 MHz, $CDCl_3$) δ 148.6, 136.5, 132.2, 132.1, 131.9, 130.1, 128.6, 128.5, 127.2, 126.9, 124.5, 123.1, 64. 8, 58.1, 57.4, 52.5, 41.3. HRMS (ESI): *m/z* calculated for $C_{34}H_{28}N_4O_4$ $[M+H]^+$ 557.2189; found 557.2163.

Methyl 2-(6-(bis(pyridin-2-ylmethyl)amino)-1,3-dioxo-1H-benzo[de]isoquinolin-2(3H)-yl)acetate (L_6)

A mixture of compound **12** (100 mg, 0.28 mmol) and 2,2'-dipicolylamine (100 μL, 0.56 mmol) was flushed with nitrogen and heated to 150 ˚C for 5 hours. The mixture was cooled to room temperature, all volatiles were removed under reduced pressure. Purification using column chromatography (silica gel, 75-95% EtOAc in hexanes + 1% Et_3N) gave the desired product as a yellow oily residue. Yield: 57 mg, 49%. ^{1}H NMR (400 MHz, $CDCl_3$) δ 8.94 (d, *J* = 8.5 Hz, 1H), 8.6 (dd, *J* = 13.1, 6 Hz, 3H), 8.38 (d, *J* = 8.1 Hz, 1H), 7.73 (m, 1H). 7.6 (t, *J* = 7.5 Hz, 2H), 7.34 (d, *J* = 7.8 Hz, 2H), 7.19 (dd, *J* = 12.8, 7.7 Hz, 4H), 4.93 (s, 2H), 4.74 (s, 4H), 3.76 (s, 3H). ^{13}C NMR (100 MHz, $CDCl_3$) δ 168.7, 164.1, 146.8, 138.9, 138.5, 133.1, 131.8, 131.4, 130.5, 129.5, 128.1, 127.2, 122.6, 121.6, 52.7, 41.4, 32.9, 8.8. HRMS (ESI): *m/z* calculated for $C_{27}H_{22}N_4O_4$ $[M+H]^+$: 467.1719, found 467.1719.

***fac*-[Re(CO)$_3$(L_1)]OTf (ReL_1)**

A solution of **L_1** (8 mg, 0.014 mmol) in 2:1 methanol:dH_2O and 0.1 M solution of $[Re(CO)_3(H2O)_3]OTf$ (1.2 equiv.) in H_2O, were added to a 2 mL microwave vial. The reaction was heated to 110 °C for 15 minutes under microwave irradiation. Removal of methanol under reduced pressure resulted in the precipitation of the product which was filtered and washed with cold dH_2O. Purity of the complex was analyzed by reverse

phase analytical HPLC (05–95% Solvent A in B) t_R = 1.9 min. Yield = 13 mg, 84%. ^{1}H NMR (400 MHz; $CDCl_3$) δ 8.68 (d, *J* = 5.5 Hz, 2H), 8.60 (dd, *J* = 7.3, 1 Hz, 1H), 8.54 (d, *J* = 8.1 Hz, 1H), 8.40 (dd, *J* = 8.5, 1 Hz, 1H), 7.84 (m, 4H), 7.70 (m, 1H), 7.28-7.23 (b, 3H), 5.77 (d, *J* = 16.2 Hz, 2H), 4.95 (s, 2H), 4.45 (d, *J* = 16.3 Hz, 2H), 3.85 (d, *J* = 4.8 Hz, 2H), 3.77 (s, 3H), 3.67 (d, *J* = 12.1 Hz, 2H), 3.21 (t, *J* = 11.6 Hz, 2H), 2.28 (d, *J* = 12.2 Hz, 2H), 1.88 (m, 2H). ^{13} C NMR (100 MHz, $CDCl_3$) δ 197.0, 186.6, 168.9, 165.0, 163.8, 161.0, 156.8, 150.8, 140.7, 139.5, 133.3, 131.6, 130.9, 126.50, 125.7, 125.6, 125.2, 122.9, 116.1, 115.5, 67.5, 53.1, 52.6, 41.3, 33.7, 33.4, 1.2. HRMS (ESI): *m/z* calculated for $C_{36}H_{33}N_5O_7$ ^{185}Re $[M]^+$: 832.1910, found 832.1892.

***fac*-[Re(CO)$_3$(L$_2$)]OTf (ReL$_2$)**

Synthesized same as ReL$_1$ but with **L$_2$** (8 mg, 0.014 mmol). HPLC (30–95% Solvent A in B) t_R = 11.84 min. Yield = 11 mg, 90%. ^{1}H NMR (400 MHz, CD_3OD) δ 9.01 (d, *J* = 5.7 Hz, 2H), 8.74 (d, *J* = 9.3 Hz, 2H), 8.63 (d, *J* = 6.6 Hz, 2H), 8.38 (d, *J* = 8.5 Hz, 1H), 8.15 (m, 2H), 7.79 (d, *J* = 8.5 Hz, 3H), 7.69 (d, *J* = 9.1 Hz, 2H), 7.36 (d, 8.5 Hz, 2H), 5.61 (d, *J* = 16.6 Hz, 2H), 5.22 (s, 2H), 5.11 (d, *J* = 16.4 Hz, 2H), 3.79(s, 3H). ^{13}C NMR (100 MHz, CD_3OD) δ 197.0, 195.9, 169.1, 163.6, 160.5, 151.8, 140.2, 132.3, 131.2, 130.3, 125.5, 123.3, 72.4, 67.5, 29.4, 8.3. HRMS (ESI): *m/z* calculated for $C_{36}H_{27}N_5O_7$^{185}Re $[M\ ]^+$: 826.1441, found 826.1455.

***fac*-[Re(CO)$_3$(L$_3$)]OTf (ReL$_3$)**

Synthesized same as ReL$_1$ but with **L$_3$** (7 mg, 0.015 mmol). HPLC (30–95% Solvent A in B) t_R = 12.07 min. Yield = 10 mg, 82%. ^{1}H NMR (400 MHz, CD_3OD,) δ 8.92 (d, *J* = 5.5 Hz 2H), 8.69 (dd, *J* = 9.6, 7.5 Hz, 2H), 8.42 (d, *J* = 8.5 Hz, 1H), 7.99 (d, *J* = 7.9 Hz, 2H), 7.94 (t, *J* = 7.7 Hz, 2H), 7.87 (t, *J* = 7.4 Hz, 2H), 7.78 (d, *J* = 7.8 Hz, 2H), 7.54 (d, *J* = 7.8 Hz, 2H), 7.39 (m, 2H), 5.26 (d, *J* =15.6 Hz, 2H), 4.98 (s, 2H), 4.62 (d, *J* = 15.4 Hz, 2H) 3.76 (s, 3H). ^{13}C NMR (100 MHz, CD_3OD) δ 198.6, 197.5, 170.7, 165.22, 162.1,

153.4, 141,8, 133.5, 132.0, 129.5, 128.7, 127.1, 124.9, 123.9, 123.1, 74.1, 69.1, 31.0, 9.9. HRMS (ESI): *m/z* calculated for $C_{36}H_{26}N_4O_7{}^{185}Re$ $[M]^+$ 811.1332; found 811.1345

***fac*-[Re(CO)$_3$(L$_4$)]OTf (ReL$_4$)**

Synthesized same as ReL$_1$ but with **L$_4$** (8 mg, 0.014 mmol). HPLC (30–95% Solvent A in B) t_R = 12.39 min. Yield = 11 mg, 89%. ^{1}H NMR (400 MHz, $(CD_3)_2CO$) δ 9.01 (d, *J* =5.3 Hz, 2H), 8.66 (dd, *J* = 11.1, 7.8 Hz, 2H), 8.42 (d, *J* = 8.42 Hz, 1H), 8.15 (d, *J* = 8.14, 2H), 7.91 (m, 2H), 7.82 (d, *J* = 8 Hz, 2H), 7.68 (d, *J* = 7.8 Hz, 2H), 7.49 (m, 2H), 5.49 (d, *J* = 16.2 Hz, 2H), 5.3 (s, 2H), 4.91 (d, J = 16.2 Hz, 4H), 3.76 (s, 3H). ^{13}C NMR (100 MHz, $(CD_3)_2CO$) δ 196.6, 194.3, 182. 2, 161. 8, 153. 2, 141.6, 133.8, 131.8, 131.5, 129.2, 128.5, 126.9, 125.0, 124.9, 73.5, 68.8, 52.8, 41.9. HRMS (ESI): *m/z* calculated for $C_{37}H_{28}N_4O_7{}^{185}Re$ $[M]^+$ 825.1488 found 825.1492

***fac*-[Re(CO)$_3$(L$_6$)]OTf (ReL$_6$)**

Synthesized same as ReL$_1$ but with L$_2$ (8mg, 0.015mmol). HPLC (30–95% Solvent A in B) t_R = 11.16 min. Yield = 9 mg, 82 %. ^{1}H NMR (400 MHz, $(CD_3)_2CO$) δ 9.05 (d, *J* = 5.4 Hz, 2H), 8.66 (d, *J* = 8.4, 1H), 8.53 (dd, *J* = 14, 7.9 Hz, 2H), 8.25 (d, *J* = 9.7 Hz, 1H) 8.17 (t, *J* = 7.8 Hz, 2H) 7.86 (d, *J* = 7.9Hz, 2H), 7.72-7.63 (m, 3H), 5.98 (d, *J* = 16.4 Hz, 2H), 5.61 (d, *J* = 16.9 Hz, 2H) 4.83 (s, 2H), 3.67 (s, 3H). ^{13}C NMR (100 MHz, $(CD_3)_2CO$) δ 195.7, 195.3, 169.3, 153.7, 142.4, 132.6, 132.2, 128.2, 127.7, 126.1, 125.6, 117.7, 71.3, 52.8, 41.9. HRMS (ESI): *m/z* calculated for $C_{30}H_{22}N_4O_7{}^{185}Re$ $[M]^+$ 735.1018 found 735.1028

2.3 References

(1) Houston, J. P.; Ke, S.; Wang, W.; Li, C.; Sevick-Muraca, E. M. *J. Biomed. Opt.* **2005**, *10* (5), 1.

(2) Li, C.; Wang, W.; Wu, Q.; Ke, S.; Houston, J.; Sevick-Muraca, E.; Dong, L.; Chow, D.; Charnsangavej, C.; Gelovani, J. G. *Nucl. Med. Biol.* **2006**, *33* (3), 349.

(3) Nairne, J.; Iveson, P. B.; Meijer, A. Lawton, G., Witty, D. R. B. T.-P. in M. C.,

Eds.; Elsevier, 2015; Vol. 54, pp 231–280.

(4) Liew, H. S.; Mai, C.-W.; Zulkefeli, M.; Madheswaran, T.; Kiew, L. V; Delsuc, N.; Low, M. L. *Molecules* . 2020,.

(5) Zhao, G.-W.; Zhao, J.-H.; Hu, Y.-X.; Zhang, D.-Y.; Li, X. *Synth. Met.* **2016**, *212*, 131.

(6) Liu, Z.; He, W.; Guo, Z. *Chem. Soc. Rev.* **2013**, *42* (4), 1568.

(7) Raszeja, L. J.; Siegmund, D.; Cordes, A. L.; Güldenhaupt, J.; Gerwert, K.; Hahn, S.; Metzler-Nolte, N. *Chem. Commun.* **2017**, *53* (5), 905.

(8) Balasingham, R. G.; Coogan, M. P.; Thorp-Greenwood, F. L. *Dalt. Trans.* **2011**, *40* (44), 11663.

(9) Clède, S.; Policar, C. *Chem. – A Eur. J.* **2015**, *21* (3), 942.

(10) Bu, L.; Shen, B.; Cheng, Z. *Adv. Drug Deliv. Rev.* **2014**, *76*, 21.

(11) Cherry, S. R. *Semin. Nucl. Med.* **2009**, *39* (5), 348.

(12) Kobayashi, H.; Koyama, Y.; Barrett, T.; Hama, Y.; Regino, C. A. S.; Shin, I. S.; Jang, B.-S.; Le, N.; Paik, C. H.; Choyke, P. L.; Urano, Y. *ACS Nano* **2007**, *1* (4), 258.

(13) Jia, B.; Zhang, X.; Wang, B.; Chen, M.; Lv, F.; Wang, S.; Wang, F. *ACS Appl. Mater. Interfaces* **2018**, *10* (7), 6646.

(14) Azhdarinia, A.; Ghosh, P.; Ghosh, S.; Wilganowski, N.; Sevick-Muraca, E. M. *Mol. imaging Biol.* **2012**, *14* (3), 261.

(15) Dai, F.; Jin, F.; Long, Y.; Jin, X.-L.; Zhou, B. *Free Radic. Res.* **2018**, *52* (11–12), 1288.

(16) Ge, S.; Li, B.; Meng, X.; Yan, H.; Yang, M.; Dong, B.; Lu, Y. *Dye. Pigment.* **2018**, *148*, 147.

(17) Bao, X.; Wu, X.; Berry, S. N.; Howe, E. N. W.; Chang, Y.-T.; Gale, P. A. *Chem. Commun.* **2018**, *54* (11), 1363.

(18) Liu, J.; Tu, G.; Zhou, Q.; Cheng, Y.; Geng, Y.; Wang, L.; Ma, D.; Jing, X.; Wang, F. *J. Mater. Chem.* **2006**, *16* (15), 1431.

(19) Szakács, Z.; Rousseva, S.; Bojtár, M.; Hessz, D.; Bitter, I.; Kállay, M.; Hilbers, M.; Zhang, H.; Kubinyi, M. *Phys. Chem. Chem. Phys.* **2018**, *20* (15), 10155.

(20) Bojinov, V.; Konstantinova, T. *Dye. Pigment.* **2002**, *54* (3), 239.

(21) Tian, Y.; Su, F.; Weber, W.; Nandakumar, V.; Shumway, B. R.; Jin, Y.; Zhou, X.; Holl, M. R.; Johnson, R. H.; Meldrum, D. R. *Biomaterials* **2010**, *31* (29), 7411.

(22) Poteau, X.; Brown, A. I.; Brown, R. G.; Holmes, C.; Matthew, D. *Dye. Pigment.* **2000**, *47* (1), 91.

(23) Banerjee, S.; Veale, E. B.; Phelan, C. M.; Murphy, S. A.; Tocci, G. M.; Gillespie, L. J.; Frimannsson, D. O.; Kelly, J. M.; Gunnlaugsson, T. *Chem. Soc. Rev.* **2013**, *42* (4), 1601.

(24) Langdon-Jones, E. E.; Symonds, N. O.; Yates, S. E.; Hayes, A. J.; Lloyd, D.; Williams, R.; Coles, S. J.; Horton, P. N.; Pope, S. J. A. *Inorg. Chem.* **2014**, *53* (7), 3788.

(25) Turnbull, W. L.; Yu, L.; Murrell, E.; Milne, M.; Charron, C. L.; Luyt, L. G. *Org. Biomol. Chem.* **2019**, *17* (3), 598.

(26) Day, A. H.; Domarkas, J.; Nigam, S.; Renard, I.; Cawthorne, C.; Burke, B. P.; Bahra, G. S.; Oyston, P. C. F.; Fallis, I. A.; Archibald, S. J.; Pope, S. J. A. *Dalt. Trans.* **2020**, *49* (2), 511.

(27) Turnbull, W. L.; Murrell, E.; Bulcan-gnirss, M.; Majeed, M.; Milne, M.; Luyt, L. G. *Dalt. Trans.* **2019**, *48* (37), 14077.

(28) Cao, X.; Meng, L.; Li, Z.; Mao, Y.; Lan, H.; Chen, L.; Fan, Y.; Yi, T. *Langmuir* **2014**, *30* (39), 11753.

(29) Rurack, K.; Resch-Genger, U.; Bricks, J. L.; Spieles, M. *Chem. Commun.* **2000**, No. 21, 2103.

(30) Panchenko, P. A.; Arkhipova, A. N.; Zakharko, M. A.; Jonusauskas, G.; Fedorov, Y. V; Fedorova, O. A. *Russ. Chem. Bull.* **2016**, *65* (10), 2444.

(31) McAdam, C. J.; Morgan, J. L.; Robinson, B. H.; Simpson, J.; Rieger, P. H.; Rieger, A. L. *Organometallics* **2003**, *22* (24), 5126.

(32) Rémy, C.; Allain, C.; Leray, I. *Photochem. Photobiol. Sci.* **2017**, *16* (4), 539.

(33) Zhang, J. F.; Park, M.; Ren, W. X.; Kim, Y.; Kim, S. J.; Jung, J. H.; Kim, J. S. *Chem. Commun.* **2011**, *47* (12), 3568.

(34) Seubert, K.; Böhme, D.; Kösters, J.; Shen, W.; Freisinger, E.; Müller, J. *Zeitschrift für Anorg. und Allg. Chemie* **2012**, *638*.

(35) Goforth, S. K.; Walroth, R. C.; McElwee-White, L. *Inorg. Chem.* **2013**, *52* (10), 5692.

(36) Yoshizawa, A.; Feula, A.; Leach, A. G.; Male, L.; Fossey, J. S. *Front. Chem.* **2018**,

6, 211.

(37) Fülöp, A.; Arian, D.; Lysenko, A.; Mokhir, A. *Bioorganic Med. Chem. Lett.* **2009**, *19* (11), 3104.

(38) Schmidt, S. P.; Nitschke, J.; Trogler, W. C.; Huckett, S. I.; Angelici, R. J. *Inorganic Syntheses*. January 1, 1989, pp 113–117.

(39) He, H.; Lipowska, M.; Xu, X.; Taylor, A. T.; Carlone, M.; Marzilli, L. G. *Inorg. Chem.* **2005**, *44* (15), 5437.

(40) Loving, G. S.; Sainlos, M.; Imperiali, B. *Trends Biotechnol.* **2010**, *28* (2), 73.

(41) González-Vera, J. A.; Fueyo-González, F.; Alkorta, I.; Peyressatre, M.; Morris, M. C.; Herranz, R. *Chem. Commun.* **2016**, *52* (62), 9652.

(42) Rettig, W. *Angew. Chemie Int. Ed. English* **1986**, *25* (11), 971.

(43) Grabowski, Z. R.; Rotkiewicz, K.; Rettig, W. *Chem. Rev.* **2003**, *103* (10), 3899.

Chapter 3 : Conclusions and Future Work

Each imaging modality is able to provide some insight about disease. However, it is a combination of two or more modalities that can lead to an accurate diagnosis. Multi-modality imaging using hybrid-imaging platforms has been an alternative to address the inaccuracies of image fusion. While clinically available platforms such as PET/CT and SPECT/CT seek to acquire anatomical and functional information, the combination of modalities such as SPECT and optical imaging can be used to substantiate the results, due to their complimentary nature.

In vivo optical imaging is an emerging domain promising high resolution and high sensitivity of images while being non-invasive and cost effective. Major limitations of *in vivo* optical imaging are its limited depth of penetration and auto-fluorescence of cells in the visible spectrum of light. The use of near-infrared fluorescent tags has been instrumental in overcoming this restriction. Eventually, probes encompassing a radionuclide for SPECT imaging and near-infrared emitting dye have been envisioned as a dual-modality imaging probe for use in pre-operative diagnosis and intra-operative guidance[1–5]. Continuing efforts in this field have also sought to incorporate fluorophores to cater to other optical imaging methods including *ex vivo* imaging. d^6Metal-based systems have been receiving attention for their favourable properties such as resistance to photobleaching, large Stoke's shift and narrow emission bands. In addition, tunability of emission in combination with a variety of ligands and cellular uptake capability make them suitable for fluorescence microscopy and related applications[6–10]. Particularly, rhenium complexes are being explored due to their isostructural relationship with ^{99m}Tc complexes for developing multi-modality imaging probes[10,11].

Re(I) tricarbonyl complexes appended with a 1,8-naphthalimide derivative have been previously examined as cell imaging agents as well as potential SPECT/fluorescence imaging agents for CXCR4 targeted imaging[12–14]. Based on the structure of dual-imaging probes, the linker that connects the two imaging entities can be exploited to modulate the pharmacokinetics of the imaging probe. In addition, length, flexibility and lipophilicity of the linker can be used to fine-tune the photophysical properties[15].

In this work, we designed 1,8-naphthalimide based imaging agents to examine the effect of extended π-conjugation and rigidity on their photophysical properties. Absorption and fluorescence spectra as well as absolute quantum yield measurements of all the synthesized ligands and their Re(I)tricarbonyl complexes were obtained. In comparison to previously reported derivatives, the inclusion of rigid linkers resulted in large Stoke's shift. Due to the lowering of HOMO-LUMO gap in π-conjugated systems, emissions of longer wavelength were anticipated. In contrast, all emission and excitation maxima values were found to be in the shorter wavelengths. This can be attributed to the fact that the ICT transitions in these systems are more influenced by the electron-donating capacity of the substituents than the extension of π-conjugation[16]. Lower quantum yield may be due to the possibility of twisted ICT excited states in 1,8-naphthalimide derivatives containg two π-systems[17,18].

Current fluorescence imaging platforms utilize excitations in the range of visible light. Thus, it can be inferred that some of the newly synthesized naphthalimide derivatives which need to be excited at wavelengths below 400 nm may not be useful in fluorescence imaging. However, derivatives with excitation wavelengths of 418 nm have potential applications in cell imaging. Successful formation of the rhenium complexes suggests the possibility of radiolabelling with ^{99m}Tc to study the biodistribution of the probes when administered in an animal model.

Future work involving these 1,8-naphthalimide derivatives will focus on obtaining the crystal structures of the rhenium complexes to study the orientation of the linkers with respect to the naphthalimide entity. This will allow us to confirm the possibility of TICT excited states and correlate its effect to the measured photophysical properties. Further, lipophilicity and cell uptake studies will be carried out with suitable derivatives to establish the effect of lipophilicity on the linkers. Radiolabelling with ^{99m}Tc will be attempted to examine the suitability as SPECT tracers.

3.1 References

(1) Rijpkema, M.; Oyen, W. J.; Bos, D.; Franssen, G. M.; Goldenberg, D. M.; Boerman, O. C. *J. Nucl. Med.* **2014**, *55* (9), 1519 LP.

(2) Liu, C.; Zhang, X.; Song, Y.; Wang, Y.; Zhang, F.; Zhang, Y.; Zhang, Y.; Lan, X. *Atherosclerosis* **2016**, *254*, 263.

(3) Feng, G.-K.; Liu, R.-B.; Zhang, M.-Q.; Ye, X.-X.; Zhong, Q.; Xia, Y.-F.; Li, M.-Z.; Wang, J.; Song, E.-W.; Zhang, X.; Wu, Z.-Z.; Zeng, M.-S. *J. Control. Release* **2014**, *192*, 236.

(4) Welling, M. M.; Bunschoten, A.; Kuil, J.; Nelissen, R. G. H. H.; Beekman, F. J.; Buckle, T.; van Leeuwen, F. W. B. *Bioconjug. Chem.* **2015**, *26* (5), 839.

(5) Hekman, M. C. H.; Rijpkema, M.; Bos, D. L.; Oosterwijk, E.; Goldenberg, D. M.; Mulders, P. F. A.; Boerman, O. C. *J. Nucl. Med.* **2017**, *58* (5), 706.

(6) Haas, K. L.; Franz, K. J. *Chem. Rev.* **2009**, *109* (10), 4921.

(7) Patra, M.; Gasser, G. *ChemBioChem* **2012**, *13* (9), 1232.

(8) Li, K.-B.; Chen, F.-Z.; Zhang, S.; Shi, W.; Han, D.-M.; Cai, C.; Chen, C.-X. *Anal. Methods* **2017**, *9* (45), 6443.

(9) Li, C.; Yu, M.; Sun, Y.; Wu, Y.; Huang, C.; Li, F. *J. Am. Chem. Soc.* **2011**, *133* (29), 11231.

(10) Lee, L. C.-C.; Leung, K.-K.; Lo, K. K.-W. *Dalt. Trans.* **2017**, *46* (47), 16357.

(11) Ranasinghe, K.; Handunnetti, S.; Perera, I. C.; Perera, T. *Chem. Cent. J.* **2016**, *10*, 71.

(12) Langdon-Jones, E. E.; Symonds, N. O.; Yates, S. E.; Hayes, A. J.; Lloyd, D.;

Williams, R.; Coles, S. J.; Horton, P. N.; Pope, S. J. A. *Inorg. Chem.* **2014**, *53* (7), 3788.

(13) Turnbull, W. L.; Yu, L.; Murrell, E.; Milne, M.; Charron, C. L.; Luyt, L. G. *Org. Biomol. Chem.* **2019**, *17* (3), 598.

(14) Turnbull, W. L.; Murrell, E.; Bulcan-gnirss, M.; Majeed, M.; Milne, M.; Luyt, L. G. *Dalt. Trans.* **2019**, *48* (37), 14077.

(15) Day, A. H.; Domarkas, J.; Nigam, S.; Renard, I.; Cawthorne, C.; Burke, B. P.; Bahra, G. S.; Oyston, P. C. F.; Fallis, I. A.; Archibald, S. J.; Pope, S. J. A.; Martorana, A.; Yang, Y.; Zhao, Y.; Li, Q.; Su, X.; Goldfarb, D. *Dalt. Trans.* **2020**, *1* (II), 511.

(16) Rémy, C.; Allain, C.; Leray, I. *Photochem. Photobiol. Sci.* **2017**, *16* (4), 539.

(17) Rettig, W. *Angew. Chemie Int. Ed. English* **1986**, *25* (11), 971.

(18) Grabowski, Z. R.; Rotkiewicz, K.; Rettig, W. *Chem. Rev.* **2003**, *103* (10), 3899.

Appendices

Appendix A : ^{1}H and ^{13}C NMR Spectroscopy Data of Synthesized Compounds

^{1}H NMR spectrum (400 MHz; $CDCl_3$) of **1**

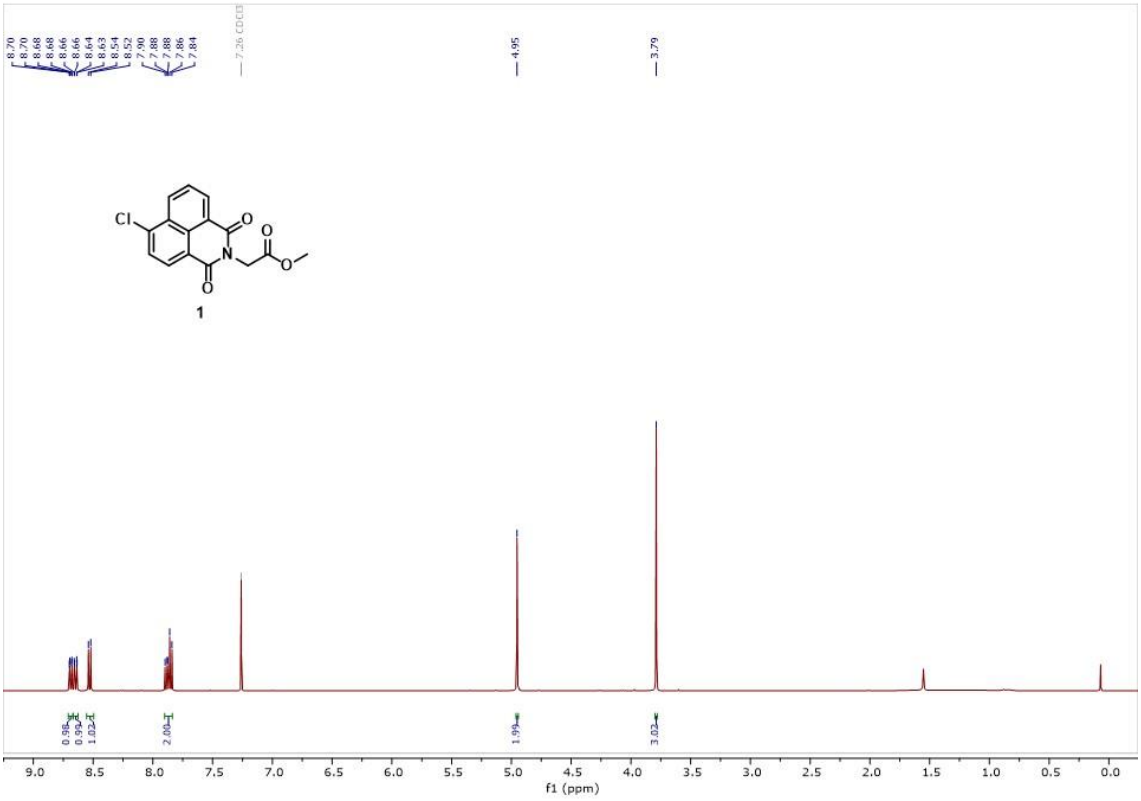

^{13}C NMR spectrum (100 MHz; $CDCl_3$) of **1**

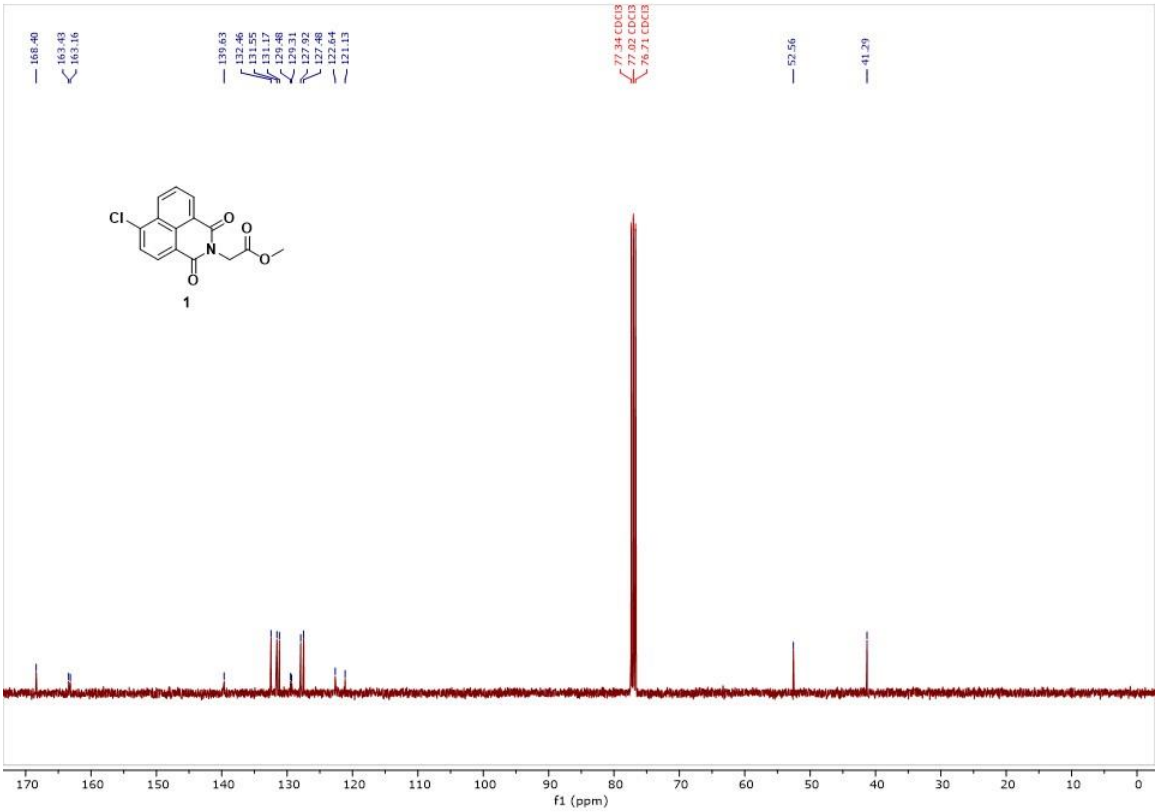

^{1}H NMR spectrum (400 MHz; $CDCl_3$) of **2**

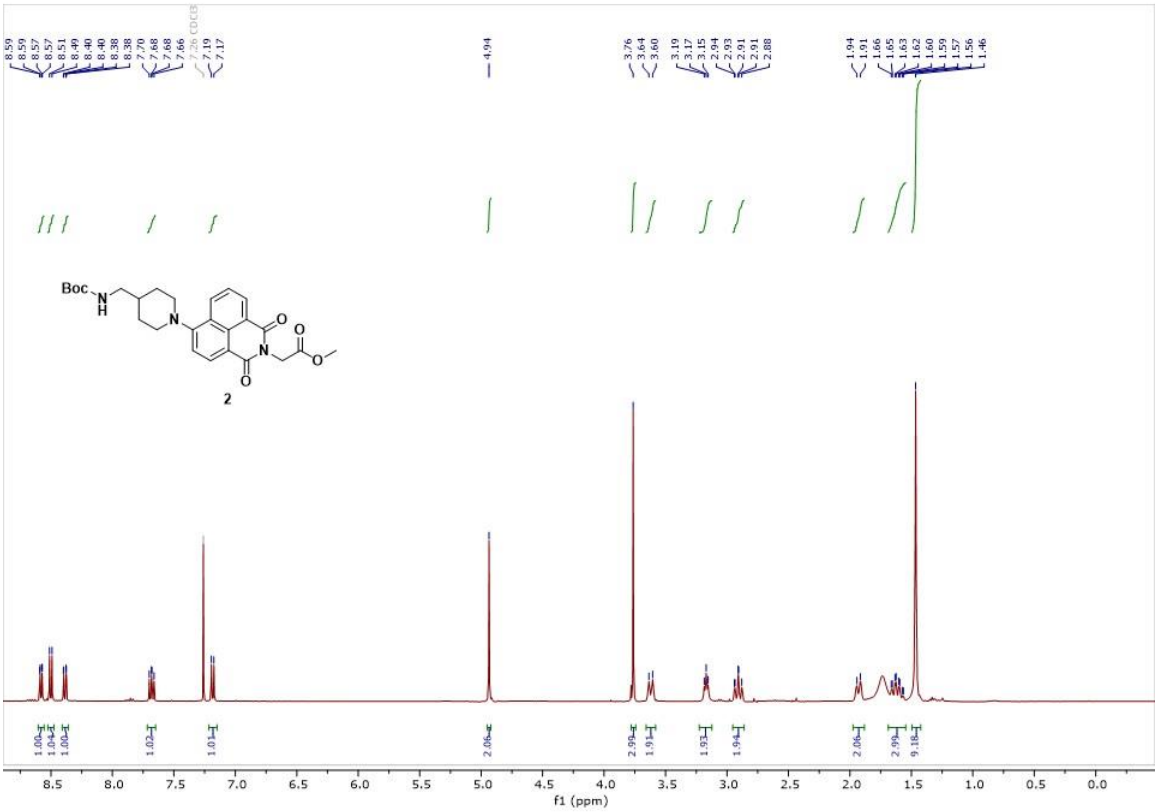

^{13}C NMR spectrum (100 MHz; $CDCl_3$) of **2**

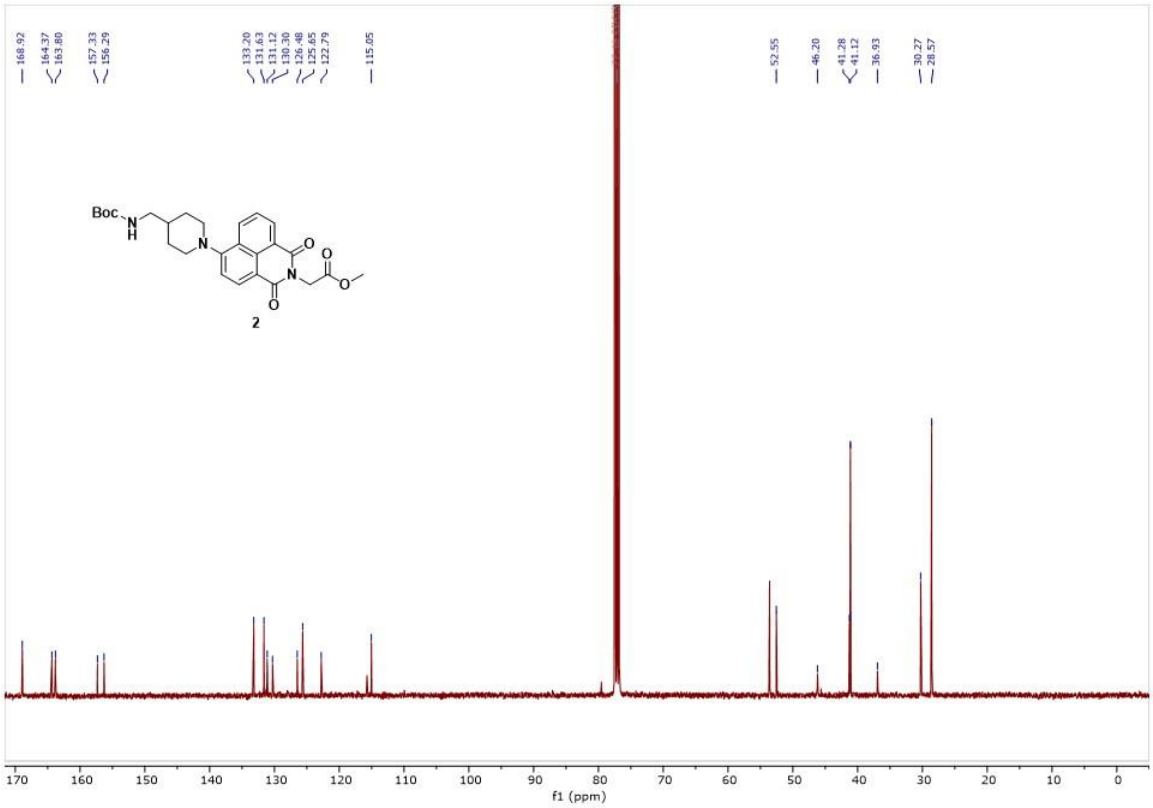

^{1}H NMR spectrum (400 MHz; $CDCl_3$) of **3**

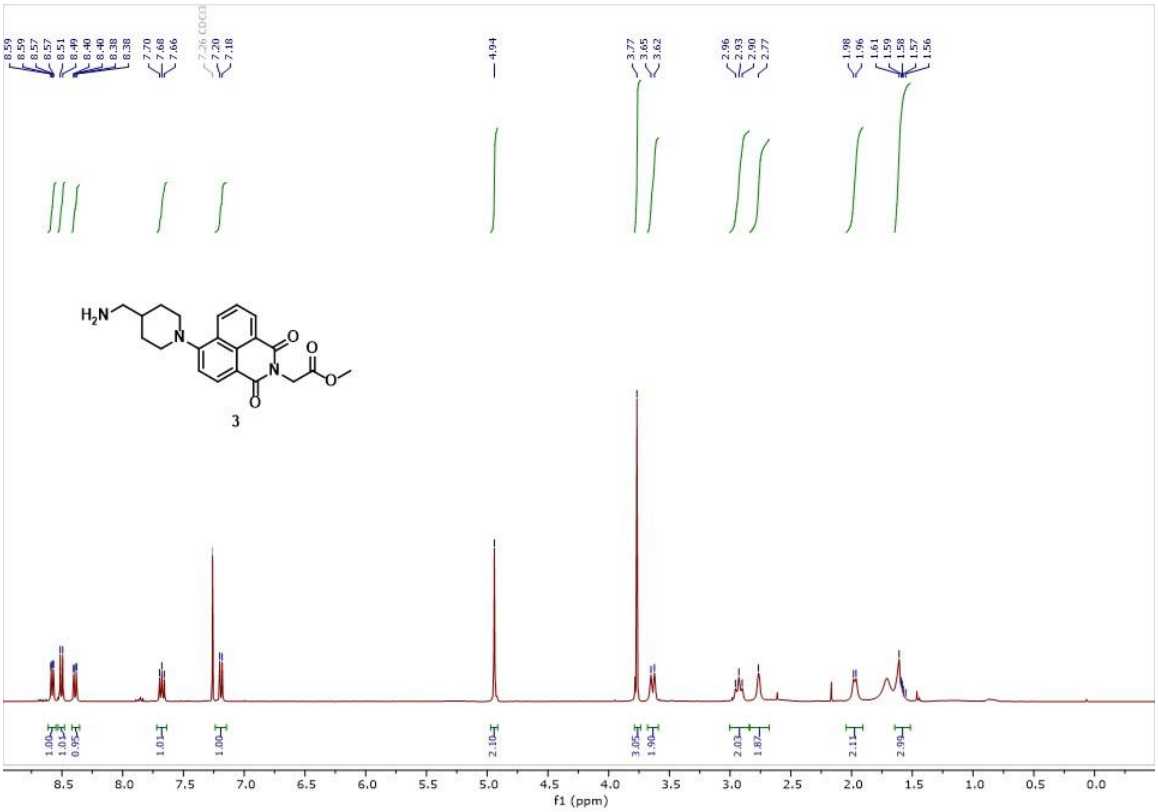

^{13}C NMR spectrum (100 MHz; $CDCl_3$) of **3**

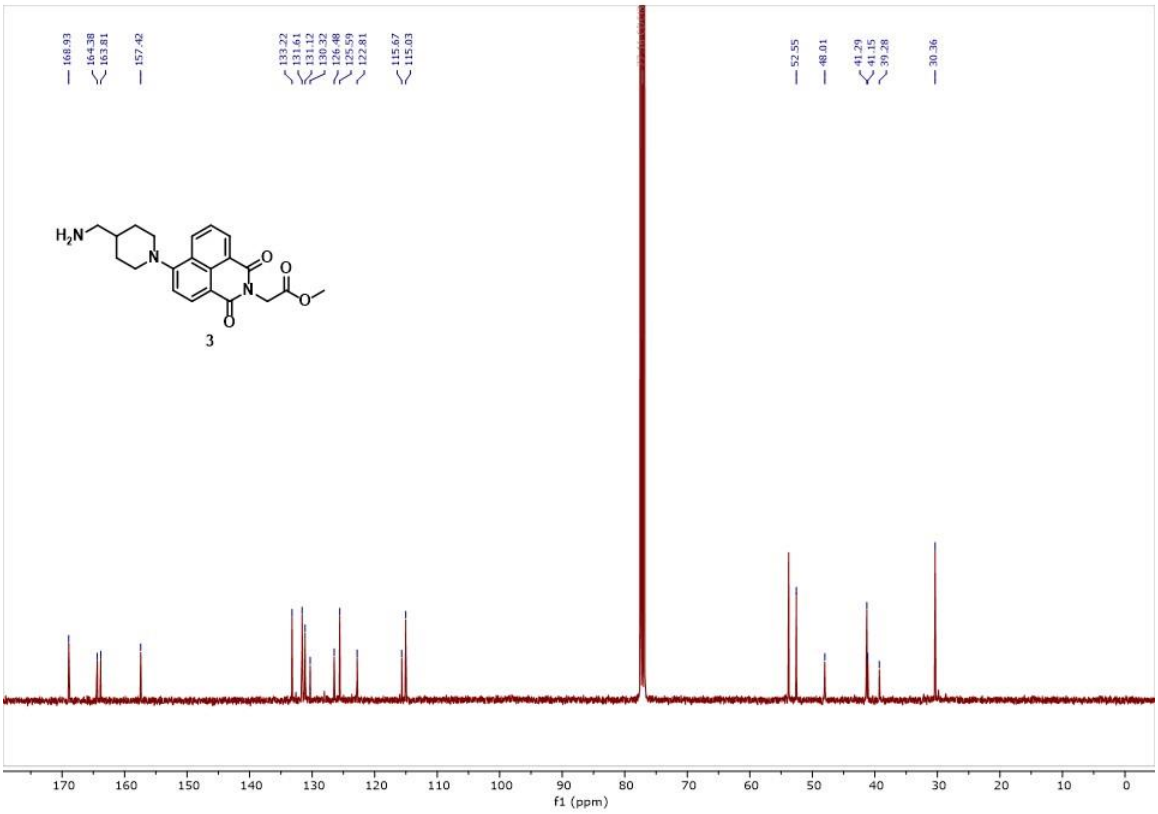

^{1}H NMR spectrum (400 MHz; $CDCl_3$) of **L_1**

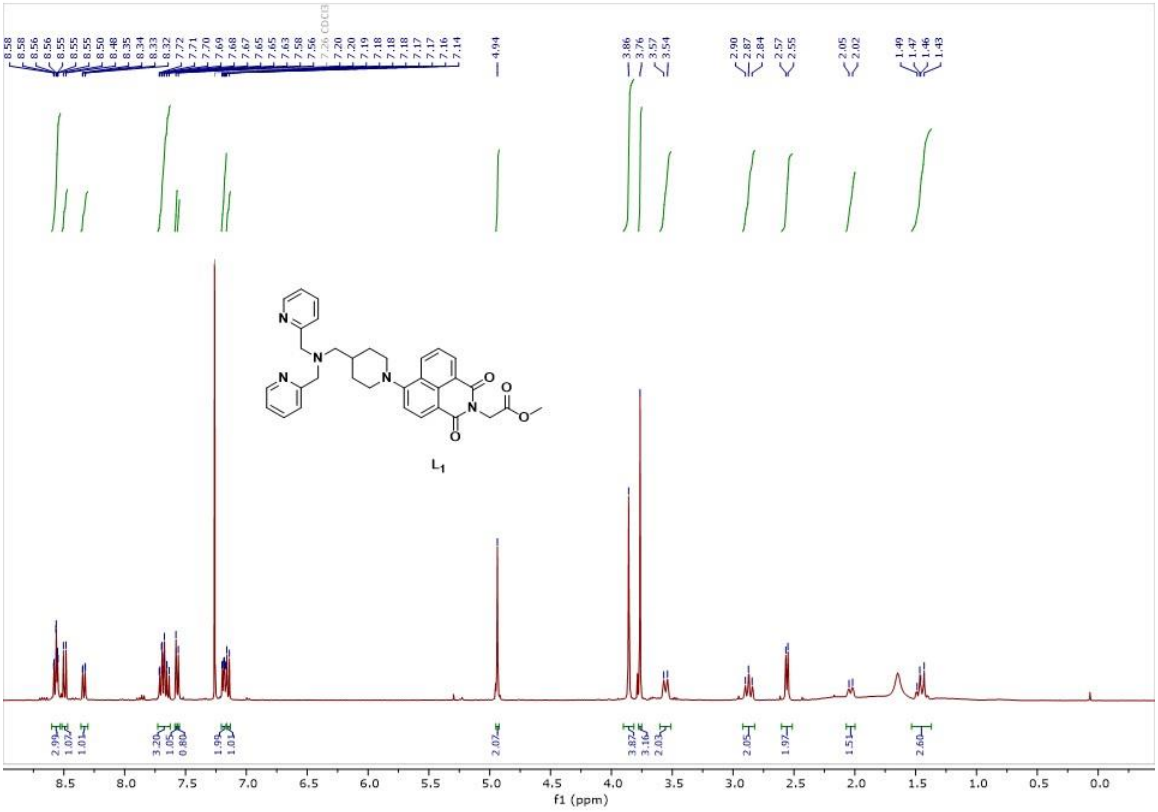

^{13}C NMR spectrum (100 MHz; $CDCl_3$) of **L_1**

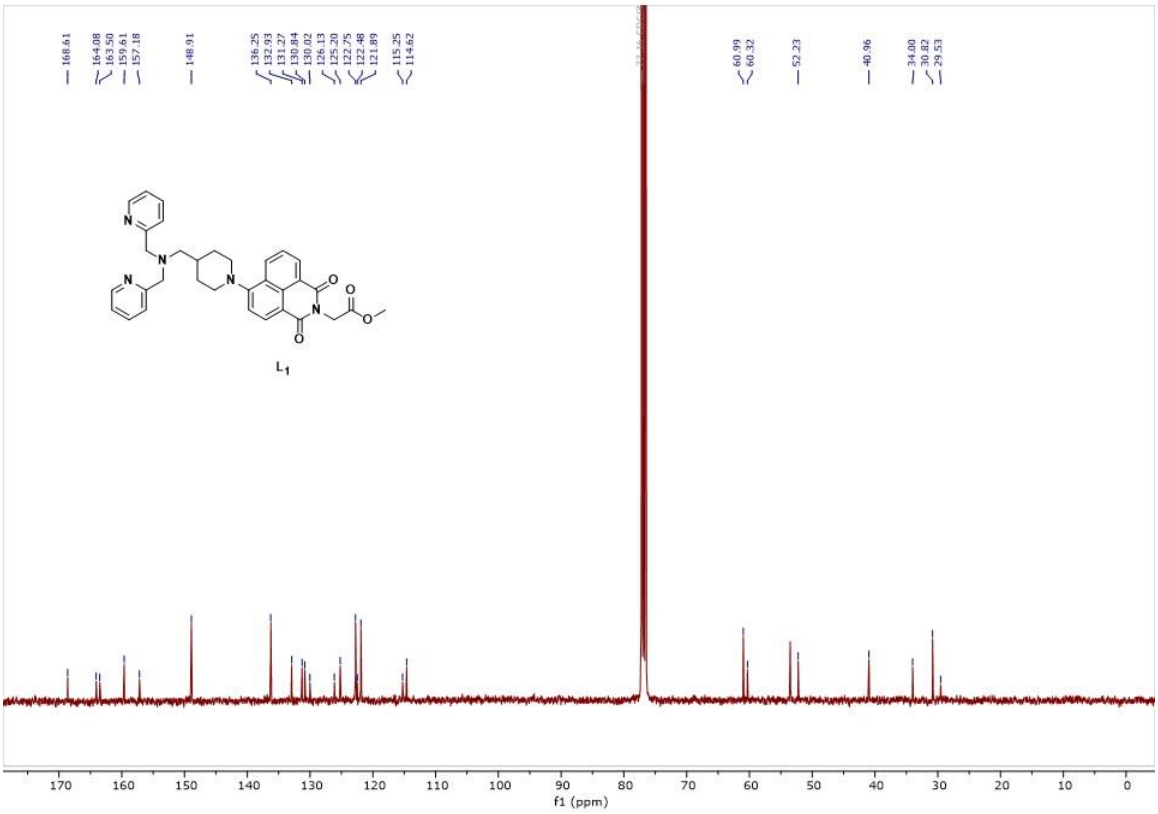

^{1}H NMR spectrum (400 MHz; $CDCl_3$) of **5**

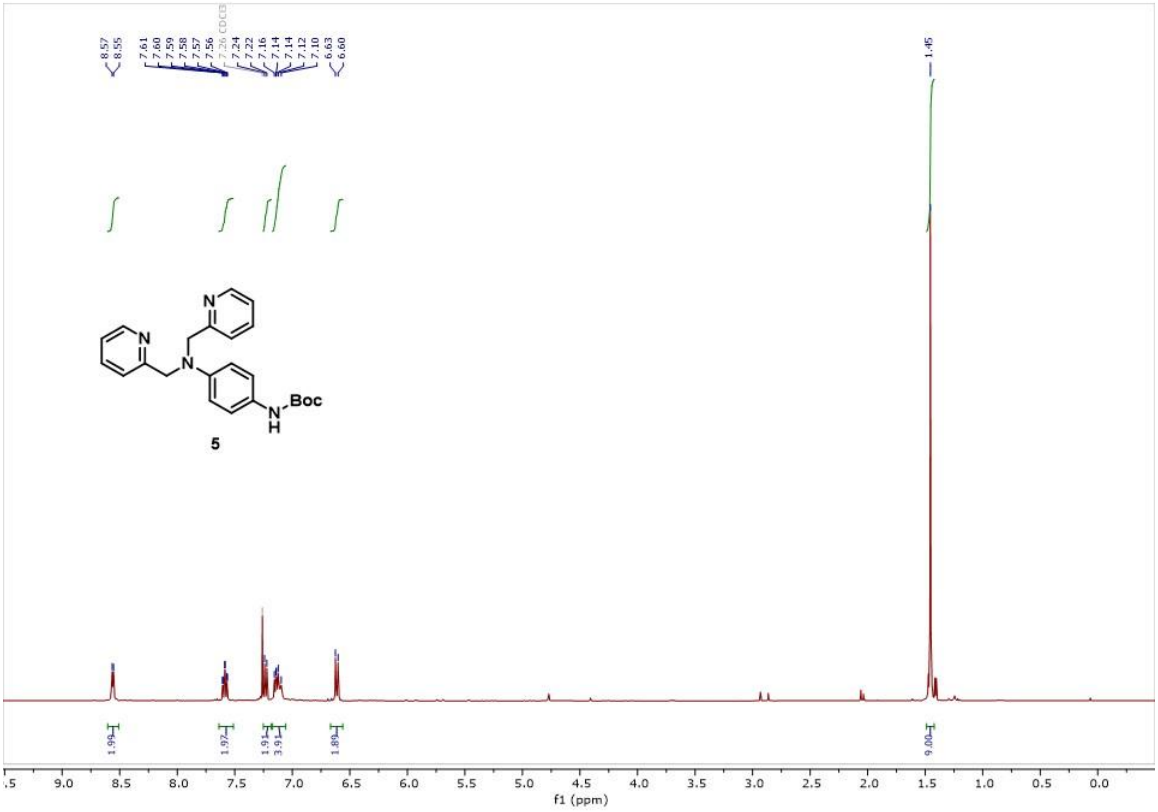

^{13}C NMR spectrum (100 MHz; $CDCl_3$) of **5**

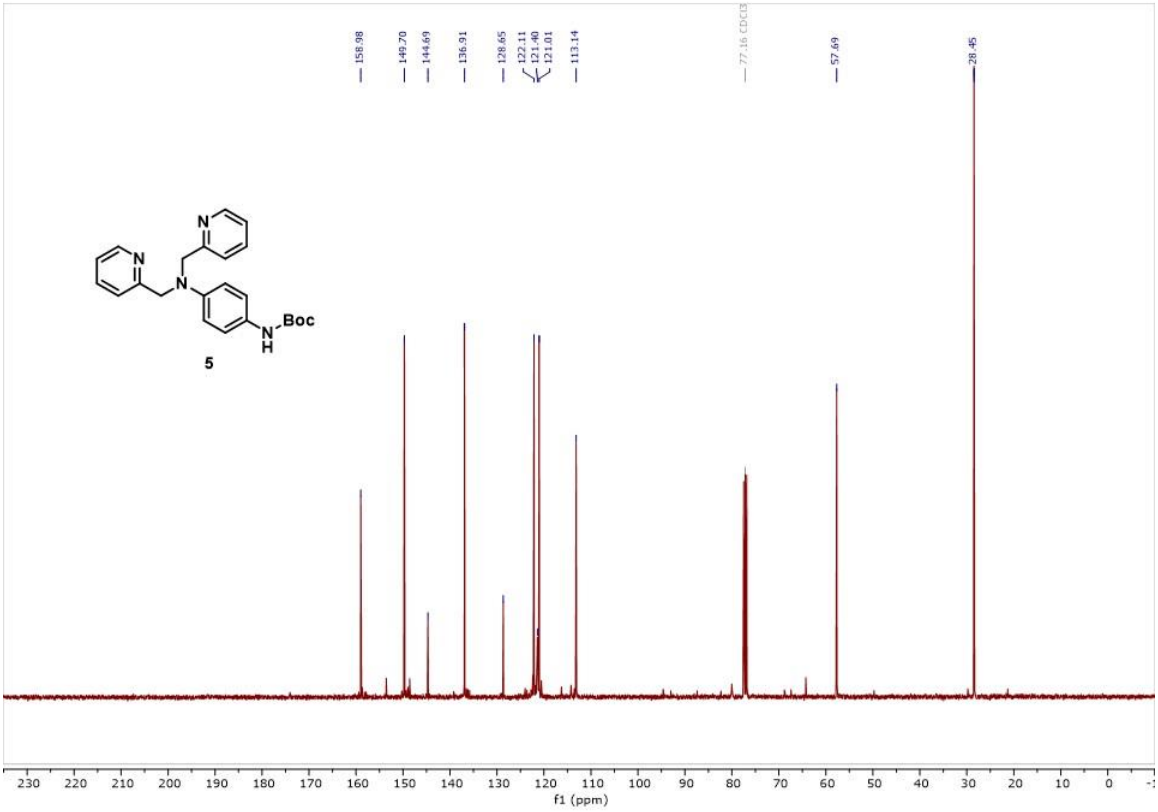

^{1}H NMR spectrum (400 MHz; $CDCl_3$) of **6**

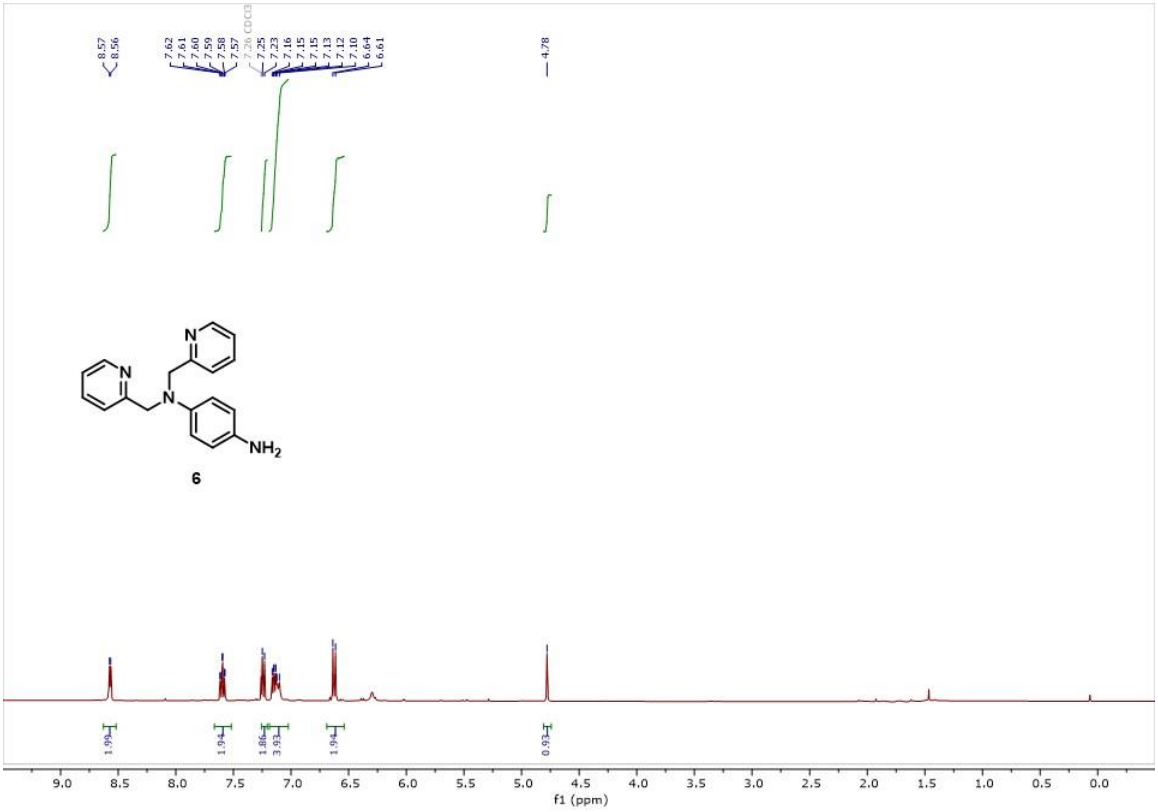

^{13}C NMR spectrum (100 MHz; $CDCl_3$) of **6**

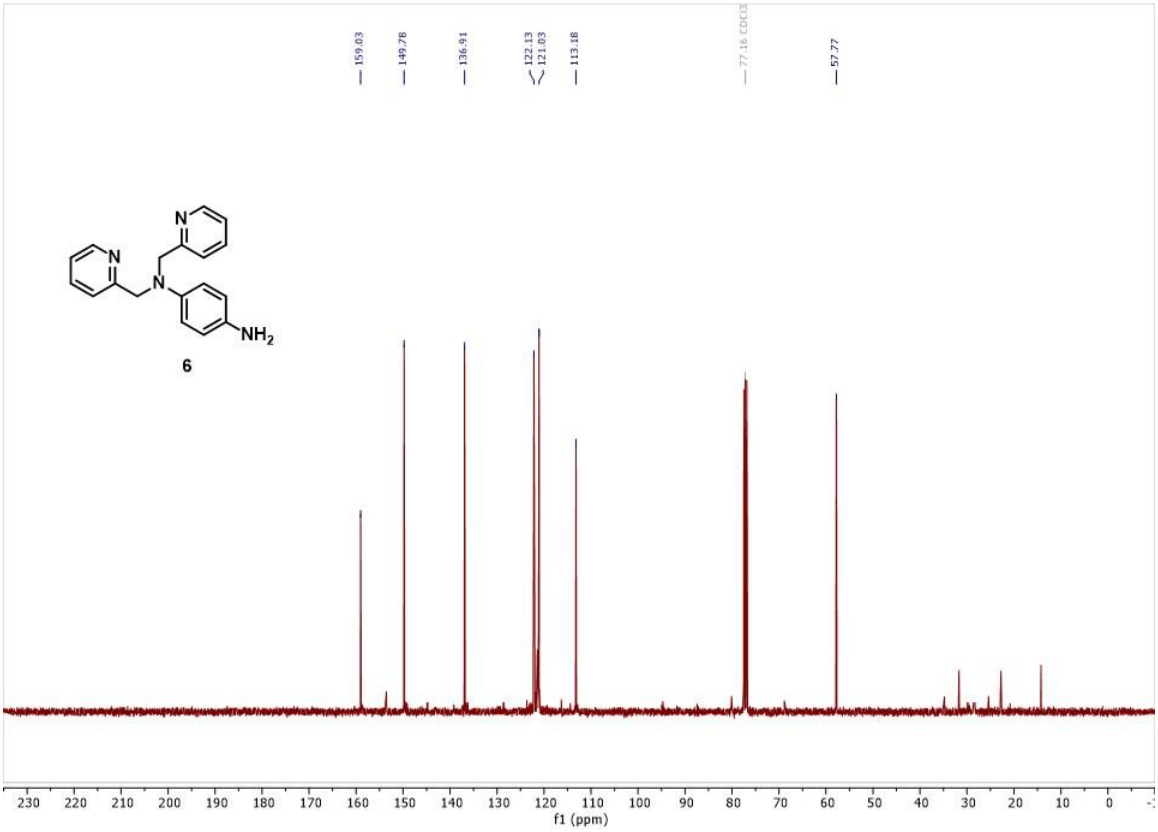

^{1}H NMR spectrum (400 MHz; $CDCl_3$) of **12**

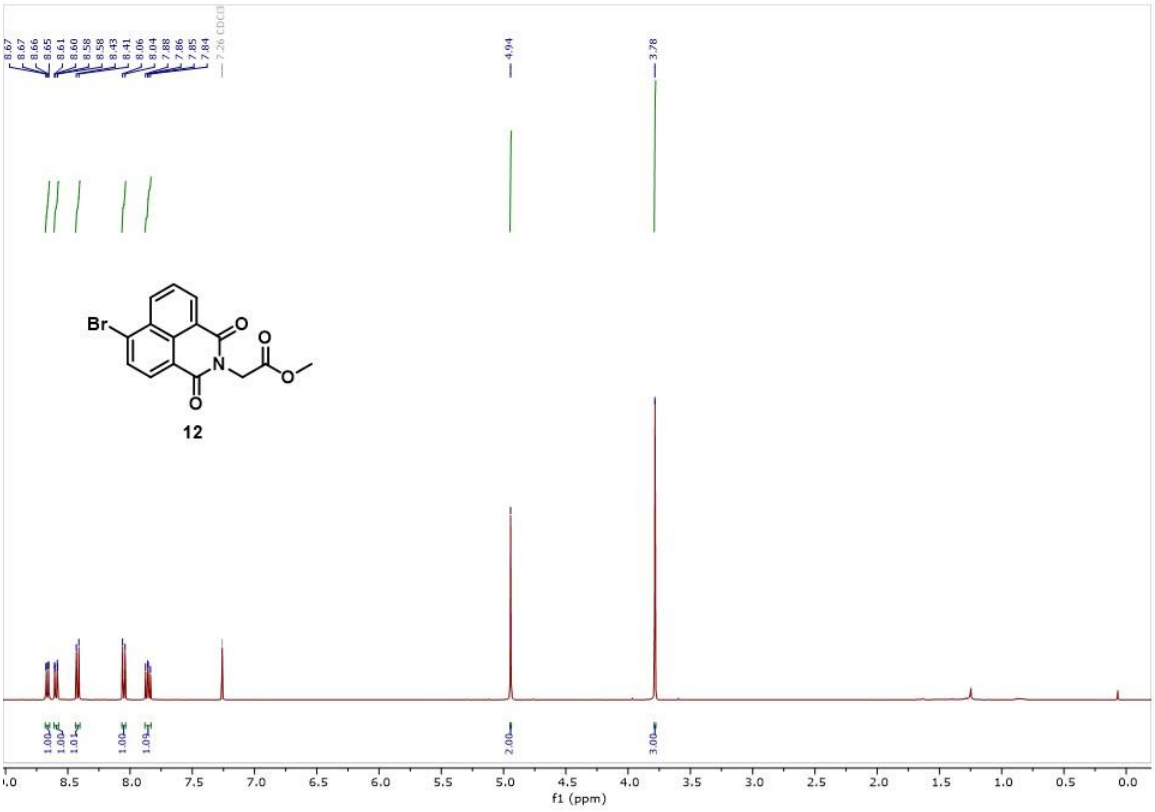

^{13}C NMR spectrum (100 MHz; $CDCl_3$) of **12**

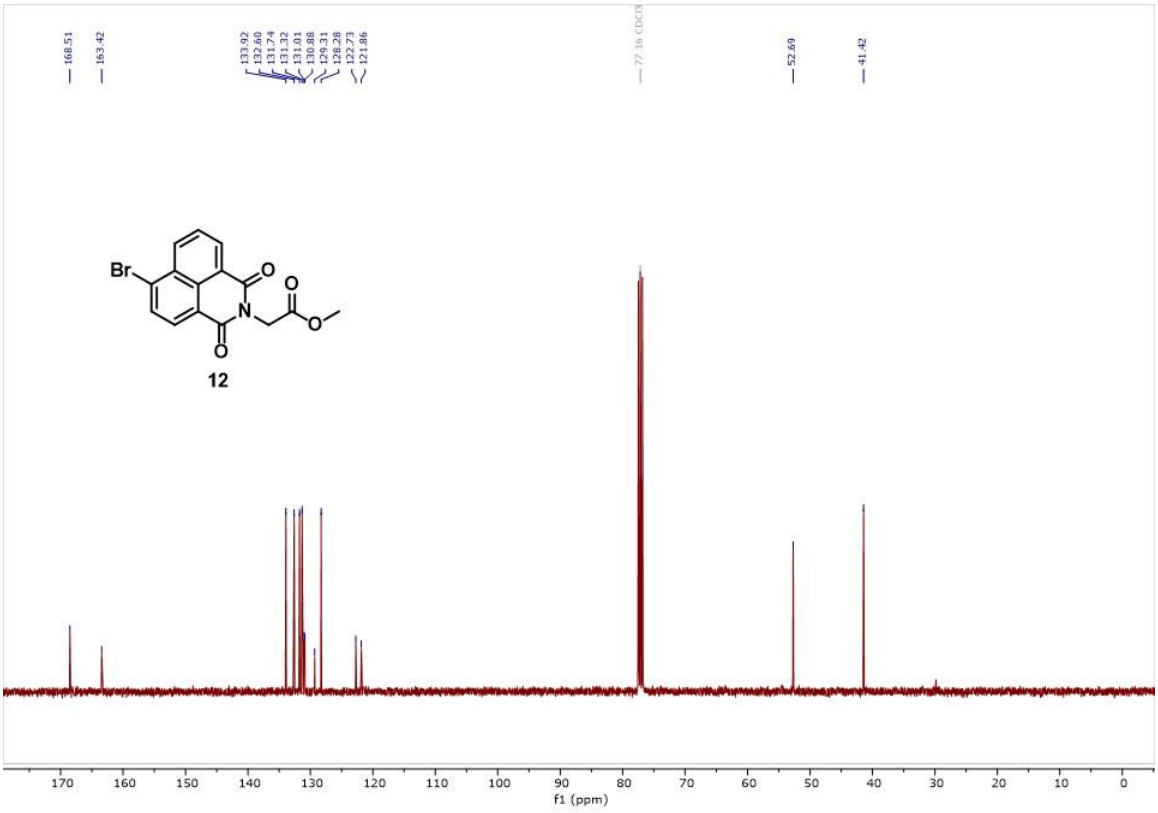

^{1}H NMR spectrum (400 MHz; $CDCl_3$) of **L_2**

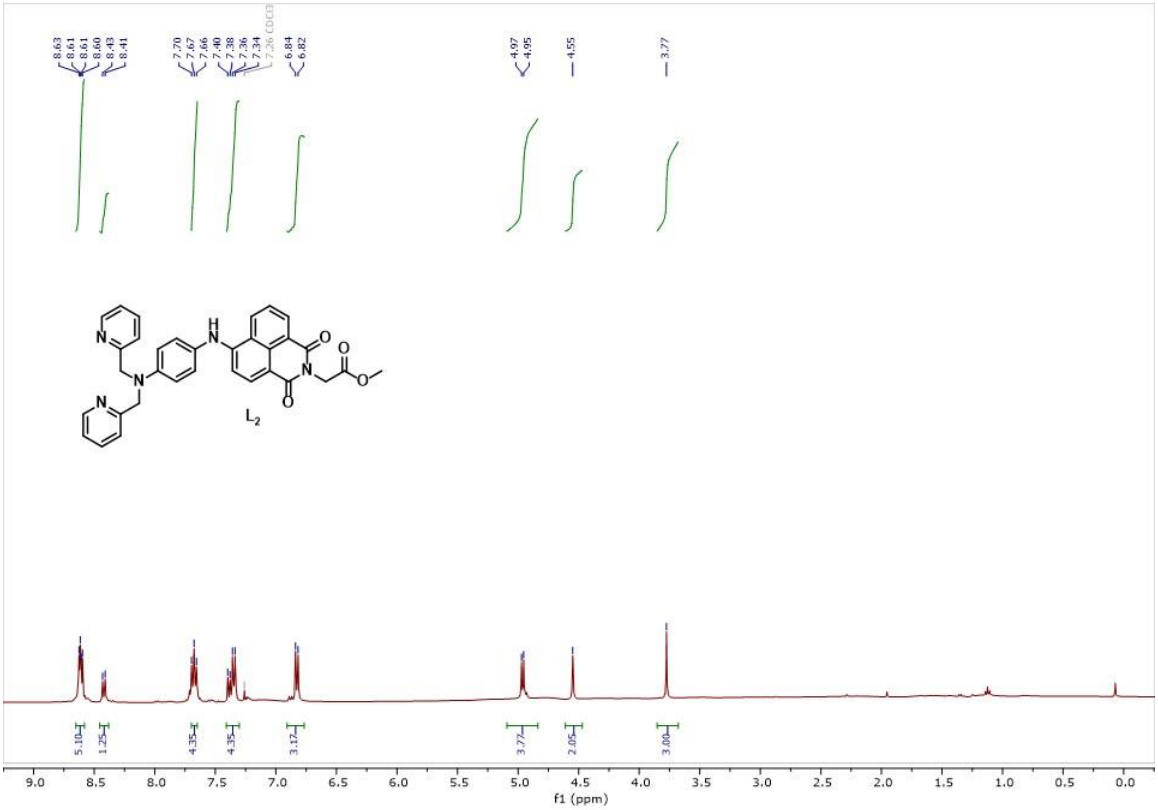

^{13}C NMR spectrum (100 MHz; $CDCl_3$) of **L_2**

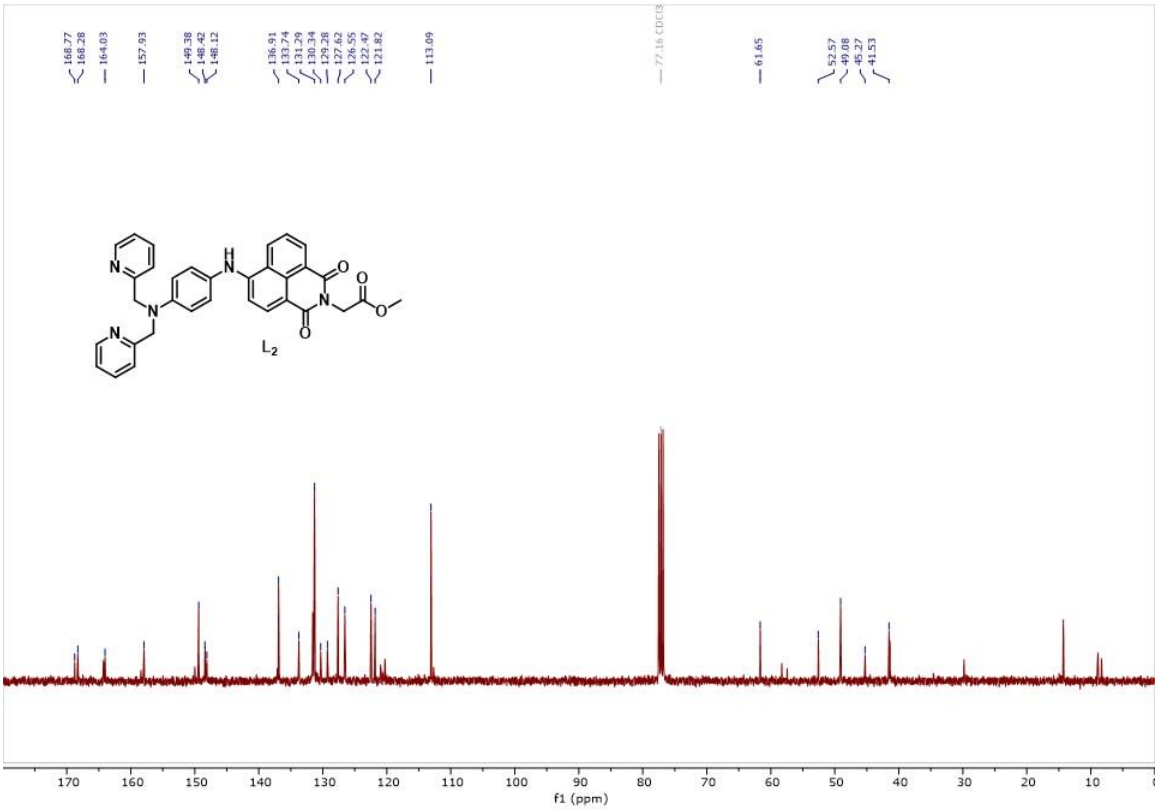

^{1}H NMR spectrum (400 MHz; $CDCl_3$) of **13**

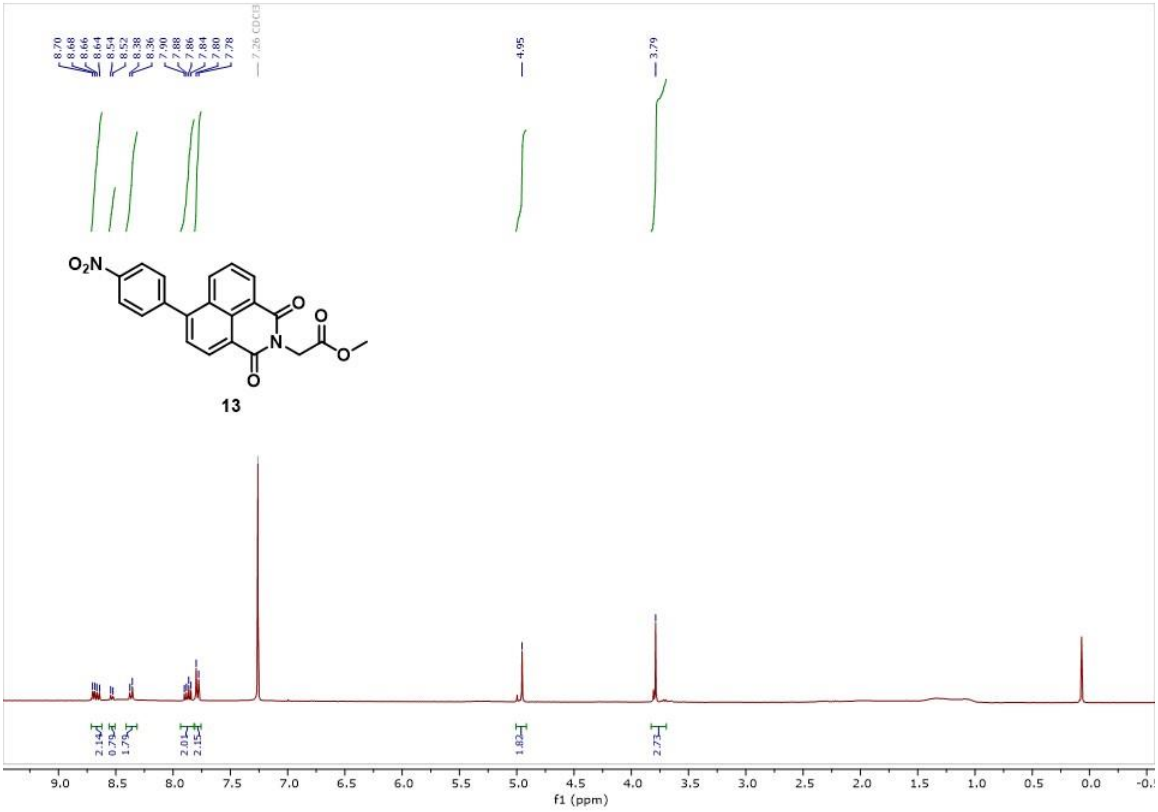

^{13}C NMR spectrum (100 MHz; $CDCl_3$) of **13**

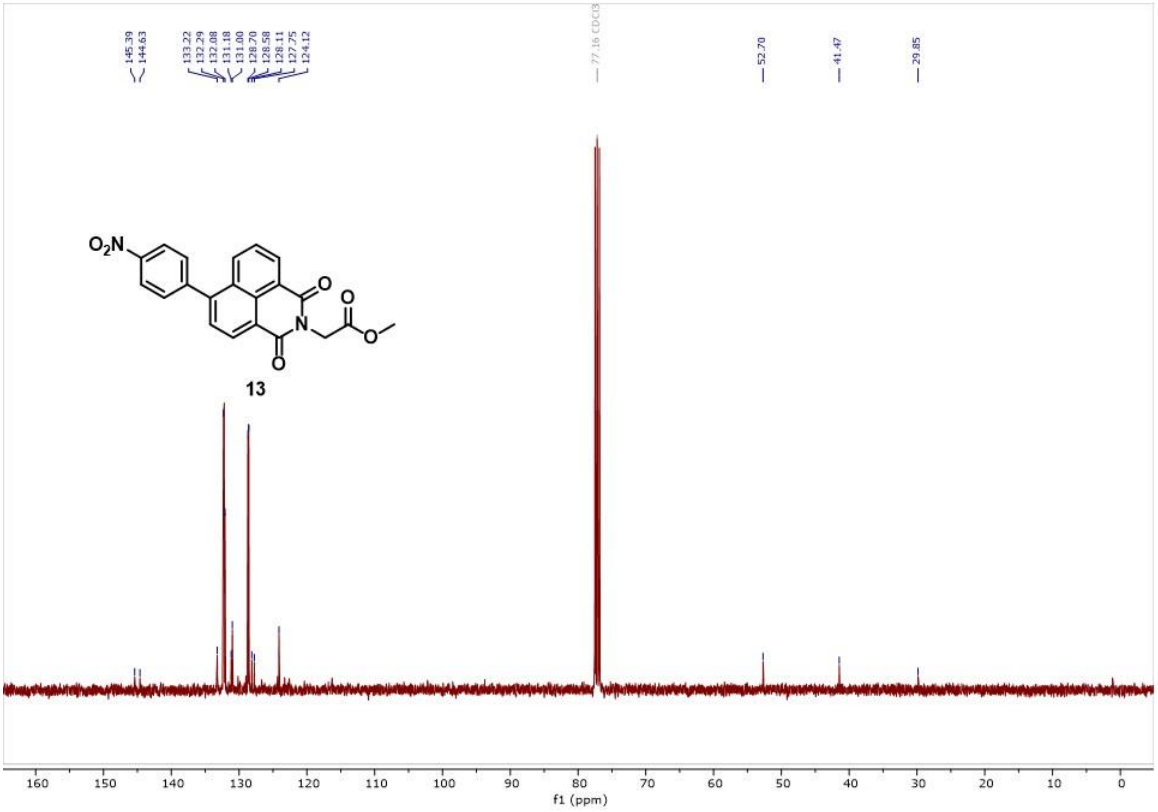

^{1}H NMR spectrum (400 MHz; $CDCl_3$) of reduction product of **13**

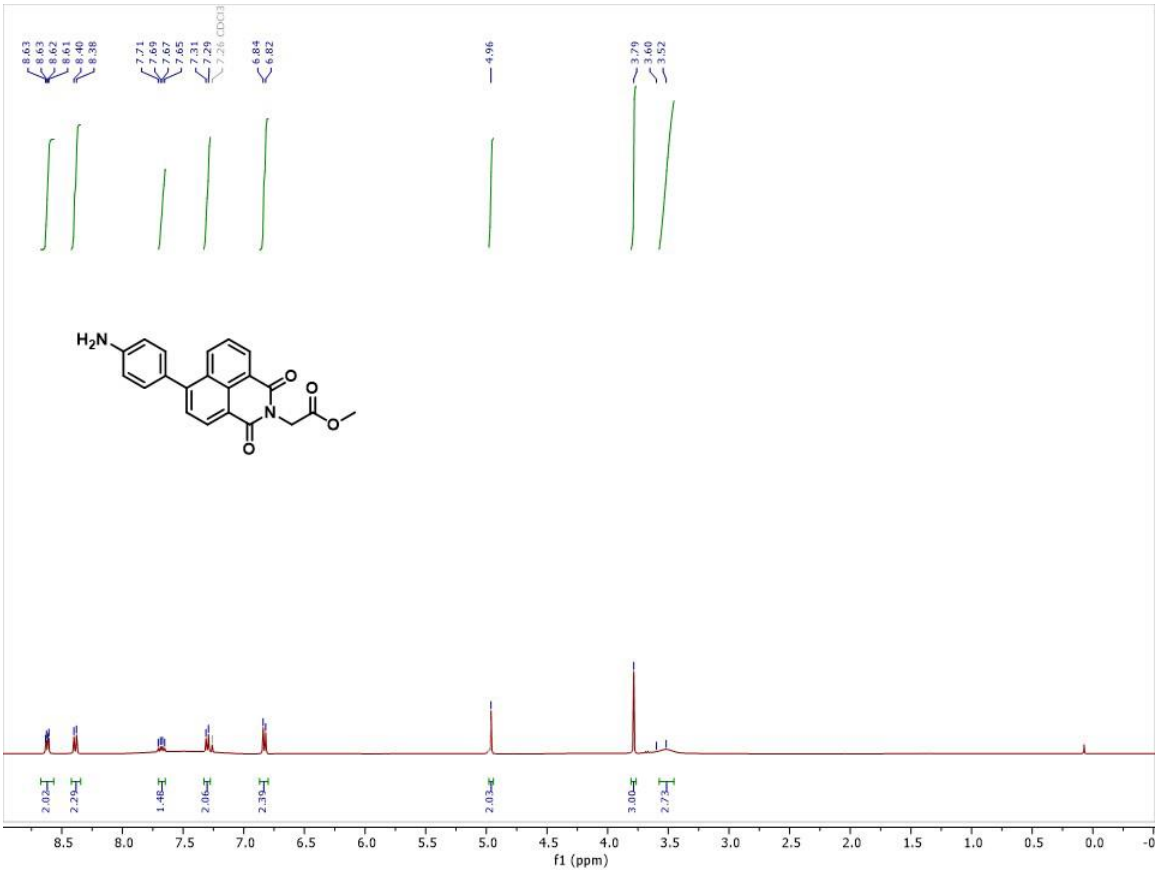

^{13}C NMR spectrum (100 MHz; $CDCl_3$) of reduction product of **13**

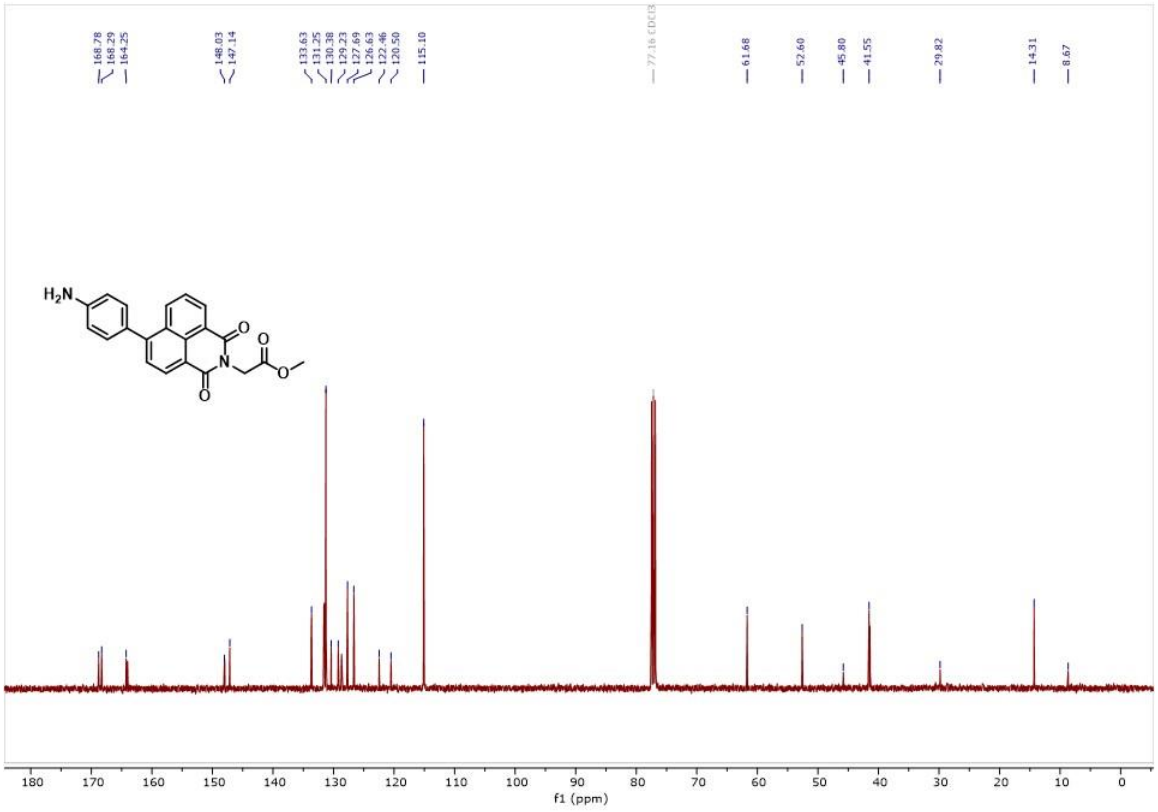

^{1}H NMR spectrum (400 MHz; $CDCl_3$) of **L_3**

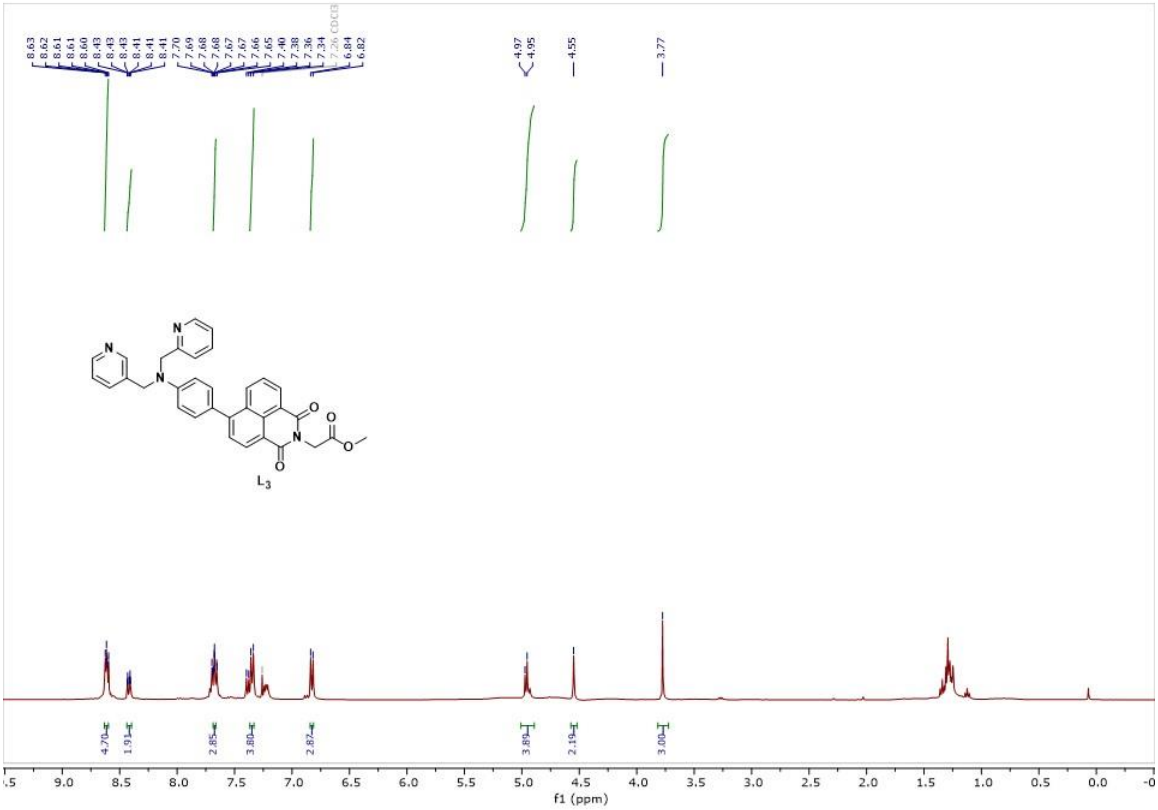

^{13}C NMR spectrum (100 MHz; $CDCl_3$) of **L_3**

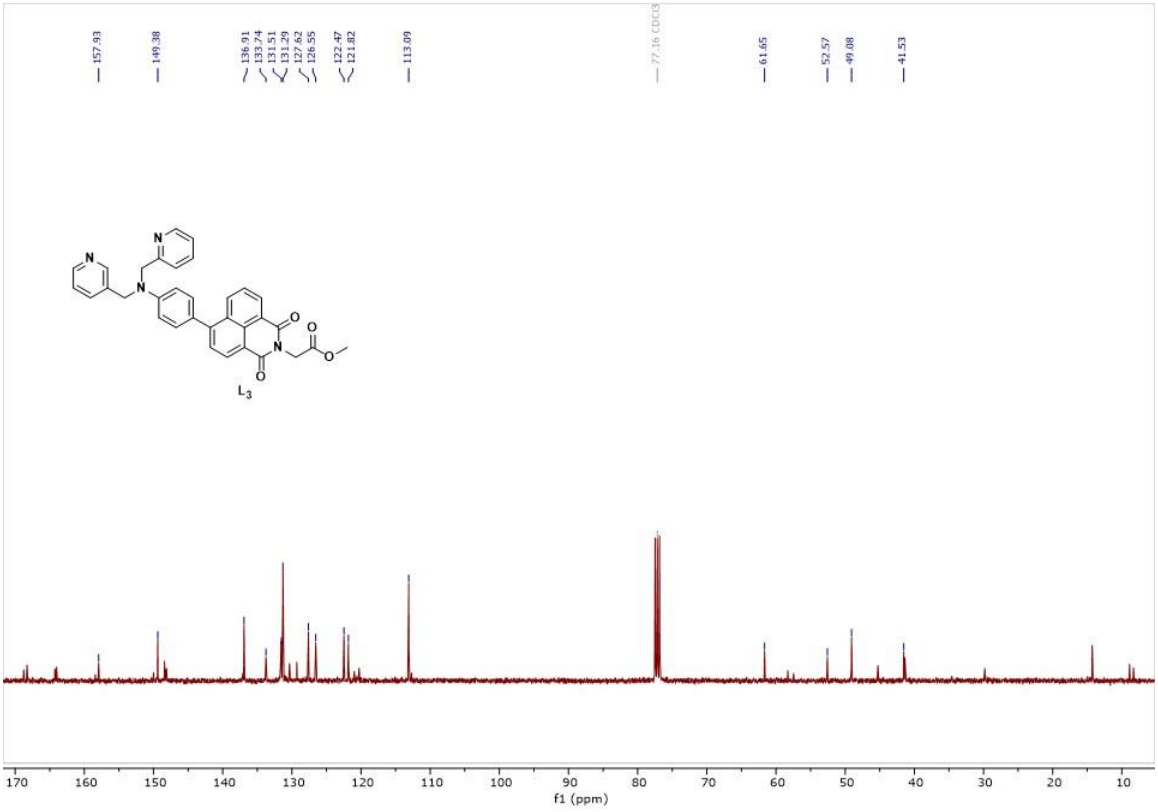

^{1}H NMR spectrum (400 MHz; $CDCl_3$) of **14**

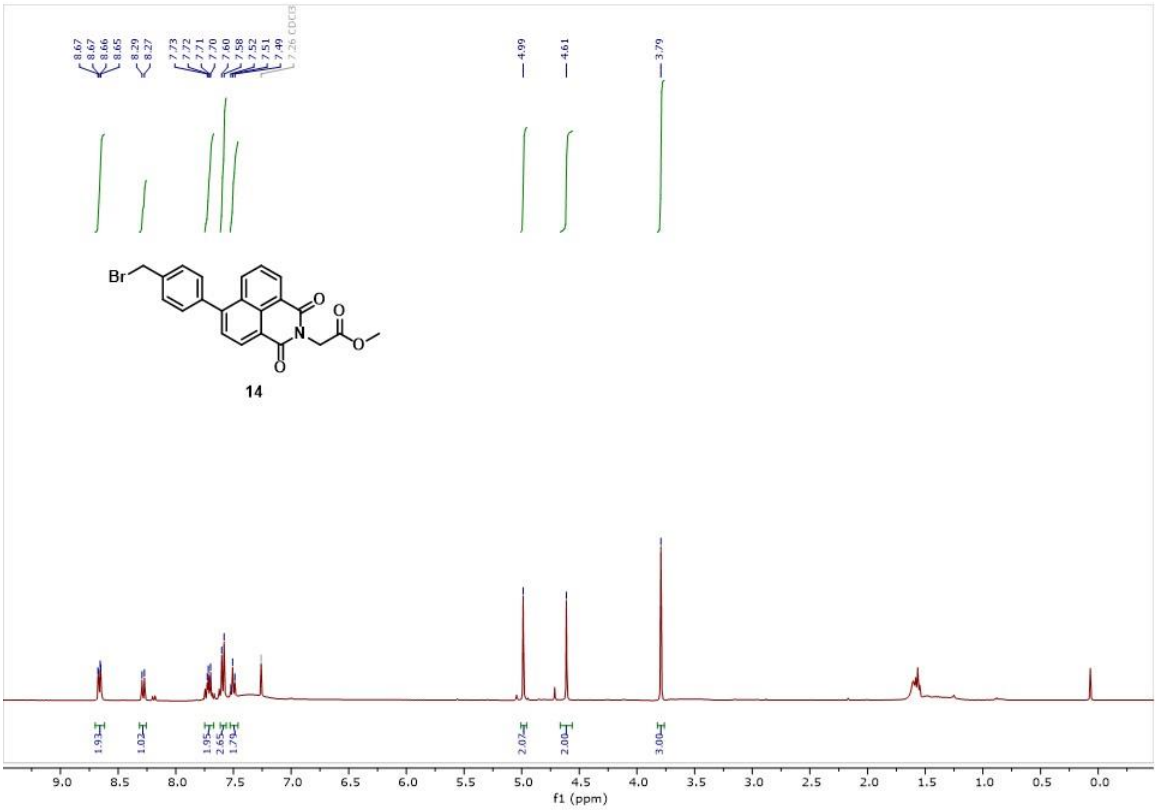

^{13}C NMR spectrum (100 MHz; $CDCl_3$) of **14**

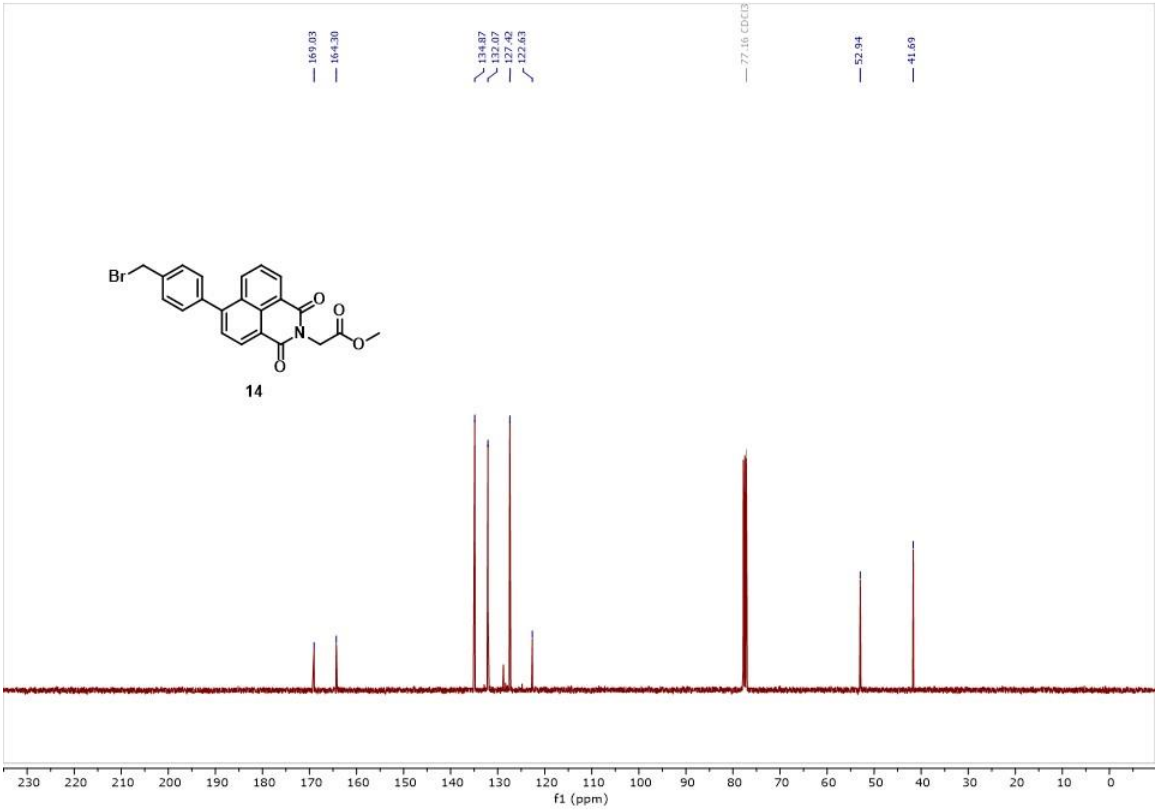

^{1}H NMR spectrum (400 MHz; $CDCl_3$) of **L_4**

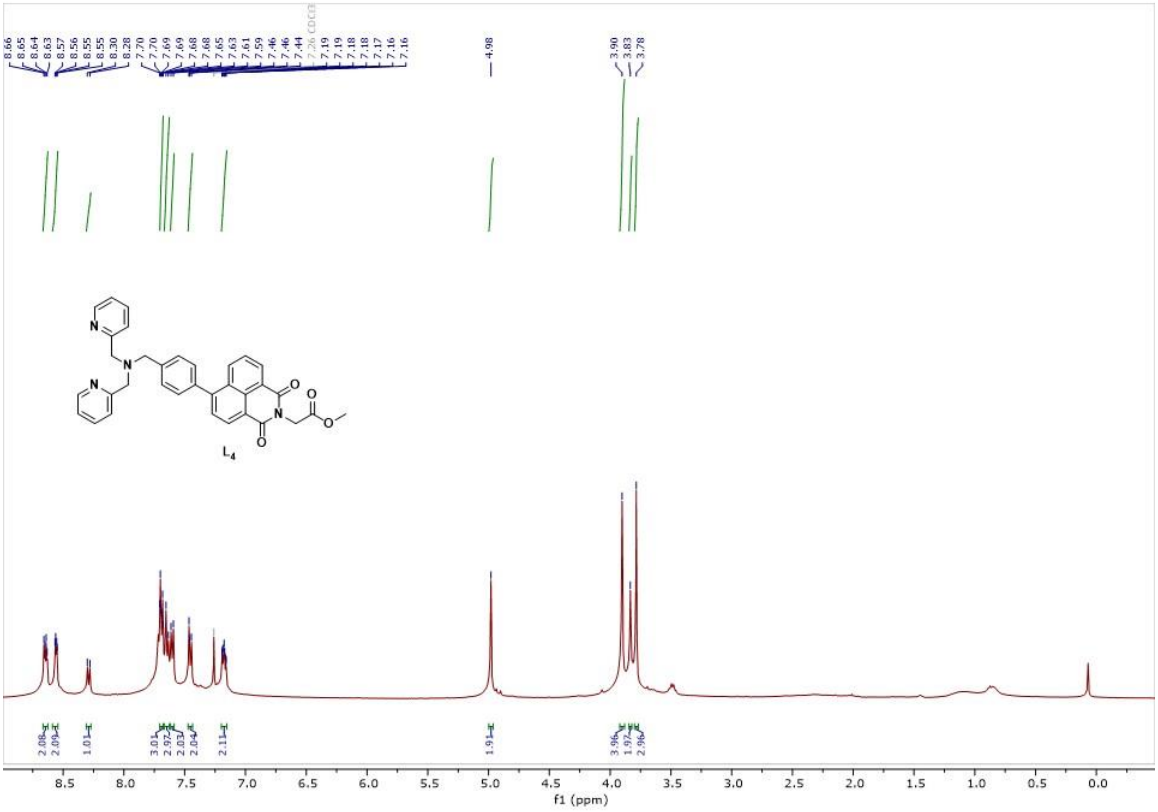

^{13}C NMR spectrum (100 MHz; $CDCl_3$) of **L_4**

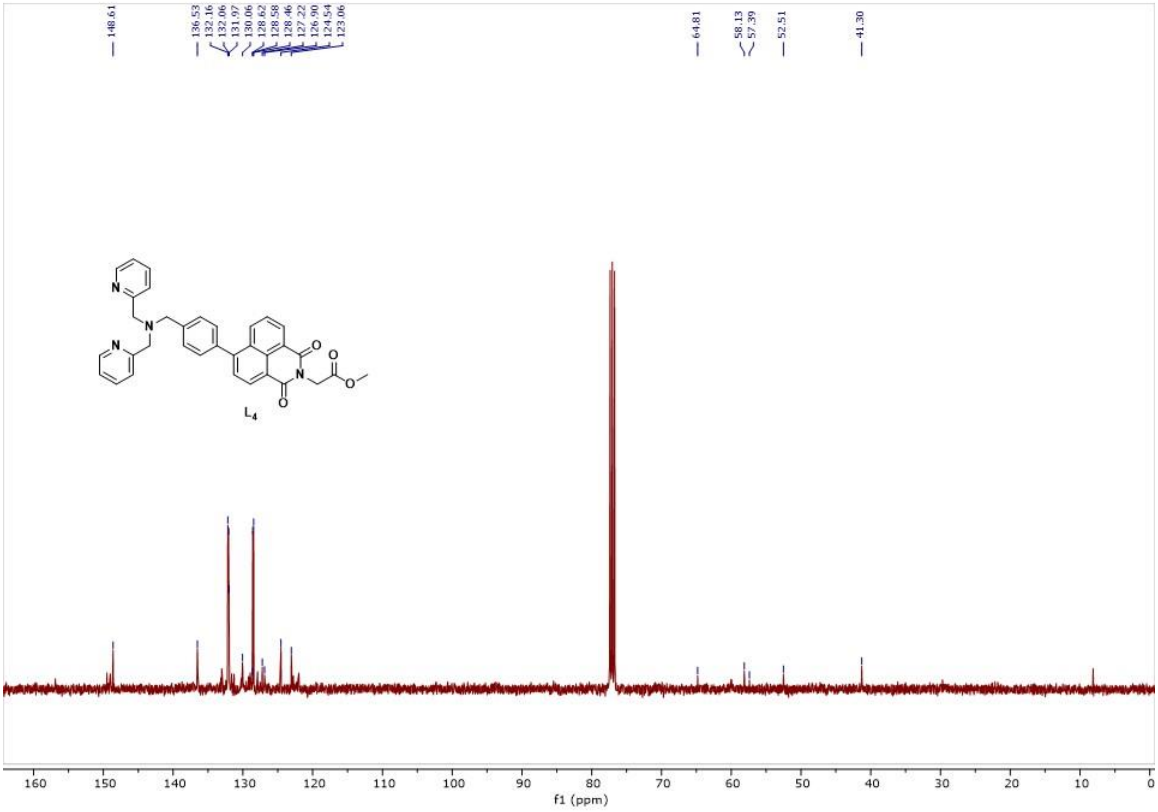

^{1}H NMR spectrum (400 MHz; $CDCl_3$) of **L_6**

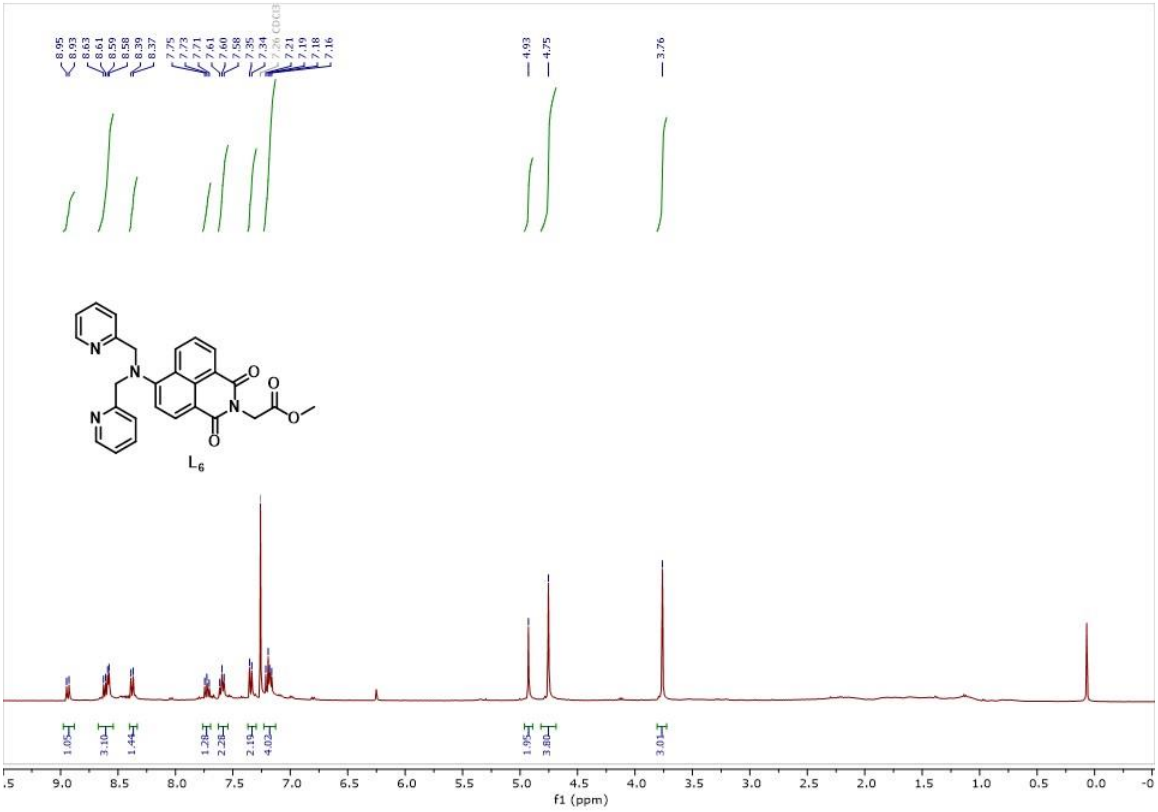

^{13}C NMR spectrum (100 MHz; $CDCl_3$) of **L_6**

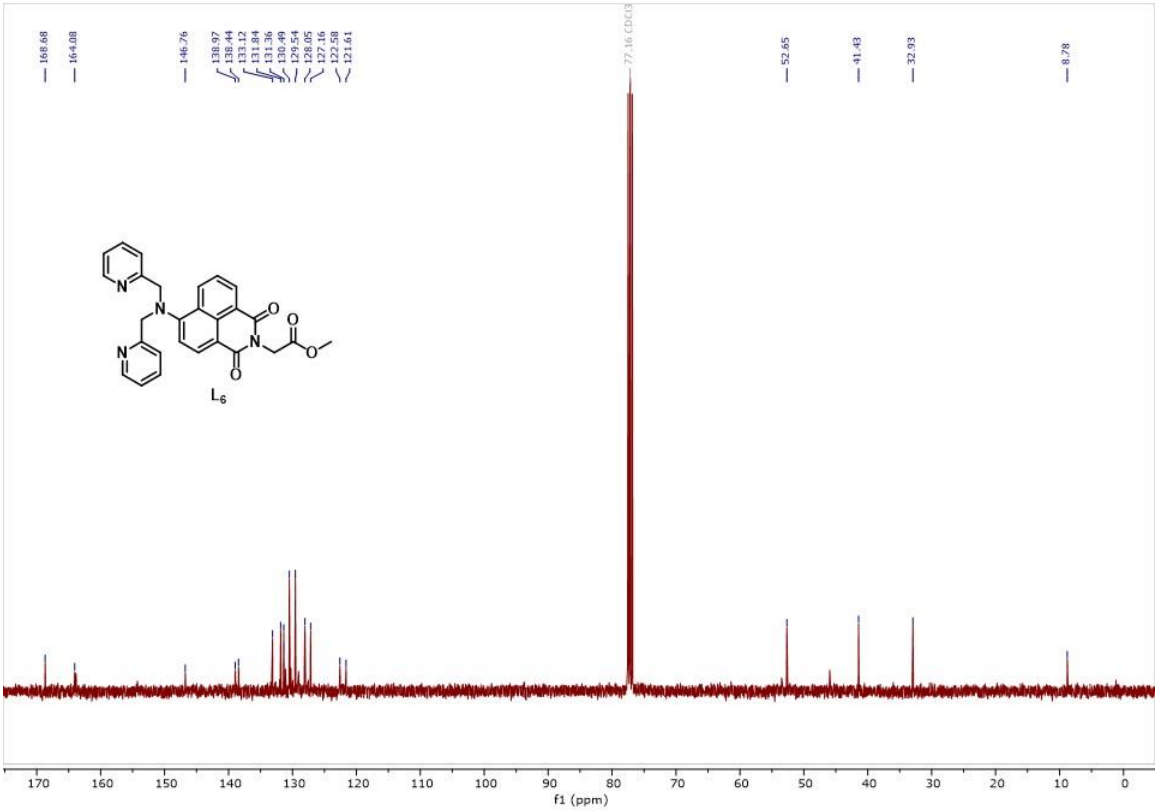

^{1}H NMR spectrum (400 MHz; $CDCl_3$) of **ReL$_1$**

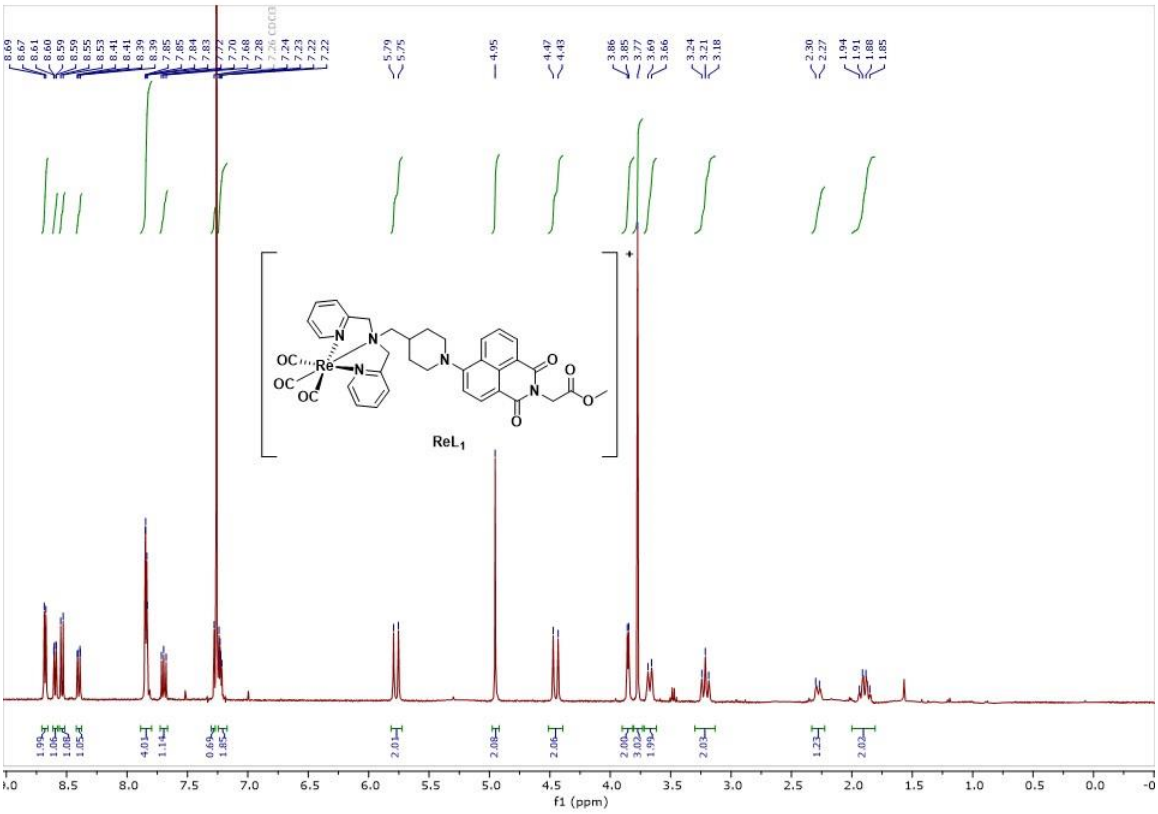

^{13}C NMR spectrum (100 MHz; $CDCl_3$) of **ReL$_1$**

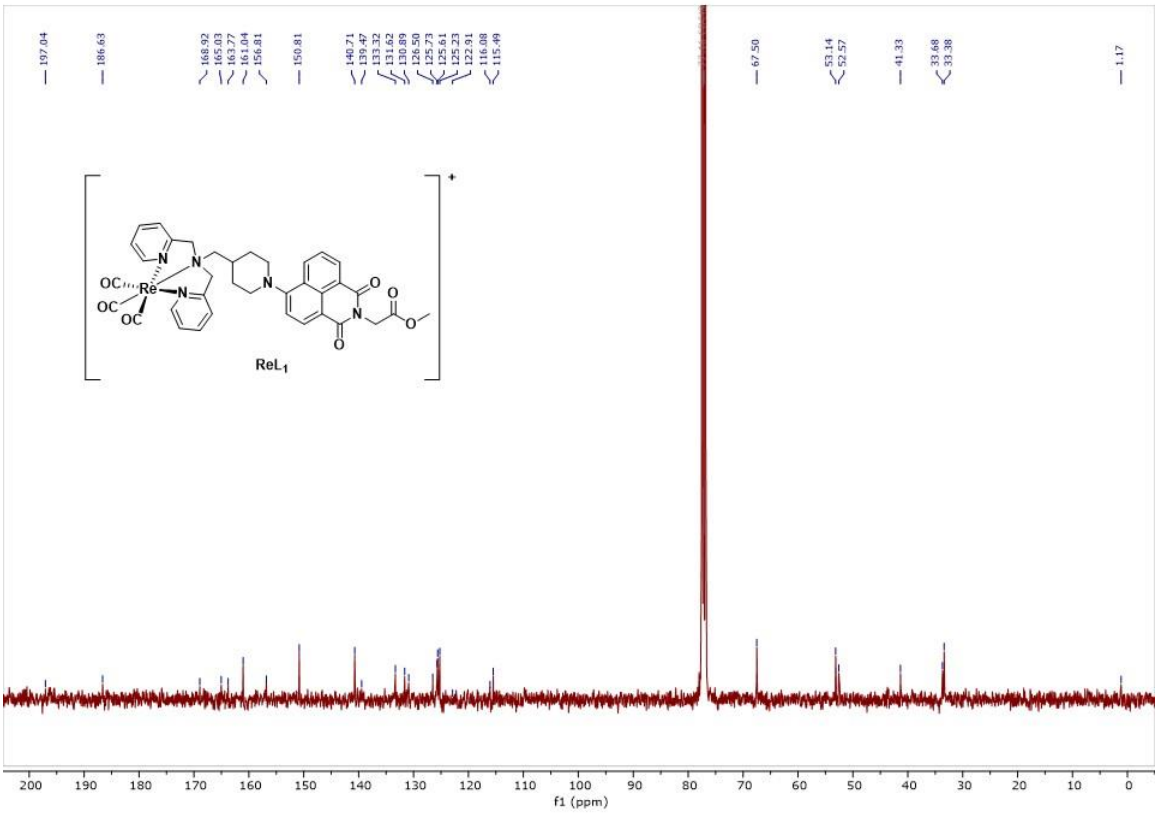

^{1}H NMR spectrum (400 MHz; CD_3OD) of **ReL$_2$**

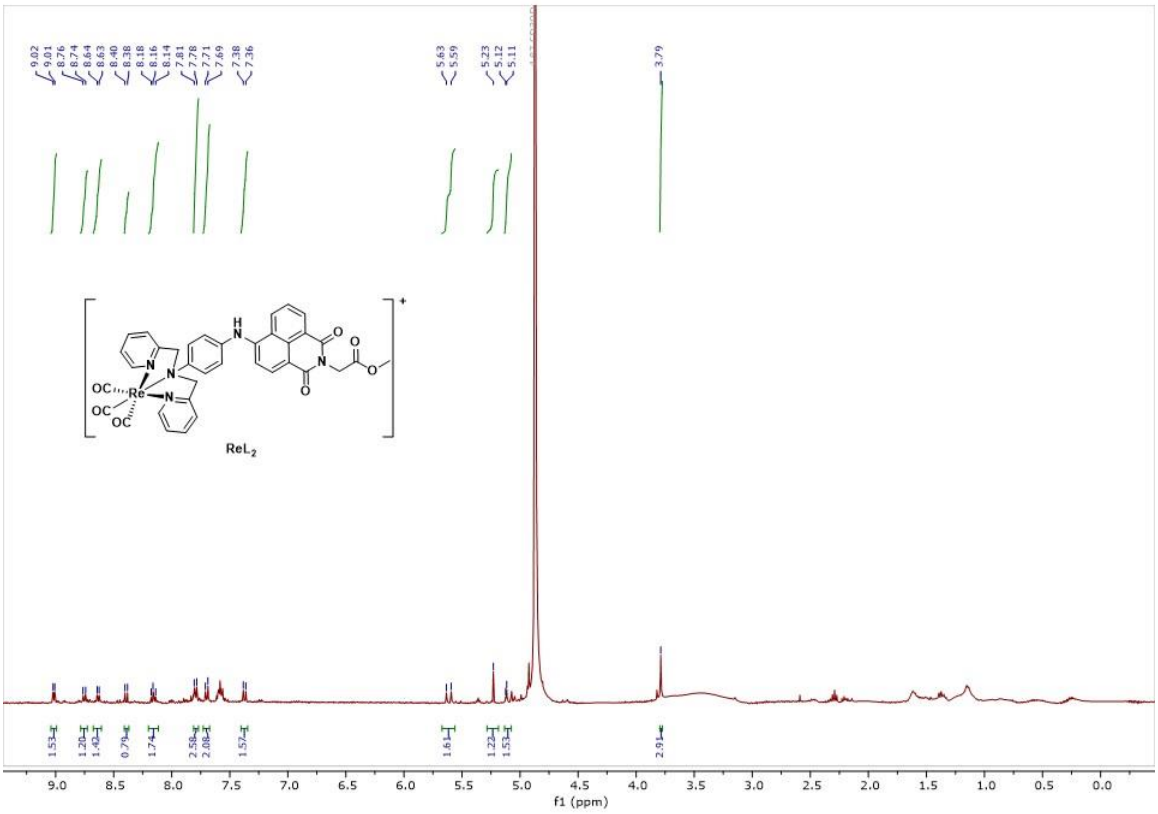

^{13}C NMR spectrum (100 MHz; CD_3OD) of **ReL$_2$**

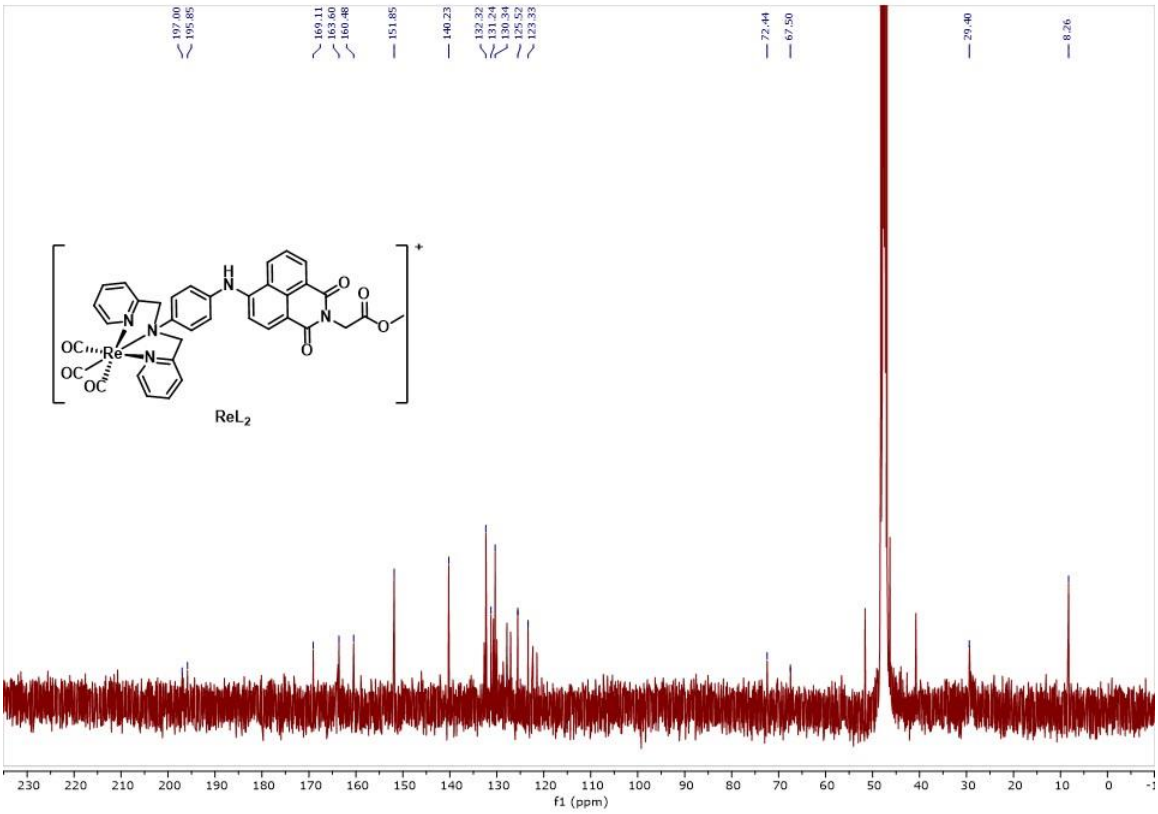

^{1}H NMR spectrum (400 MHz; CD_3OD) of **ReL$_3$**

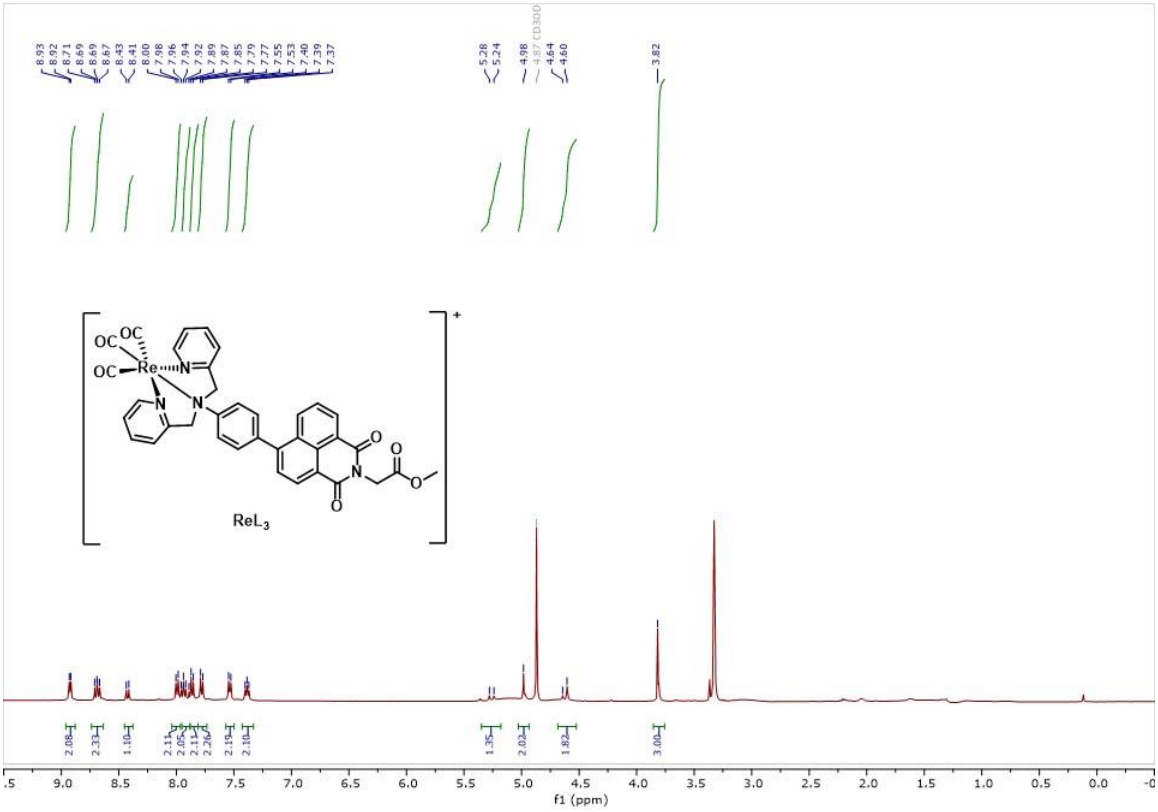

^{13}C NMR spectrum (100 MHz; CD_3OD) of **ReL$_3$**

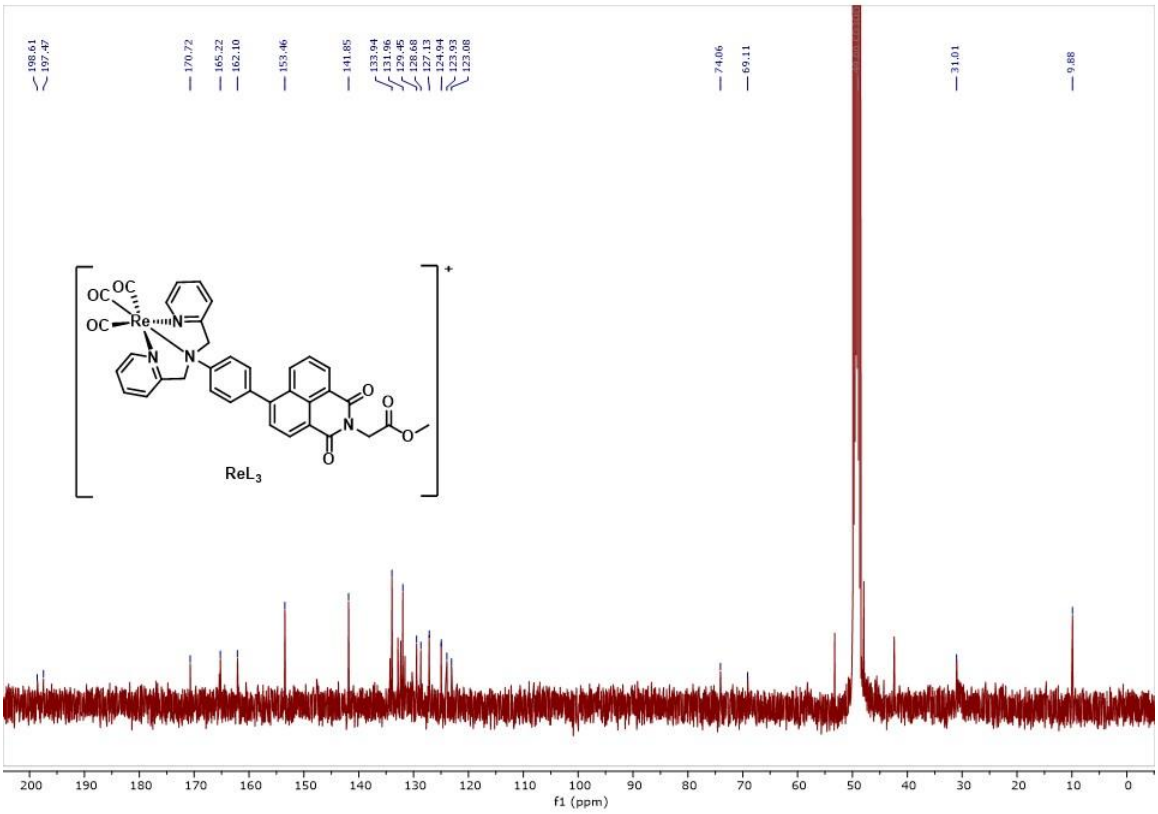

^{1}H NMR spectrum (400 MHz; $(CD_3)_2CO$) of **ReL$_4$**.

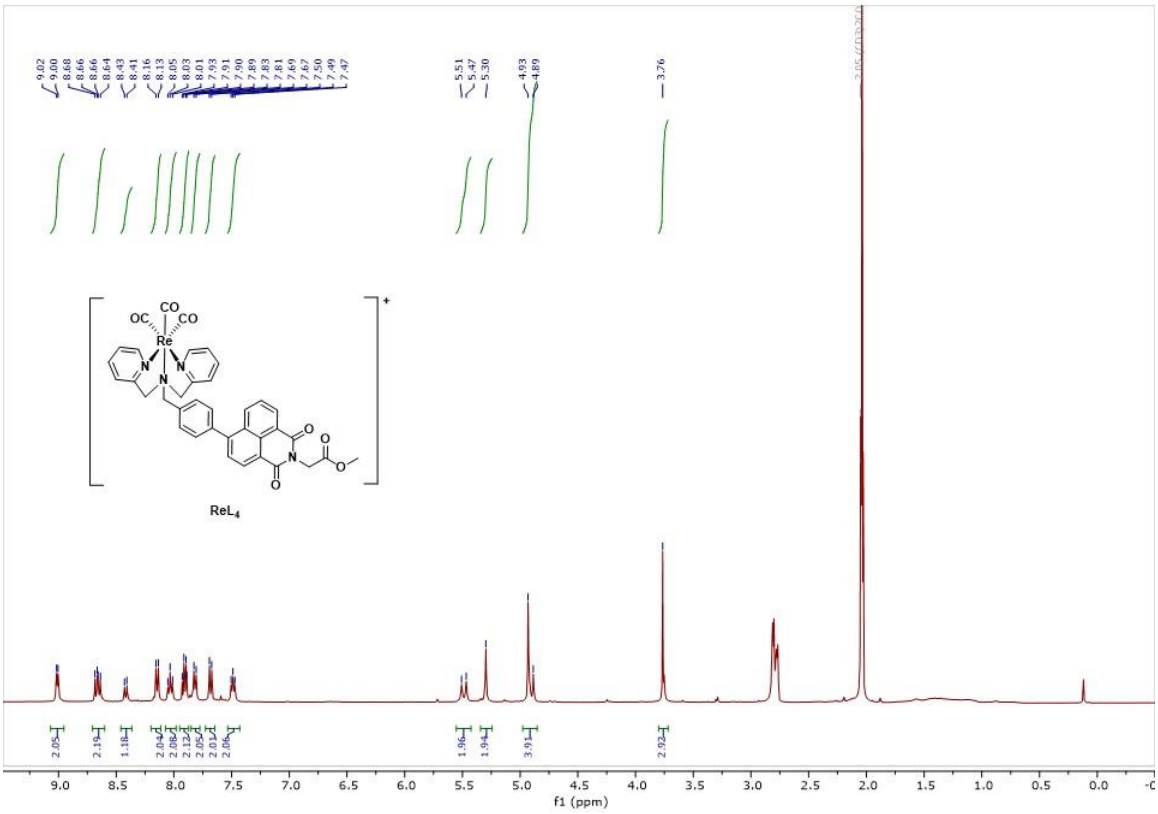

^{13}C NMR spectrum (100 MHz; $(CD_3)_2CO$) of **ReL$_4$**

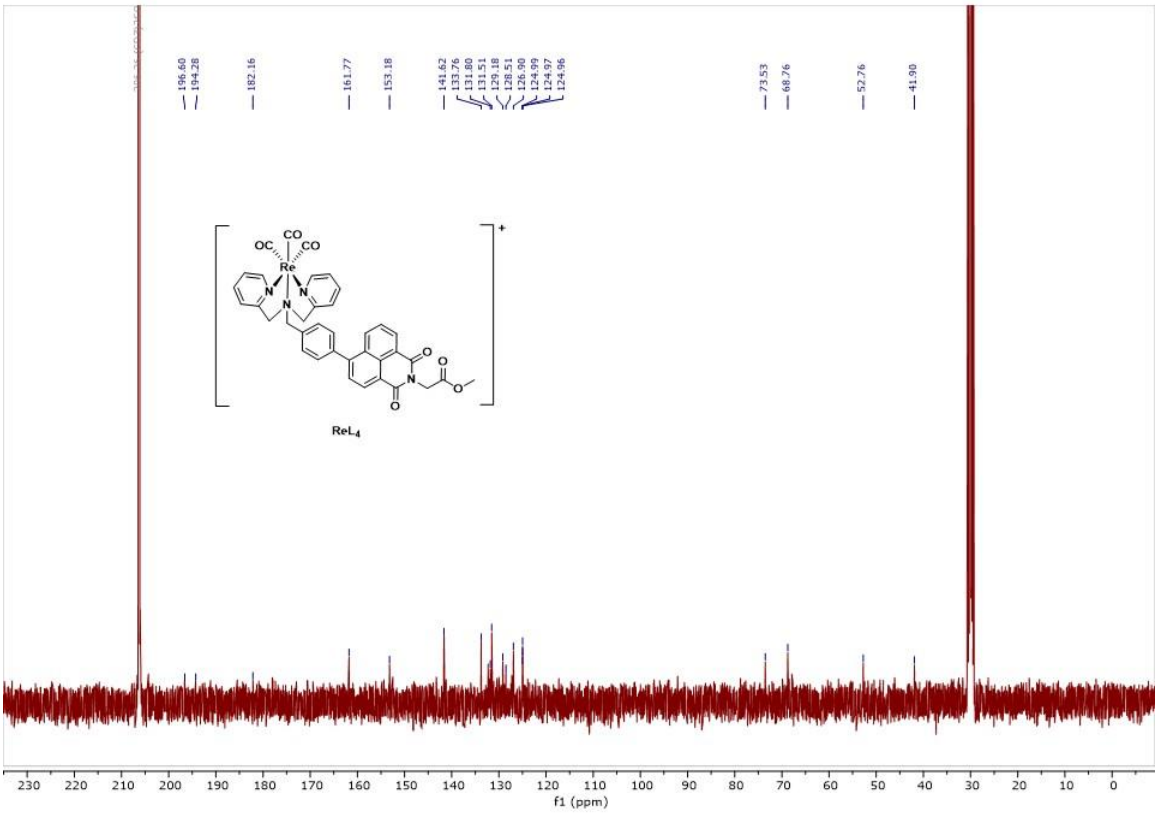

^{1}H NMR spectrum (400 MHz; $(CD_3)_2CO$) of **ReL$_6$**

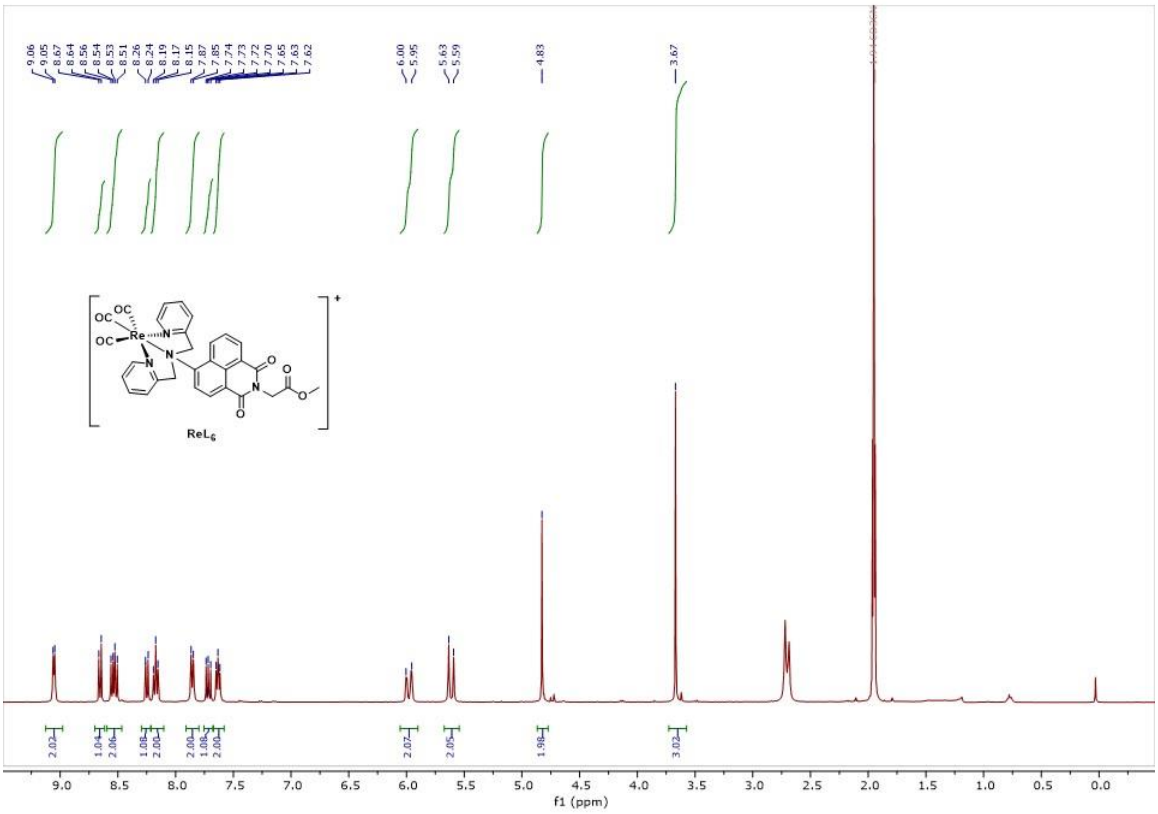

^{13}C NMR spectrum (100 MHz; $(CD_3)_2CO$) of **ReL$_6$**

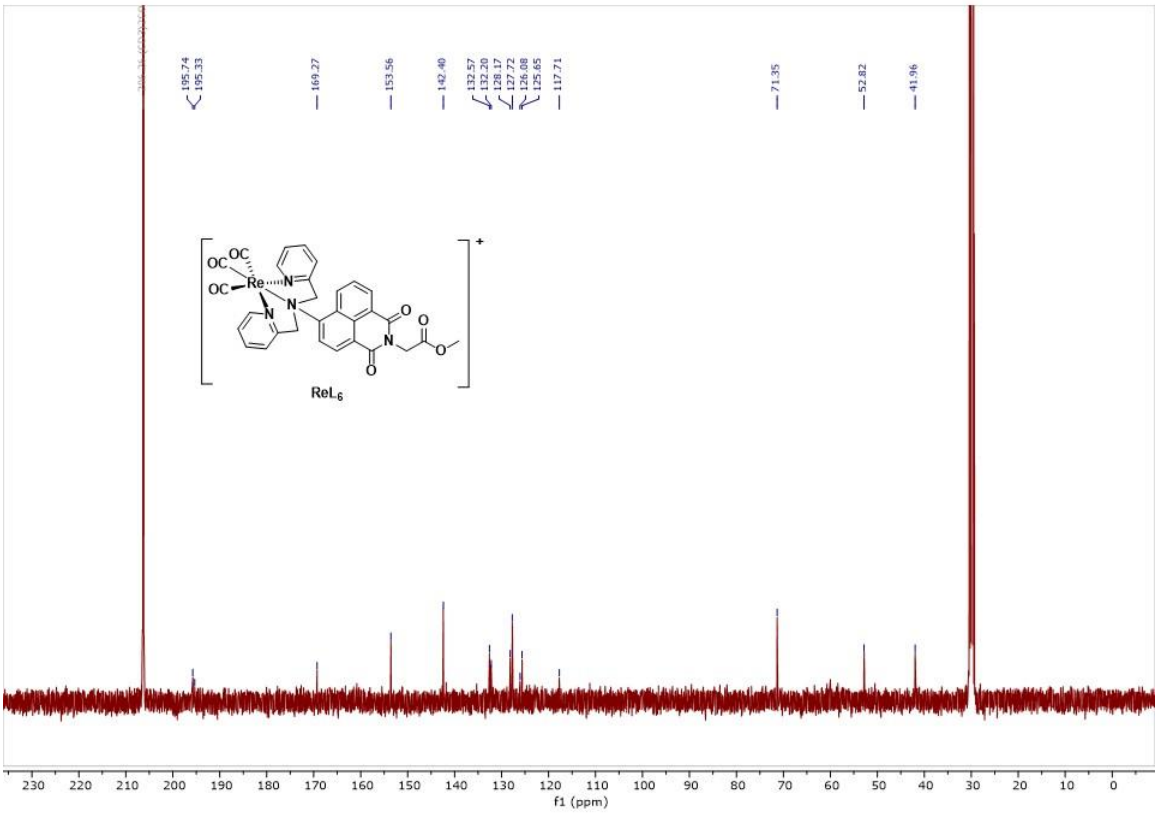

Appendix B: High Resolution Mass Spectroscopy (HRMS) Data of Synthesized Compounds

HRMS (ESI) spectrum of **1**

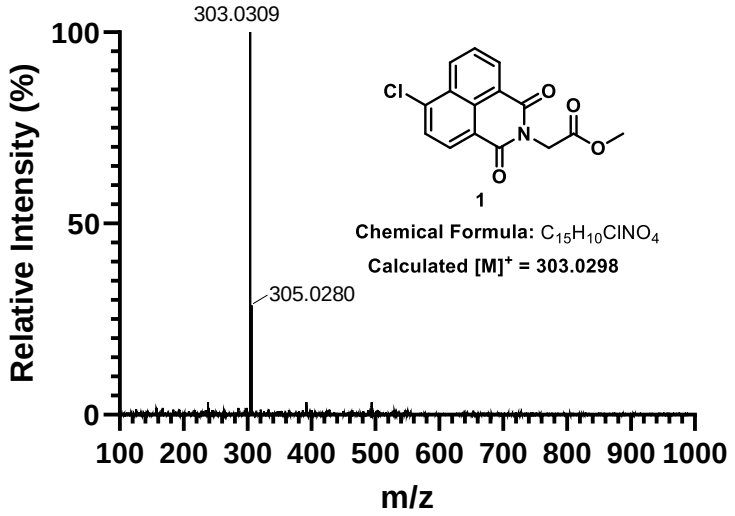

HRMS (ESI) spectrum of **2**

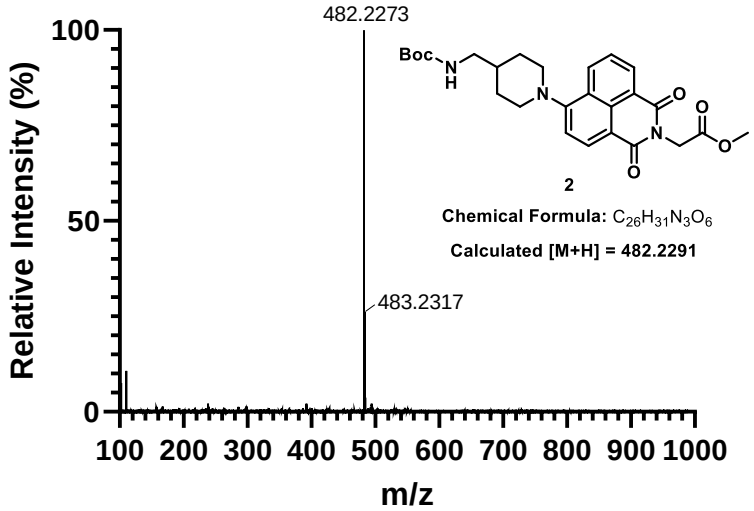

HRMS (ESI) spectrum of **3**

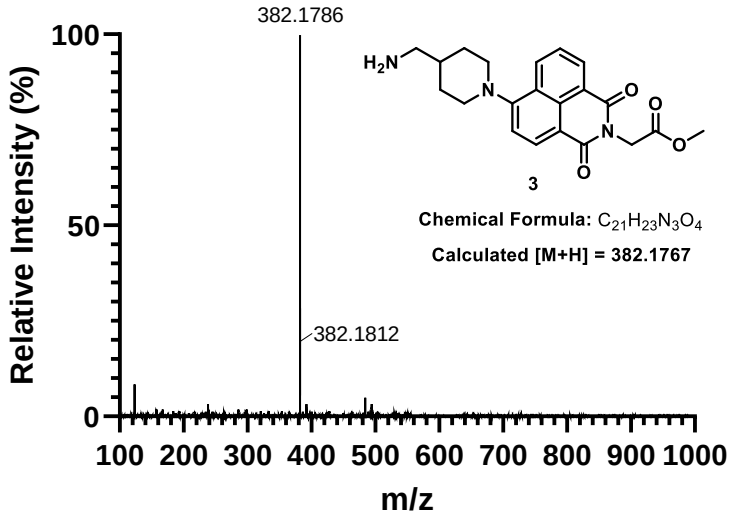

HRMS (ESI) spectrum of **L_1**

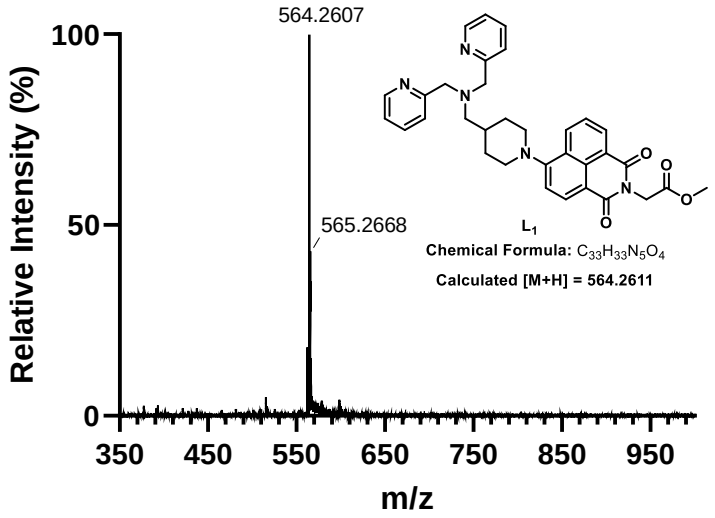

HRMS (ESI) spectrum of **5**

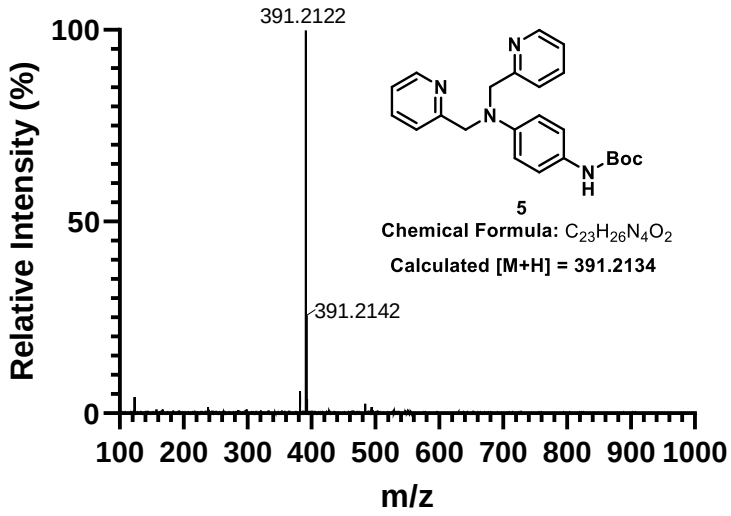

HRMS (ESI) spectrum of **6**

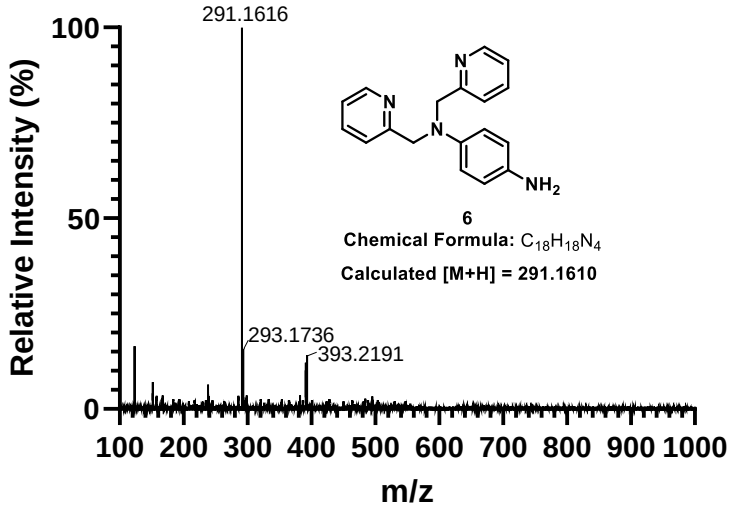

HRMS (ESI) spectrum of **12**

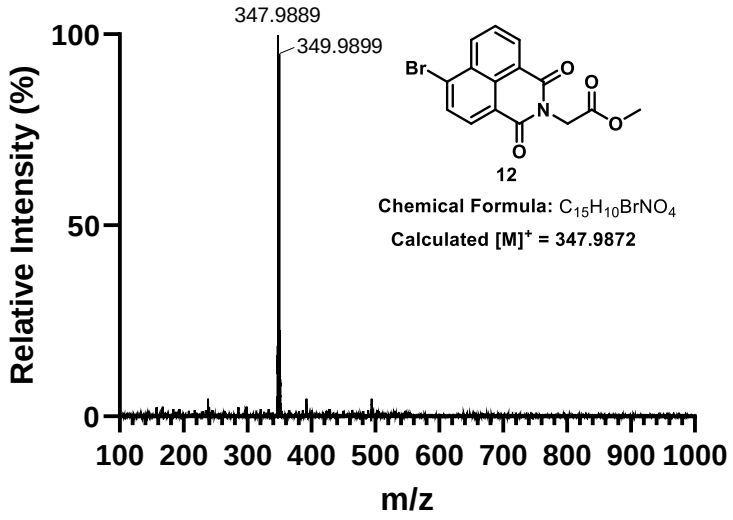

HRMS (ESI) spectrum of **L_2**

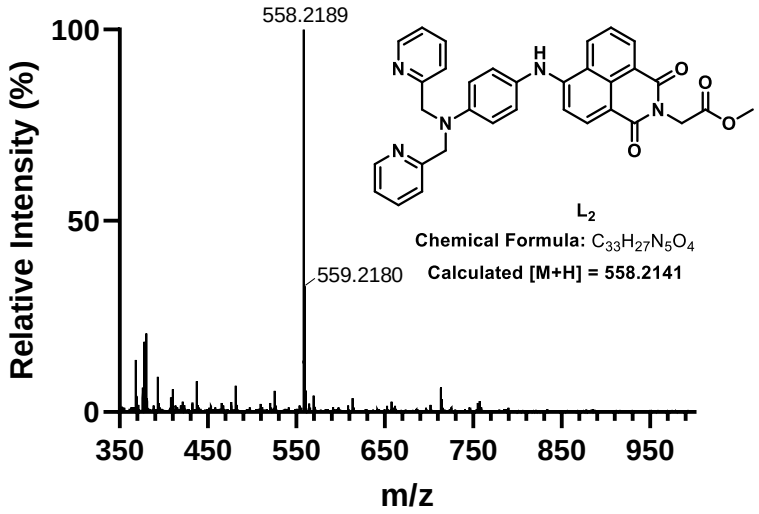

HRMS (ESI) spectrum of **13**

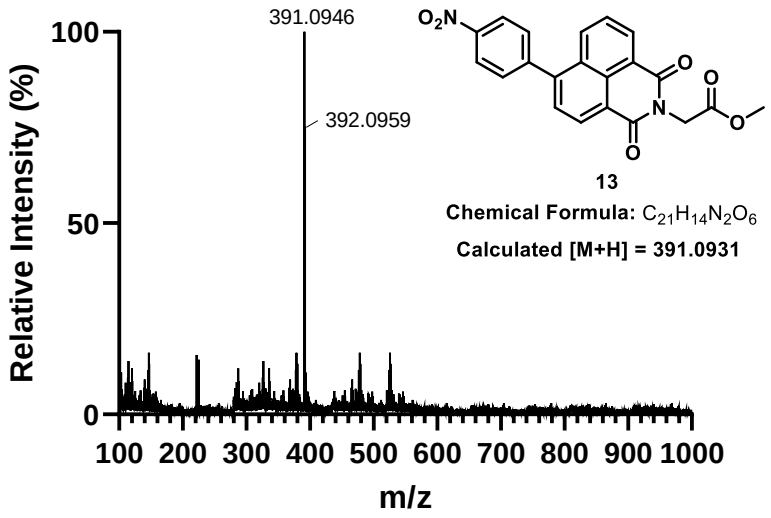

HRMS (ESI) spectrum of reduction product of **13**

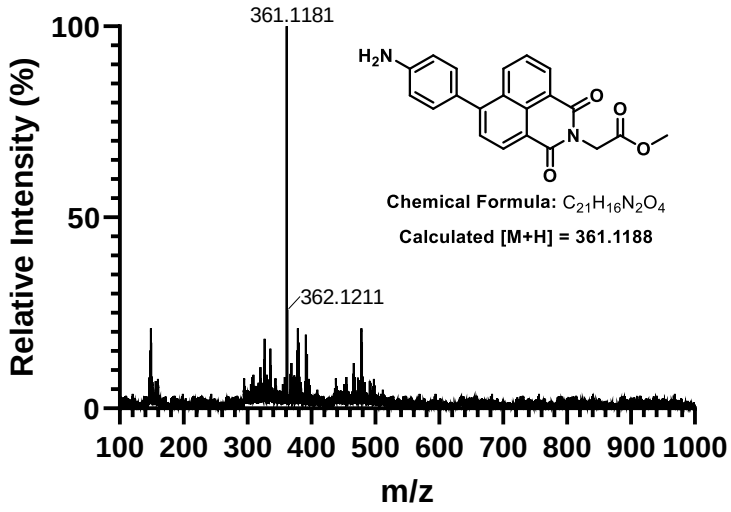

HRMS (ESI) spectrum of **L_3**

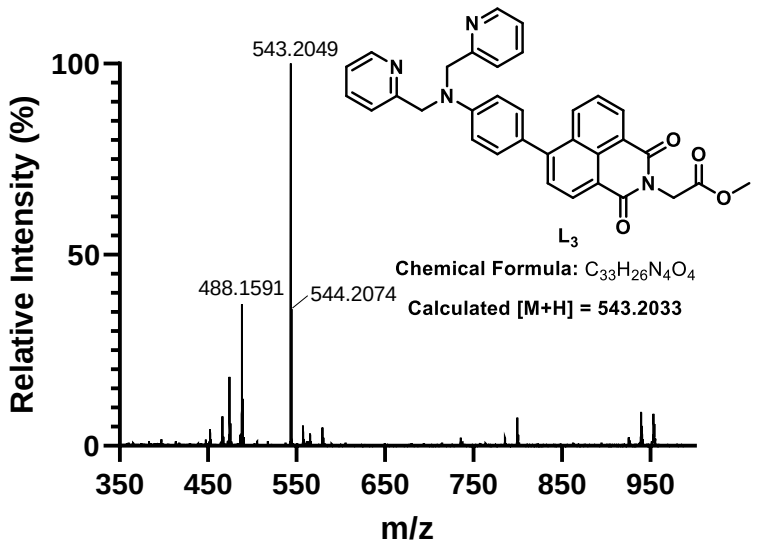

HRMS (ESI) spectrum of **14**

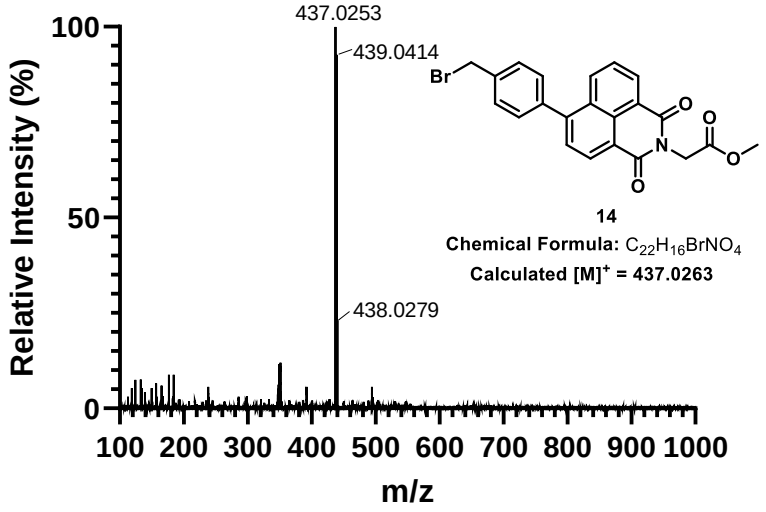

HRMS (ESI) spectrum of **L_4**

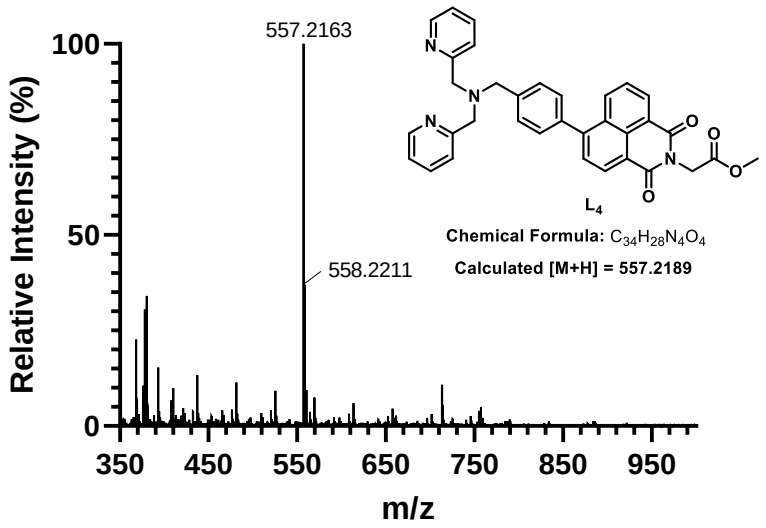

HRMS (ESI) spectrum of **L_6**

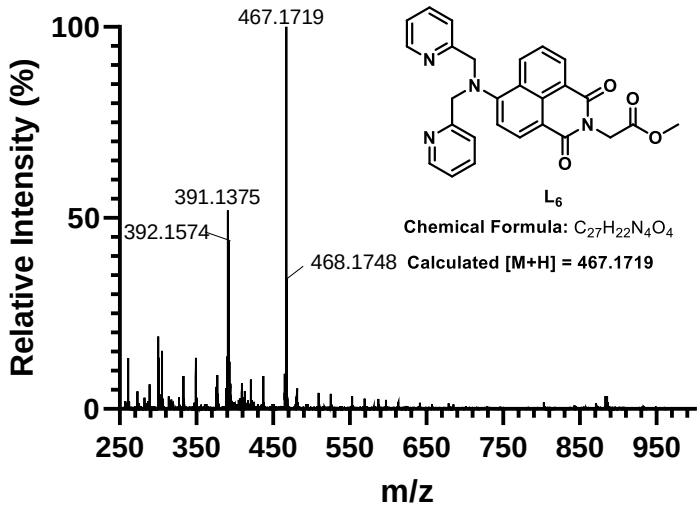

HRMS (ESI) spectrum of **ReL$_1$**

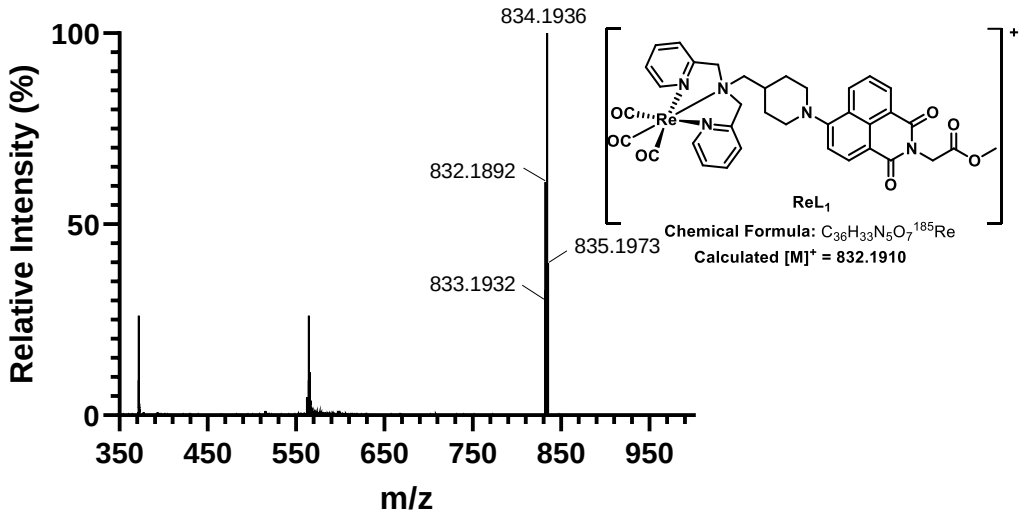

HRMS (ESI) spectrum of **ReL$_2$**

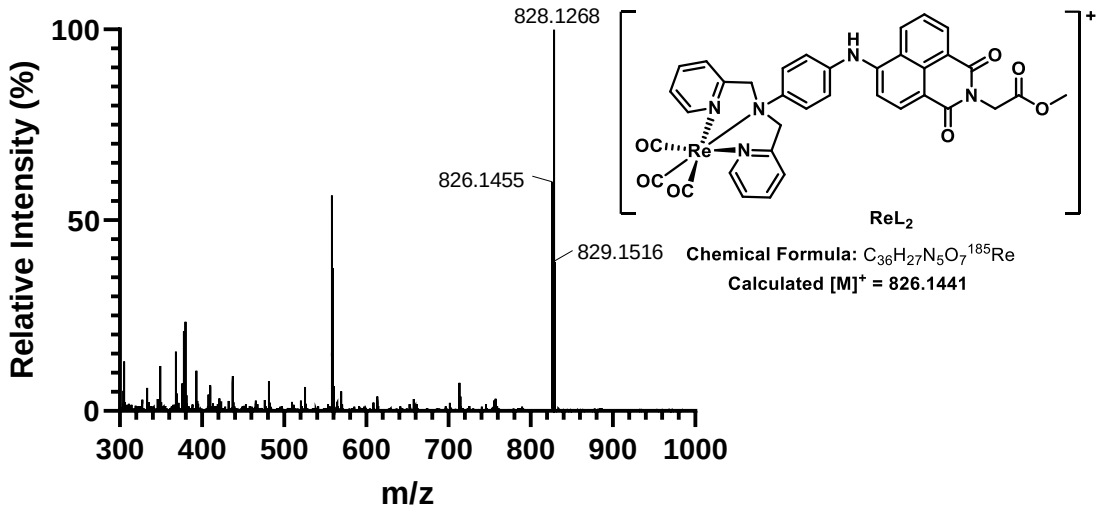

HRMS (ESI) spectrum of **ReL$_3$**

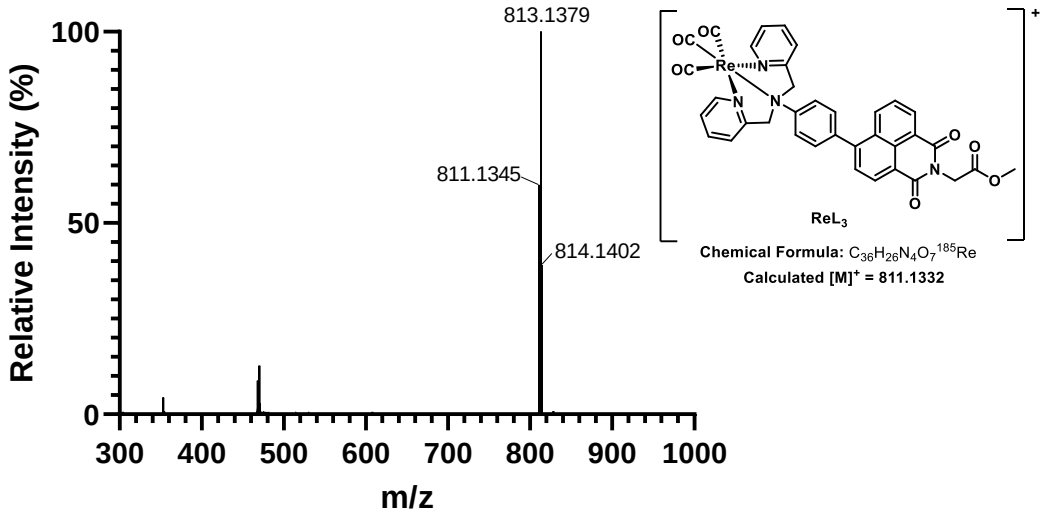

HRMS (ESI) spectrum of **ReL$_4$**

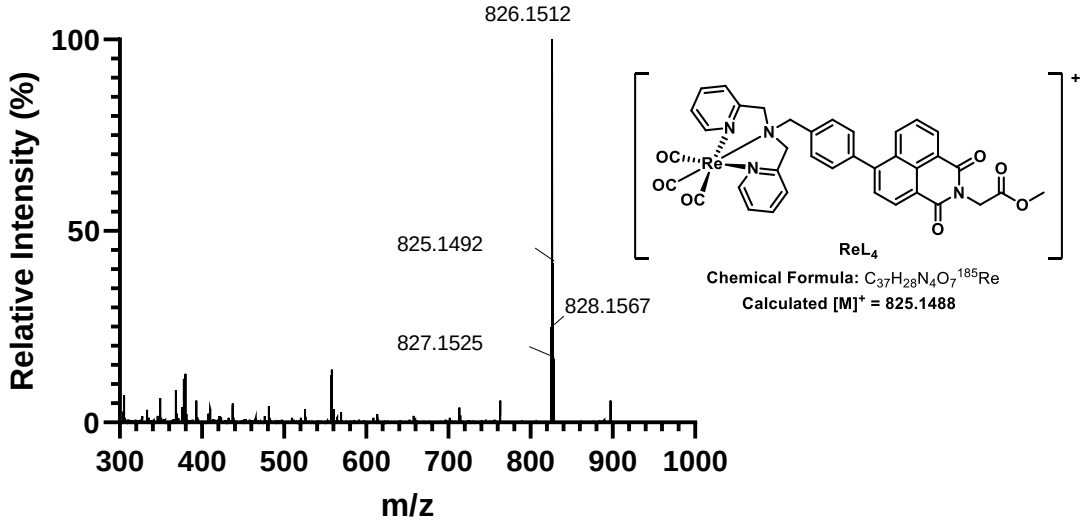

HRMS (ESI) spectrum of **ReL$_6$**

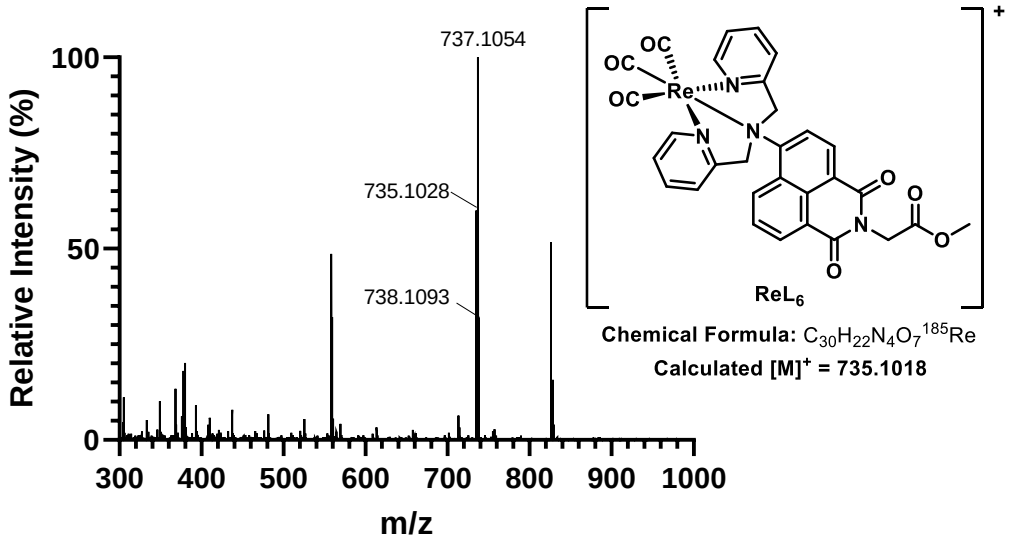

Appendix C : UV/Vis Absorbance and Fluorescence Spectra of Ligands and Rhenium complexes

UV/Vis absorbance spectra of 20 μM solutions of **L_1** and **ReL_1** in CH_3CN

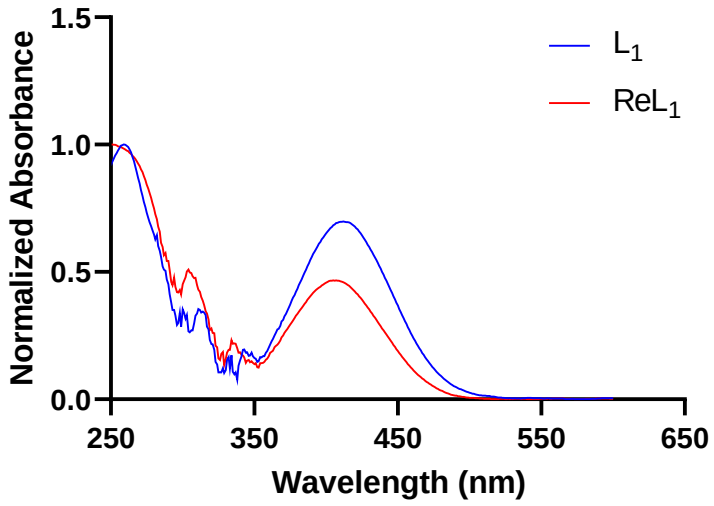

Fluorescence excitation and emission spectra of 20 μM solutions of **L_1** and **ReL_1** in CH_3CN

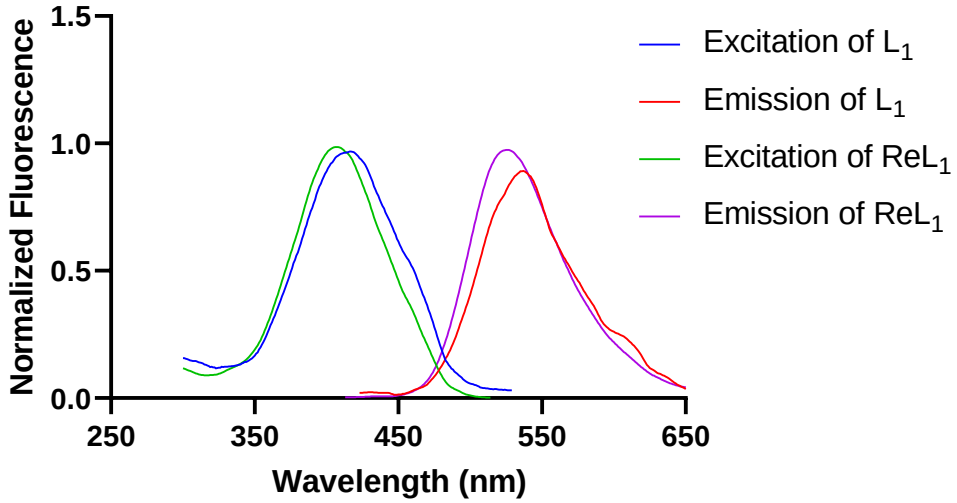

UV/Vis absorbance spectra of 20 μM solutions of **L_2** and **ReL_2** in CH_3CN

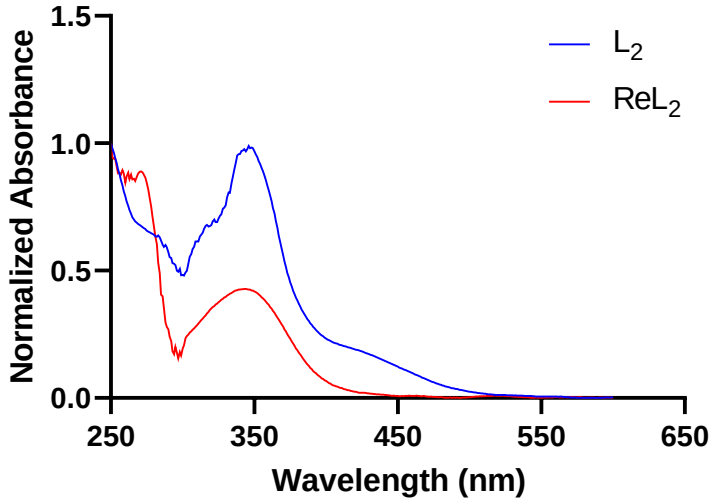

Fluorescence excitation and emission spectra of 20 μM solutions of **L_2** and **ReL_2** in CH_3CN

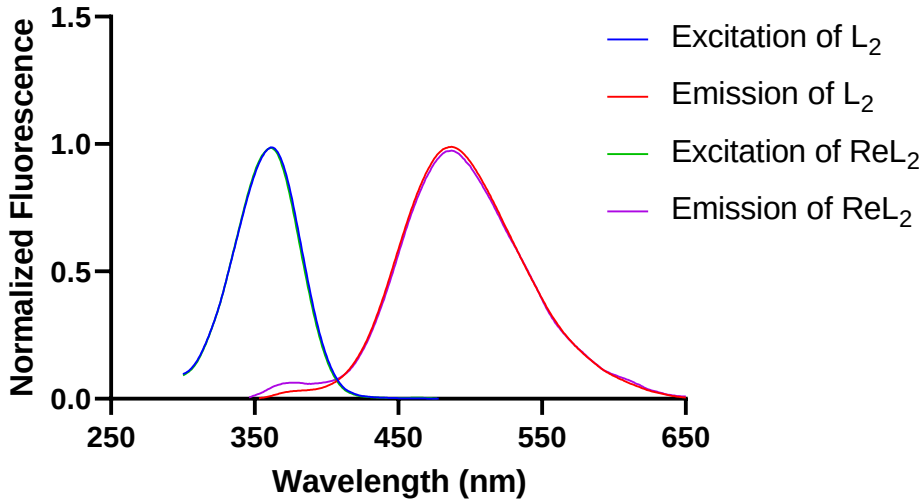

UV/Vis absorbance spectra of 20 μM solutions of **L_3** and **ReL_3** in CH_3CN

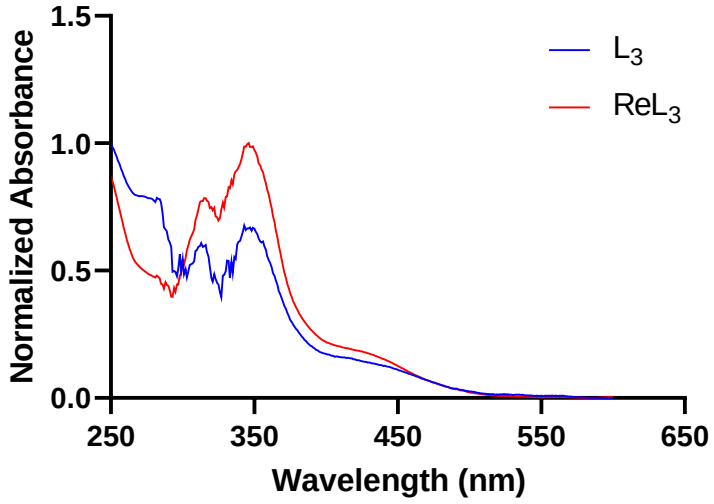

Fluorescence excitation and emission spectra of 20 μM solutions of **L_3** and **ReL_3** in CH_3CN

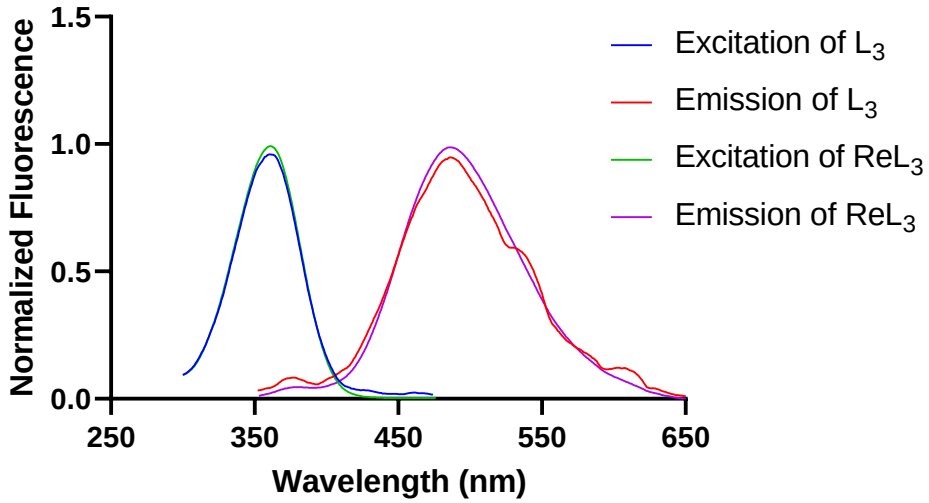

UV/Vis absorbance spectra of 20 μM solutions of **L_4** and **ReL_4** in CH_3CN

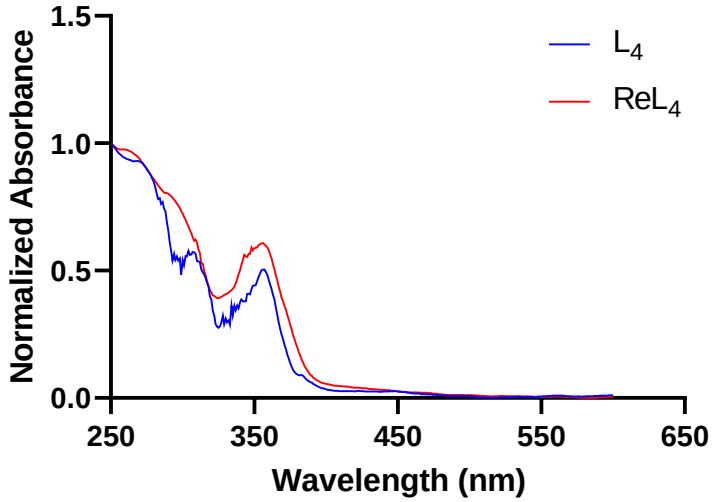

Fluorescence excitation and emission spectra of 20 μM solutions of **L_4** and **ReL_4** in CH_3CN

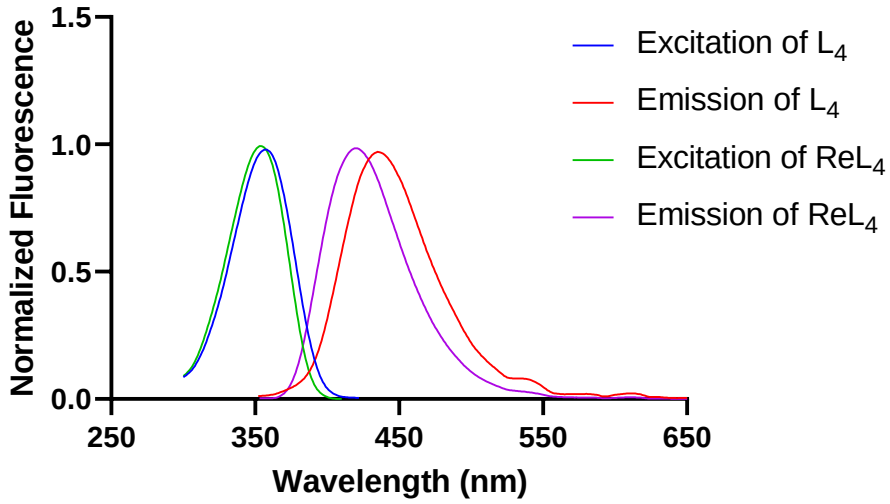

UV/Vis absorbance spectra of 20 μM solutions of **L_6** and **ReL_6** in CH_3CN

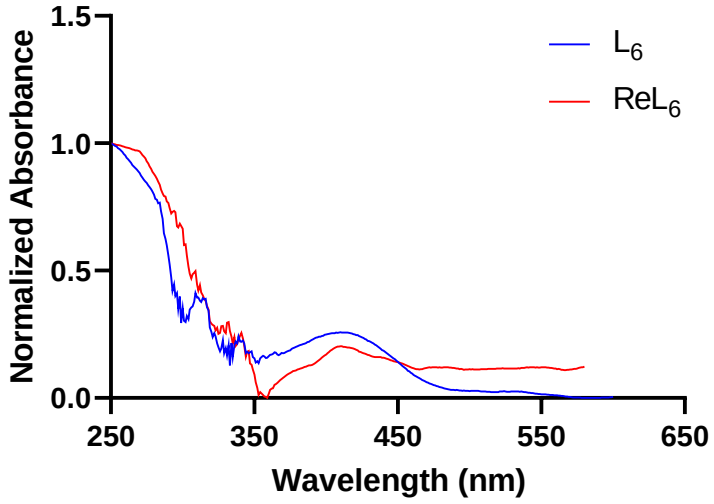

Fluorescence excitation and emission spectra of 20 μM solutions of **L_6** and **ReL_6** in CH_3CN

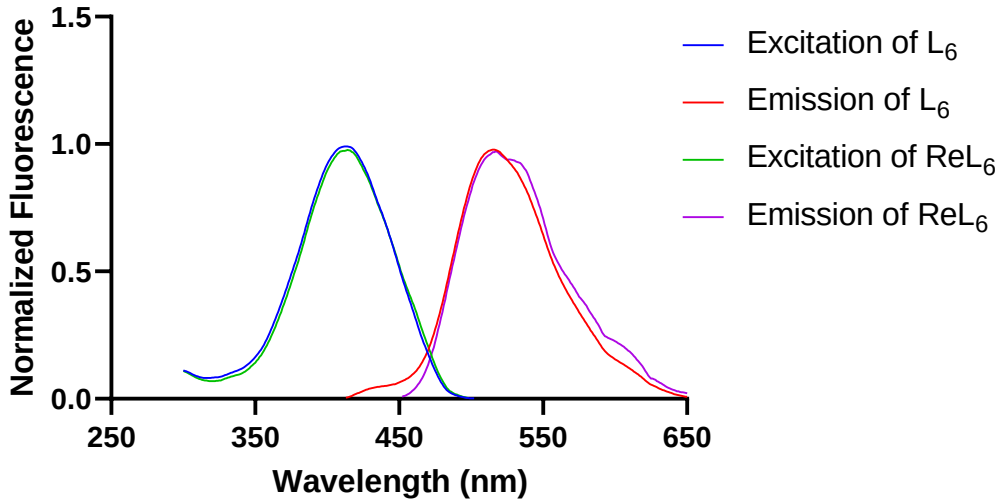

Curriculum Vitae

Name: Priyanka Jagadeesa Prabhu

Education

2019-Present	M.Sc., Organic Chemistry and Molecular Imaging
	The University of Western Ontario, Canada
	Supervisor: Prof. Leonard G. Luyt
2013-2018	BS-MS, Chemistry
	Indian Institute of Science Education and Research, India
	Supervisor: Dr. Gokulnath Sabapathi

Research Experience

2018-Winter	Thesis for the minor degree in Biology
	Indian Institute of Science Education and Research, India
	Supervisor: Dr. Nishant K.T.
2016-Summer	Research Internship
	CSIR- National Chemical Laboratory, India
	Supervisor: Dr. G. J. Sanjayan
2014 Summer	Research Internship
	Rajiv Gandhi Centre for Biotechnology, India
	Supervisor: Dr. G. S. Vinod Kumar

Awards and Scholarships

2013-2018	INSPIRE fellowship
	Department of Science and Technology, Government of India

Publications

Nadimpally, K. C.; Chakrapani, A.; **Prabhu, P. J**.; Madica, K.; Sanjayan, G. J. *ChemistrySelect* **2017**, *2* (12), 3594.

Teaching Experience

2019-Present Marking and Laboratory teaching assistantship,

The University of Western Ontario, Canada

Courses: Chem 2213 – Organic Chemistry for Life Science

Chem 2223 – Organic Chemistry of Biological Molecules

Chem 3393 – Medicinal Chemistry